AD-A273 593

DTIC
ELECTE
DEC 09 1993
A

# Vertical Motion
# in the SYNOP Central Array

93-29977

## Scott S. Lindstrom and D. Randolph Watts

93 12 8 046

## Abstract

As part of the SYNOP (Synoptic Ocean Prediction experiment) field program, twelve tall moorings measured the Gulf Stream's temperature and velocity fields with current meters (CM) at nominal depths of 400 m, 700 m, 1000 m, and 3500 m for two years, from May 1988 through August 1990. Simultaneously, 24 inverted echo sounders (IES) monitored the thermocline topography. A third observational component of the experiment was the release of isopycnal RAFOS floats; 70 such floats traversed the area monitored by the CM and the IES. This report documents the methods used to compute vertical motion for each data source, and the differences and similarities between the three methods. Typical velocities during 'strong' events, as observed by or inferred from all three instruments, was $1-2$ mm s$^{-1}$ in regions near the center of the Gulf Stream. The comparison of RAFOS vertical motions and vertical motions diagnosed from CM data showed excellent agreement; furthermore, CM vertical motions and IES vertical motions are statistically coherent for periods longer than 12 days. We conclude that we may map mesoscale fields of $w(x, y, t)$; the fields mapped are consistent with quasi-geostrophic dynamics.

# Contents

# List of Figures

# List of Tables

# 1  Introduction

The SYNoptic Ocean Prediction experiment (SYNOP) was a multi-institutional study of the Gulf Stream from 1987-1990. Designed to further the understanding of Gulf Stream meanders, and to facilitate the modeling of the meanders, the SYNOP experiment was comprised of three different arrays: an Inlet Array near Cape Hatteras, a Central Array near 68°W, and an Eastern Array near the Grand Banks at 55°W. Data collected in the Central Array to be considered in this report came from 12 tall, high-performance moorings on which were four current meters (CM) (at nominal depths of 400, 700, 1000, and 3500 m), from 24 inverted echo sounders (IES) which acoustically monitored the depth of the main thermocline, and from approximately 70 isopycnal RAFOS floats which sampled pressure and temperature along an isopycnal surface as they moved downstream through the Gulf Stream.

Vertical motion, $w$, in the Gulf Stream has been observed in previous studies (e.g. Bower and Rossby 1989) and inferred in others (Hall 1986). Here, we wish to compare the vertical motions observed by the isopycnal floats to those inferred from CM observations and those inferred from IES observations. The three methods of computing/determining vertical motion are detailed in the following section, with 23 case study events following.

# 2  Instruments and vertical motion calculations

## 2.1  RAFOS floats

### 2.1.1  Methodology

Bower and Rossby (1989) show how vertical motion is related to RAFOS float motion, namely that upward vertical motion occurs as the float moves downstream from trough to crest, and downward motion accompanies motion downstream from crest to trough. The RAFOS float recorded temperature, pressure and location at eight-hour intervals as it moved through the stream. The method for determining vertical motion from these variables is straightforward. The computed $w_{RAF}$ ($\equiv \frac{\partial p}{\partial t}$) is estimated using a second-order centered finite difference. Because $\delta t = 8$ hours, the vertical motion computed is an average over a 16-hour interval. Of the 72 RAFOS floats that were released as part of the SYNOP experiment and returned useful data, more than 90% passed directly through the Central Array, providing a large dataset of observed vertical motion.

### 2.1.2  Errors in Float vertical motion estimates

Errors introduced by the float not being perfectly isopycnal should be insignificant for the scales of motion we consider (Rossby, personal communication). However, because floats move through features, the vertical motion measured by the float, a sixteen-hour average value, may differ considerably from the point values measured by CM and IES. This is most obviously the case if the float passes through an up/down couplet in sixteen hours, in which case the average vertical motion may be near zero, although the values of upwelling or downwelling within the couplet (as sampled by a current meter mooring, perhaps) will not be. This bias error may underestimate several of the largest $w$ events by as much as 30%.

To understand this bias, consider a pattern of vertical motion that along a fluid particle trajectory varies sinusoidally such that the pressure measured by a RAFOS float and the vertical motion will be

$$P = A \sin \omega t \quad \text{and} \quad w_{true} = A \omega \cos \omega t, \tag{1}$$

respectively. How is the computed vertical motion affected by discrete, rather than continuous, sampling? The estimated vertical motion, $\hat{w}$, is

$$\hat{w} = A \frac{\sin\left[\omega(t + \Delta t)\right] - \sin\left[\omega(t - \Delta t)\right]}{2\,\Delta t} = w_{true} \frac{\sin \omega \Delta t}{\omega \Delta t}. \tag{2}$$

The ratio $\frac{\hat{w}}{w_{true}}$ approaches unity for all motions that have period $T$ much longer than the sampling time, $\Delta t$, but it crosses zero for $T = 2\Delta t$.

The RAFOS floats that generated the data used in this study sampled data at $\Delta t = 8$ hours. For $T \geq 3$ days, for example, $\frac{\hat{w}}{w_{true}} \geq 0.92$; however, for a period $T$ of 36 hours, the estimated vertical motion is 70% of true. Vertical motions in the inertial frequency range (or higher frequencies) are significantly underestimated by the 8-$h$ sampling period. For a period of 19 hours, for example, the estimated vertical motion is only 18% of the true. However, this is desirable, because we are using the floats to estimate vertical motions on meso- and synoptic scales.

The largest vertical motions that we investigate in this paper are typically associated with float displacements with period three days or less. Several of the float trajectories through the central array show strong up and down couplets, with the float moving up and down $> 200\ m$ in less than three days. Equation (2) indicates that the vertical motion as measured by the float may underestimate the true vertical motion in these cases by around 30% if the dominant period of the float is about 36 hours.

## 2.2   Current meters

### 2.2.1   Methods

Bryden (1976, 1980) was among the first[1] to use the backing (turning counterclockwise with decreasing depth) and veering (turning clockwise with decreasing depth) of current meters to infer vertical motion in the ocean. Following his notation, and that of Hall (1986), the temperature equation,

$$\frac{\partial T}{\partial t} + u\frac{\partial T}{\partial x} + v\frac{\partial T}{\partial y} + w\frac{d\theta_o}{dz} = 0, \tag{3}$$

can be transformed, using the thermal wind equation, to

$$w_{CM} = \frac{-\frac{\partial T}{\partial t} - \frac{\rho_o f}{g\alpha_o}\left[v\frac{\partial u}{\partial z} - u\frac{\partial v}{\partial z}\right]}{\frac{d\theta_o}{dz}}, \tag{4}$$

or, using $\frac{d}{dz}\tan^{-1}\phi = \frac{1}{1+\phi^2}\frac{d\phi}{dz}$, to

$$w_{CM} = \frac{-\frac{\partial T}{\partial t} - \frac{\rho_o f}{g\alpha_o} R^2 \frac{\partial \phi}{\partial z}}{\frac{d\theta_o}{dz}}. \tag{5}$$

---

[1]First in oceanography.   Árnason (1942) and Panofksy (1944) developed similar methods for the atmosphere.

Here, $R$ is magnitude of the current velocity $(u^2 + v^2)^{\frac{1}{2}}$, $\rho_o$ is mean density ($1035\ kg\ m^{-3}$), $g$ is gravitational acceleration ($9.8\ m\ s^{-2}$), $f$ is the Coriolis parameter, $\alpha_o$ is the effective thermal expansion coefficient ($\equiv \frac{\partial \rho}{\partial T} + \frac{\partial \rho}{\partial S}\frac{\partial S}{\partial T} = 1.2 \times 10^{-1} kg\ m^{-3}\ K^{-1}$) appropriate for the T-S relationship in mid-thermocline in the Gulf Stream (Hall 1985), $\frac{d\theta_o}{dz}$ is the mean stratification ($0.02\ K\ m^{-1}$), $\phi$ is the angle of the current with respect to east, and $u$ and $v$ are the eastward and northward components of the flow. The constants used in this work are consistent with a Brunt-Vaisala period of about twenty minutes. We note that $w_{CM}$ could be biased slightly by this choice of constants.

For isopycnal motions, vertical motion is proportional to the two terms in the numerator of (4) or (5). The first describes the motion of the isopycnals themselves: for instance, in the absence of horizontal motions, if the temperature at a current meter is increasing, isopycnal surfaces, and the water parcels on them, must be descending. The second term in the numerator is the heat advection in the presence of sloping isopycnal surfaces, which is proportional to the cross-frontal component of velocity in the presence of sloping isopycnal surface, as in (3), or equivalently to the turning of the current vector with height, $\frac{\partial \phi}{\partial z}$, as in (5). Where currents back or veer with height, vertical motion must exist, if the temperature is constant. Consider if the flow at 400m is towards the southeast at 80 cm s$^{-1}$ and the flow at 1000m is towards the northeast, also at 80 cm s$^{-1}$. For this case the thermal wind will point due south. Cold water is to the east, and warm water is to the west, of this vector, *i.e.* isotherms slope up to the east. The mean eastward flow encountering this upward slope to the isotherms therefore generates upward vertical motion.

### 2.2.2 Application

The CM data used in this study have been smoothed. A 40-hour low-pass filter has been applied to the data to remove high-frequency signals (diurnal and semi-diurnal tides, for example). In addition, the CM data have been adjusted to compensate for mooring motion. When strong currents surround a current meter mooring, it will tilt over more than when in an environment of weaker currents. Sensors therefore do not always remain at the same level. The method of Hogg (1991) interpolates (or extrapolates) the current meter data at variable levels to constant horizons, in this case at 400, 700, and 1000 m below the sea surface. We computed the vertical motion using data with and without the mooring motion correction and noted negligible differences. Because the corrected data also yield vertical motions at the same level throughout the domain we used in this study data corrected for mooring motion.

The vertical motion $w_{CM}$ was computed using (4), with the vertical derivatives ($\frac{\partial u}{\partial z}$ and $\frac{\partial v}{\partial z}$) approximated as centered finite differences using data at 400 and 1000 m. Current velocities ($u$ and $v$) were averages of values at 400 and 1000 m. Temperature tendencies, ($\frac{\partial T}{\partial t}$), were computed using a second-order centered-in-time finite difference scheme, with $\Delta t = 12$ hours, and data at 700 m. The vertical motion computed can be considered as a representative value about halfway between the 400 and 1000 m. We have used the formula including $v\frac{\partial u}{\partial z} - u\frac{\partial v}{\partial z}$ for two reasons. The data includes $u$ and $v$ at three levels, so less data processing is necessary than if we used the formula including $R^2 \frac{\partial \phi}{\partial z}$ (although interpretation of the results is easier using the turning current vector with height). Furthermore, the $R^2$ term introduced spikes into the computed vertical motions when current speed profile was non-linear.

Because the current speeds used in (4) are at two levels, 400 and 1000m, we originally computed the temperature tendency term, $\frac{\partial T}{\partial t}$, using the average of the values at 1000 and

400m to estimate the water column average. This introduced an error, however, for those cases in which the 400-m CM was above the main thermocline and the 1000-m CM was below. Both current meters then recorded small temperature tendencies, even though the movement of the main thermocline was large (as measured by the temperature change at 700 m). For an example, see Case 1, section 3.1. Although using the averaged temperature tendency caused an error as just described, no similar error is evident from using the average of $u$ and $v$ values at 400 and 1000 m to represent the flow at 700 m.

## 2.3 IESs

Inverted echo sounders sit on the ocean floor and acoustically monitor the depth of the main thermocline, denoted as the depth of the 12° isotherm, i.e. $z_{12}$ (Watts and Rossby 1977). Vertical motion is computed from IESs by using objectively mapped IES data (Tracey and Watts 1991) to determine a streamfunction and therefore a vorticity field as in Kim (1991). As with CM data, all IES data are 40-hour low-pass filtered to remove high-frequency signals. This smoothing is done before the objective mapping. The IES fields are objectively mapped daily for 26 months, yielding estimates not only of streamfunction and vorticity, but of the time tendencies of both. if the motion is assumed to be quasi-geostrophic, then the vorticity equation as in, for example, Holton (1979),

$$\frac{\partial \zeta_g}{\partial t} = -\vec{V}_g \cdot \nabla(\zeta_g + f) + f_o \frac{\partial w}{\partial z}, \tag{6}$$

can be rearranged to determine vertical stretching. Vertical motion in the Gulf Stream has primarily a first baroclinic mode structure (Hall 1986; Rossby 1987). The maximum vertical motion occurs below the main thermocline (Gill 1982, fig. 6.14); even for very shallow main thermoclines (i.e., $z_{12}$ around 200 m – much shallower than for any of the 23 cases considered here), the methods used by Pickart and Watts (1990) show that the maximum in vertical motion is below 500 m. Vertical motion in the the upper ocean at depth $z$ can be approximated as

$$w_{IES} = \frac{z}{f_o}[\frac{\partial \zeta_g}{\partial t} + \vec{V}_g \cdot \nabla(\zeta_g + f)] \tag{7}$$

using data at 400 m.

We have used this method of computing vertical motions instead of the quasi-geostrophic $\omega$-equation as used by Leach (1987), Tintoré et al. (1991) and Pollard and Regier (1992) because it is more suited to our data. In the other studies, roughly synoptic CTD data were available to provide data at different levels as is necessary for Q-vector computations. We have a streamfunction map at just one level, but at a sequence of times, making (6) a more natural way to compute vertical motion. Our assumption of primarily first-baroclinic mode structure is consistent with the definition of the geostrophic streamfunction (Kim 1991), namely

$$\vec{V}_g = \frac{g^*}{f_o} \hat{k} \times \nabla z_{12} , \tag{8}$$

where we have used for $g^*(\equiv g\frac{\Delta \rho}{\rho})$ a value that is a weak function of $z_{12}$. The geostrophic baroclinic current from which we compute $\frac{\partial u}{\partial z}$ is valid at 400m, and is referenced to 3500m, where no motion is assumed.

4

To generate the field of vertical motion, the time tendency $\frac{\partial \zeta_g}{\partial t}|_{t=t_o}$ was estimated using a centered finite difference ($\frac{(\zeta_g(t_o+\Delta t)-\zeta_g(t_o-\Delta t))}{2\Delta t}$), with $\Delta t = 24$ hours. Vorticity advection was computed at time $t_o$ with horizontal derivatives computed using second-order centered finite-differencing. We have smoothed the IES streamfunction fields with three applications of a Shapiro second-order filter (Shapiro 1970) to reduce the amount of noise in the highly differentiated vertical motion field. Such smoothing reduces values of extrema in the resultant vertical motion field without changing their location. The filter wavelength cutoff is $-6$ $dB$ at $133$ $km$; features with lengthscales $= k^{-1} > 37$ $km$ are passed with greater than 80% amplitude. The gridded values of $w_{IES}$ were interpolated to each CM location so that direct comparisons could be made between $w_{CM}$ and $w_{IES}$.

The vertical motion as diagnosed by (7) is forced by two effects, the local change and the advective change ($\frac{\partial \zeta_g}{\partial t}$ and $\vec{V}_g \cdot \nabla(\zeta_g + f)$, respectively). Advection of vorticity causes vertical motion because, as explained in Holton (1979), the vertical motion is required to keep the ocean hydrostatic and geostrophic. Specifically, vertical motion acts to depress the thermocline (for the case of anticyclonic vorticity advection in which case a crest is approaching) or to raise the thermocline (for the case of cyclonic vorticity advection, associated with an approaching trough). If the vorticity *locally* is changing in a positive sense, *i.e.*, becoming more cyclonic with time, then we should expect downward motion: vorticity is most easily produced locally by convergence, which will be accompanied by downward motion. Note that if the advection at a point is cyclonic and the local tendency is positive (*i.e.*, becoming more cyclonic with time), the two effects compete. If the local tendency is exactly equal to the advective tendency, then there is no vertical motion (and, incidentally, the phase speed and the float parcel speed are equal). Normally, the advective term is larger; that is the case for 75% of the 23 cases considered here.

Finally, note that the mapped IES fields are a refined version of those described in Tracey and Watts (1991); in those fields, the first guess field (*i.e.*, the so-called "mean" field) was a broad diffuse Gulf Stream (see their Figure 6). The fields in Tracey and Watts (1991) contained measurable bias that could be traced to this first-guess mean field. The first-guess field used for this study is a 31-day running mean field produced from the data in Tracey and Watts. Because the first-guess field is closer to the actual field, the objectively analyzed fields are more accurate. A further refinement, that used pseudo-IES data from CM data to fill in gaps in the IES data, and for which IES $z_{12}$ data was recomputed to reflect new B-intercepts based on a different Q curve (see Watts and Rossby 1977 for definitions), has not been incorporated into this study.

## 3    Case Study Comparisons

To compare $w_{CM}$ with $w_{RAF}$, we selected those floats that passed within 10 $km$ of a mooring on which all of the top three CMs were functioning. The 10-$km$ cutoff was chosen as a compromise between increasing error (due to the highly sheared environment) as the distance increased from CM to float versus obtaining a useful number (23) of comparisons. The requirement that the three top CM functioned was to minimize error in this preliminary study: as previously noted, the vertical motion could be calculated using data at only 2 CM levels, but this introduces an error; furthermore, requiring the presence of three levels of data minimizes the error in the mooring motion correction algorithm. Note that the data are chosen based on the CM; these sites/times chosen may not have optimal IES coverage. We will note where this may cause errors.

We carefully scrutinized the CM data records to make certain that submesoscale coherent vortices (SCVs), as described in Bane *et al.* (1989), were not present when comparisons were made. Because SCVs typically affect only one CM on a mooring, causing up to a 360° rotation in the current vector as well as a temperature perturbation, their presence obviously would adversely impact this primarily quasi-geostrophic study. No evidence of obvious SCVs was found in any 5-day interval centered on the 23 closest-passing float cases studied here. It is possible, however, that there could be cases in which subtle submesoscale features partially detected in CM data and not easily identifiable as SCVs (and therefore present in $w_{CM}$) are filtered out of the objectively mapped IES streamfunction fields (and therefore not present in $w_{IES}$), *i.e.* submesoscale eddies could cause errors as shown in Panofsky(1951).

For each of the case studies that follow, several figures are presented. The track of the RAFOS float through the Central Array, as well as the pressure record of the float will be shown. Mapped fields of $w_{IES}$ will also be shown, as will mapped fields of $\frac{\partial \zeta_g}{\partial t}$ and $\vec{V}_g \cdot \nabla(\zeta_g + f)$, *i.e.*, the two components of $w_{IES}$. We will also show a figure of the terms contributing to $w_{CM}$.

## 3.1  Case 1: Float 123, CM H4, 4 July 1988, 0000 UTC

### 3.1.1  Overview

The time surrounding float 123's passage by CM H4 (Figure 1) is one during which a series of crests and troughs propagated steadily through the Central Array. This is reflected in the float's motion through several crests and troughs (made obvious by the large vertical excursions associated with changes in path curvature), in the IES $z_{12}$ topography (Figure 2a), which shows a crest (at $x = -100$) and a trough (at $x = 40$) in the Central Array, and in the CM records, which show a distinct oscillation in current direction and temperature (Figure 3a,b) caused by propagating features.

### 3.1.2  Vertical motion results

$w_{RAF} = -0.58$ mm s$^{-1}$ , $w_{IES} = -1.42$ mm s$^{-1}$ , $w_{CM} = -0.98$ mm s$^{-1}$

Float 123 moved from 532 to 550 to 565 db (Figure 1) for the three times closest to its pass by CM H4, a mean vertical motion of $-0.58$ mm s$^{-1}$ for those 16 hours. When float 123 was closest to CM H4, the CM data suggests that vigorous downwelling was occurring. Temperatures were increasing as isotherms descended (Figure 3b) in advance of the approaching crest (at $-1.13$ mm s$^{-1}$ ) concomitant with a slight veering in the currents with decreasing depth (Figure 3a) (suggesting weak warm advection and upward vertical motion of 0.15 mm s$^{-1}$ (Figure 3e)). Note that for this case, using the average of the temperature change at 400 and 1000m to estimate the temperature change at 700m yields an incorrect answer (Figure 3d,f). $w_{IES}$ for the same time (0000 UTC 4 July 1988) was $-1.00$ mm s$^{-1}$ . Based on advection alone (Figure 2d), vertical motion should be downward at 1.67 mm s$^{-1}$ ; strong anticyclonic vorticity advection forces the local vorticity to become more and more negative. Anticyclonic spin-up would be accompanied with downward motion to force down the thermocline. The local tendency at the H4, however, contributed to upward vertical motion (0.25 mm s$^{-1}$ ). Upward motion is forced by divergence, which destroys vorticity. This is an example of the advective part of the vorticity equation being counteracted by the local tendency.

6
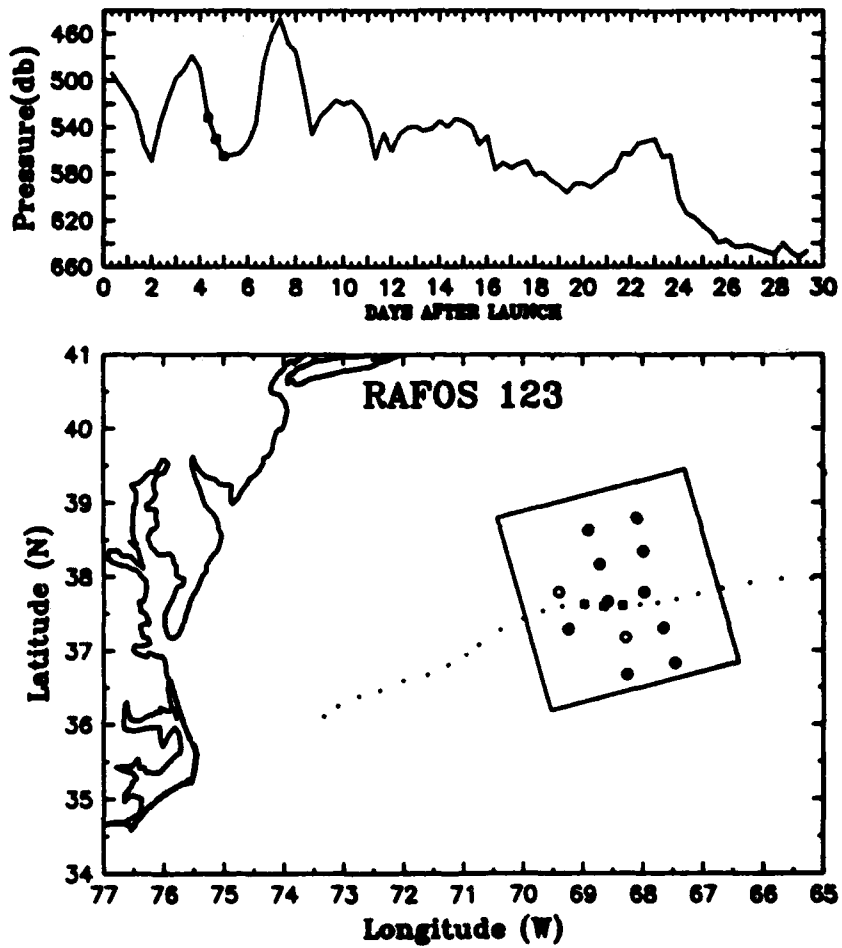
Figure 1: Pressure record in db (top) and horizontal track (bottom) – points after the first (launch) point are eight hours apart – of RAFOS float 123. CM locations within the Central Array are indicated by open circles. The three closest RAFOS fixes to CM H4 are boxed. Launch date of float: 1037 UTC, 29 June 1988.
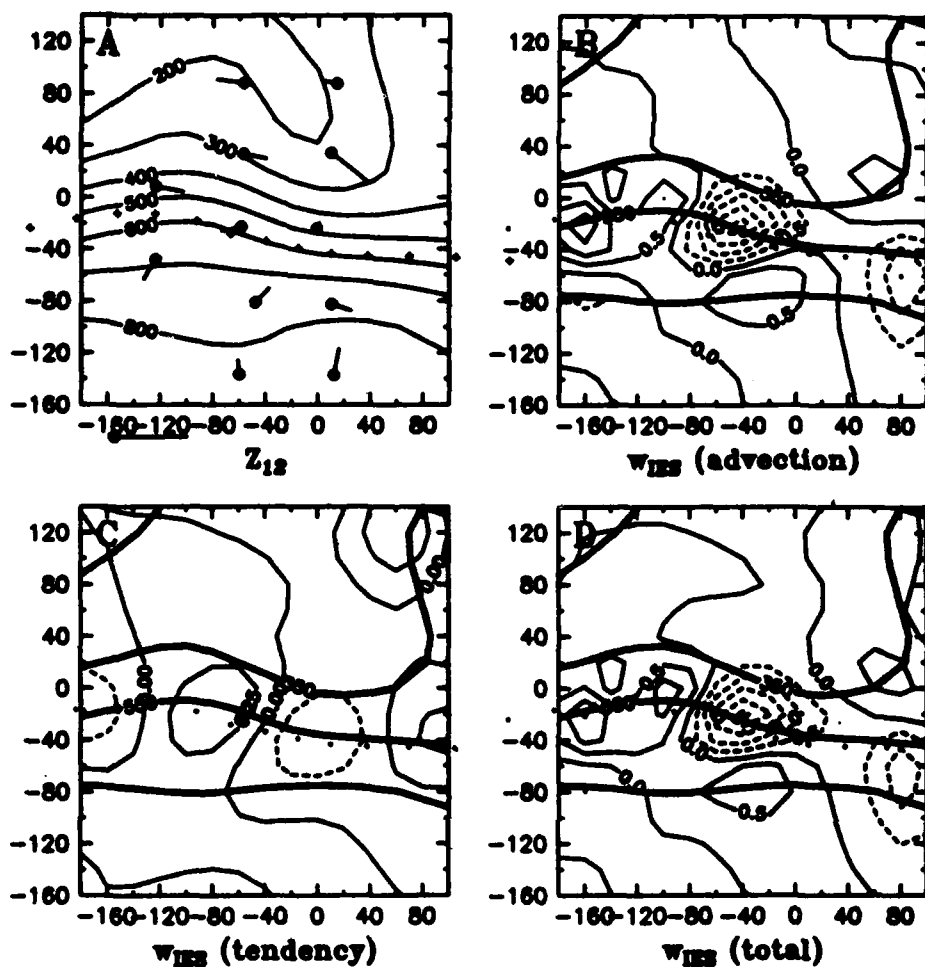
Figure 2: (A) Objectively mapped depth of 12° isotherm ($z_{12}$) as measured by IES data for 0000 UTC 4 July 1988, the time when float 123 was closest to CM H4. Contour interval every 100m. Also, deep current stick vectors plotted at CM locations, with a key (value = 0.25 m s$^{-1}$) plotted at $x = -155$, $y = -180$. (B) Objectively mapped $z_{12}$ topography (bold solid lines, contours at 150, 350, 550, 750, and 950 m) and portion of D forced by vorticity advection (thin solid lines, contour interval 0.50 mm s$^{-1}$, negative values dashed). (C) Objectively mapped $z_{12}$ topography (bold solid lines, contours at 150, 350, 550, 750, and 950m) and portion of D) forced by local vorticity tendency (thin lines, contour interval 0.25 mm s$^{-1}$, negative values dashed). (D) Objectively mapped $z_{12}$ topography (bold solid lines, contours at 150, 350, 550, 750, and 950m) and total vertical motion computed from (7) using IES data (thin lines, contour interval 0.5 mm s$^{-1}$, negative values dashed). For all four plots, the track of RAFOS float 123 is indicated by dots, and the location of CM H4 is marked by a circle.

8

100. ———— 400 m
90. —— · 700 m
80. ———— 1000 m

A

70.
60.  Direction

1 Jul          5 Jul
12 UTC        12 UTC

16.0          B
12.0
8.0   Temperature
4.0

1 Jul          5 Jul
12 UTC        12 UTC

1.60          C    ———— 400 m
1.20               —— · 700 m
0.80               ———— 1000 m
0.40  Speed
0.00

1 Jul          5 Jul
12 UTC        12 UTC

1.00          D

$T_{700}$ —0.00

avg. $T$ —−1.00  $W_{dT/dt}$

12 UTC        12 UTC

1.00          E    ———— $R^2$
                   ———— u dv/dz
0.00

−1.00  $W_{adv}$

12 UTC        12 UTC

1.00          F

$T_{700}$ —0.00

avg. $T$ —−1.00  $W_{total}$

12 UTC        12 UTC
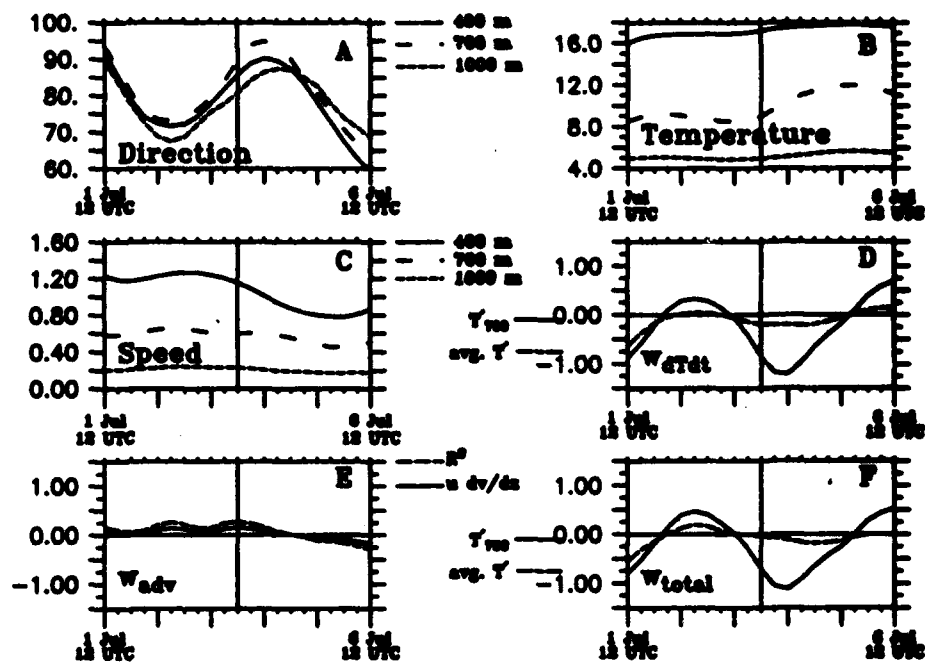
Figure 3: CM H4 data for 5 days surrounding float 123's closest approach to H4, which time is indicated by a vertical line. (A) Direction (in ° ) towards which the current is flowing (solid line: 400m; long dashed line: 700m; short dashed line: 1000m). (B) Temperature at CM site in degrees celsius (solid line: 400m; long dashed line: 700m; short dashed line: 1000m). (C) Current Speed in m s$^{-1}$(solid line: 400m; long dashed line: 700m; short dashed line: 1000m). (D) Vertical motion (in mm s$^{-1}$ ) forced by local temperature tendency (solid line: using the observed temperature tendency at 700m; dashed line: using the average of 400 and 1000 m temperature tendencies to estimate the 700m temperature tendency). (E) Vertical motion (in mm s$^{-1}$ ) forced by backing/veering current (dashed line: computed as in (4) using $v\frac{\partial u}{\partial z} - u\frac{\partial v}{\partial z}$; solid line: computed as in (5) using $R^2\frac{\partial \phi}{\partial z}$. (F) Total vertical motion in mm s$^{-1}$ , i.e. the sum of E (dashed line) and E (solid and dashed line as in D).

## 3.2 Case 2: Float 129, CM I4, 23 September 1988, 0800 – 1600 UTC

### 3.2.1 Overview

RAFOS float 129 spent considerable time in the Central Array (Figure 4). Although it entered moving steadily on an anticyclonically curved path, it then apparently escaped temporarily from the stream and moved only slowly before a meander trough moved through and started to steer the float again steadily to the northeast. The IES topography for the dates when the float was closest to CM I4 (Figures 5, 6) do show a considerable trough near the center of the Central Array. CM currents (Figure 7) are weak (less than 0.5 m s$^{-1}$). Temperatures are slowly increasing.



Figure 4: As in Figure 1, but for float 129. The four closest RAFOS fixes to CM I4 are boxed. Launch date: 0638 UTC, 31 August 1988.

### 3.2.2 Vertical motion results

$w_{RAF} = 0.19$ mm s$^{-1}$ , $w_{CM} = 0.53$ mm s$^{-1}$ , $w_{IES} = 0.04$ mm s$^{-1}$ (0800 UTC)

10
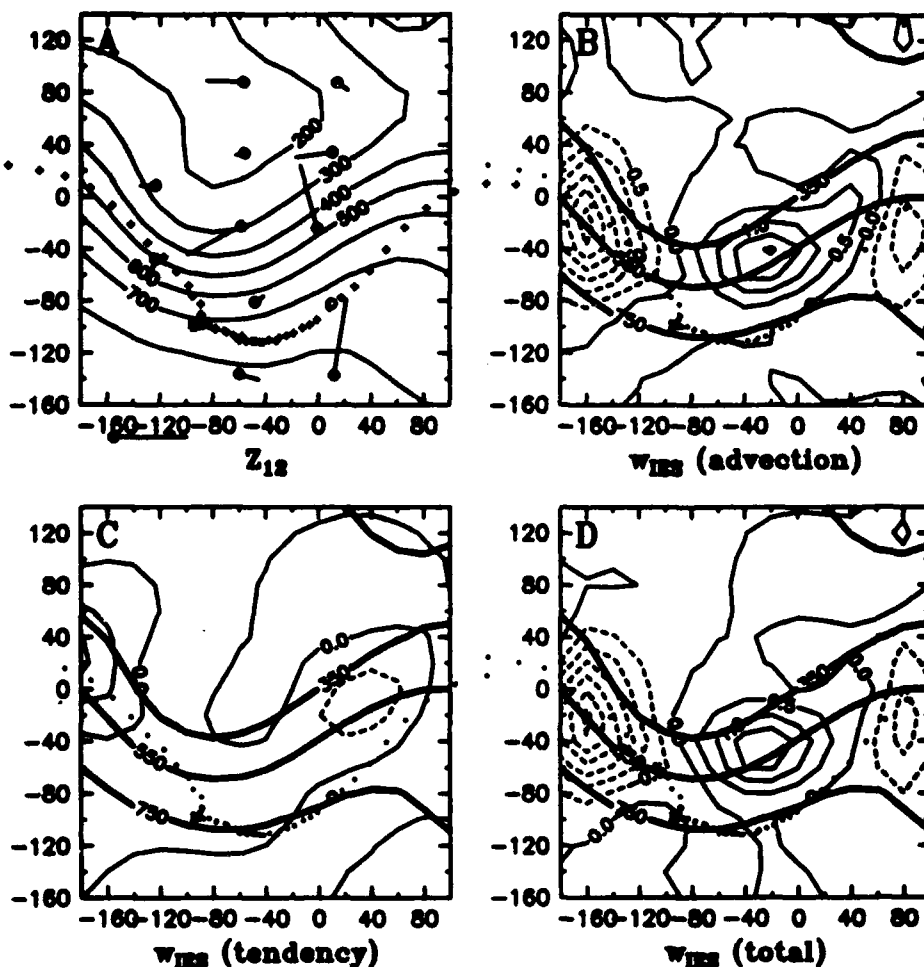
Figure 5: As in Figure 2, except for 0800 UTC 23 September 1988. The track of float 129 is indicated by dots, and the location of CM I4 is marked by a circle.
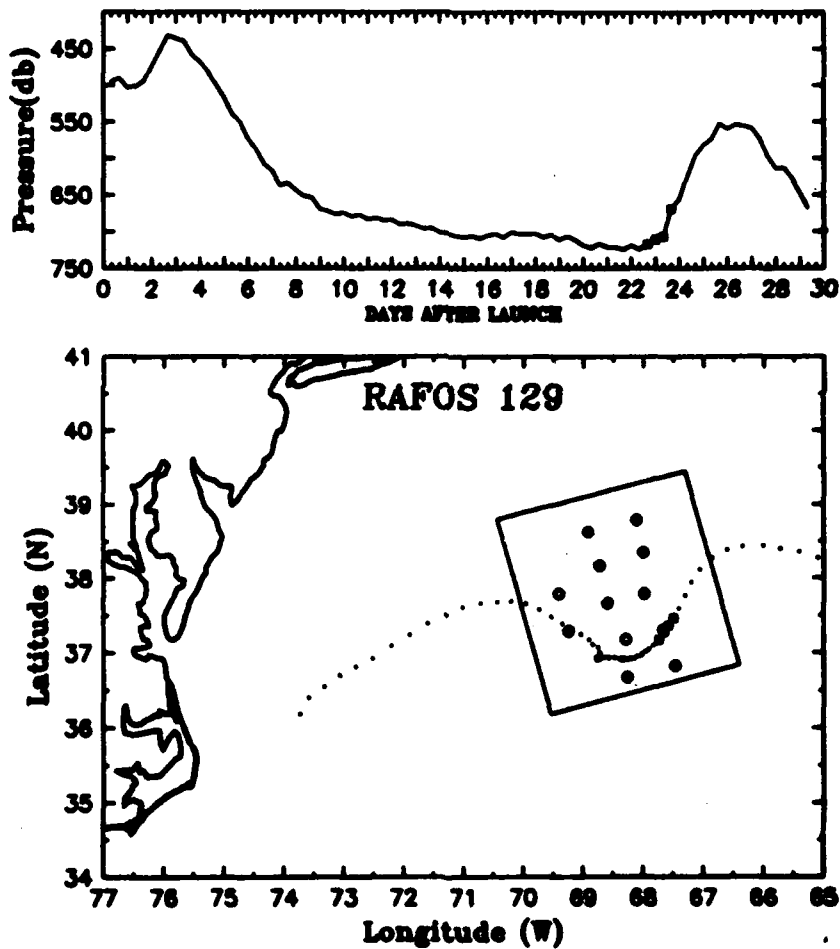
$$w_{RAF} = 0.72 \text{ mm s}^{-1} \text{ , } w_{CM} = 0.48 \text{ mm s}^{-1} \text{ , } w_{IES} = 0.05 \text{ mm s}^{-1} \text{ (1600 UTC)}$$

For the four closest float locations to CM I4 (Figure 4), the float upwelled from 717 to 711 to 706 to 669 db (between 00 UTC 23 Sep and 00 UTC 24 Sep); the two mean values of vertical motion are 0.19 and 0.72 mm s$^{-1}$. Clearly, the float is beginning to accelerate upwards as it moves out of its position at the base of a trough. CM data also suggest rising motion. Temperatures are cooling, suggesting that isotherms are rising (Figure 7d,e). At the same time, there is significant veering to the currents from which we can infer rising motion (Figure 7a-c). The vertical motion as estimated by the thermocline topography (IES data) is considerably smaller, about 0.04 mm s$^{-1}$ for both times (Figures 5,6). That part due to advection is nearly zero and the part due to local tendency is about 0.04 mm s$^{-1}$. We note, however, that a large area of ascent is located just to the north of I4.

11
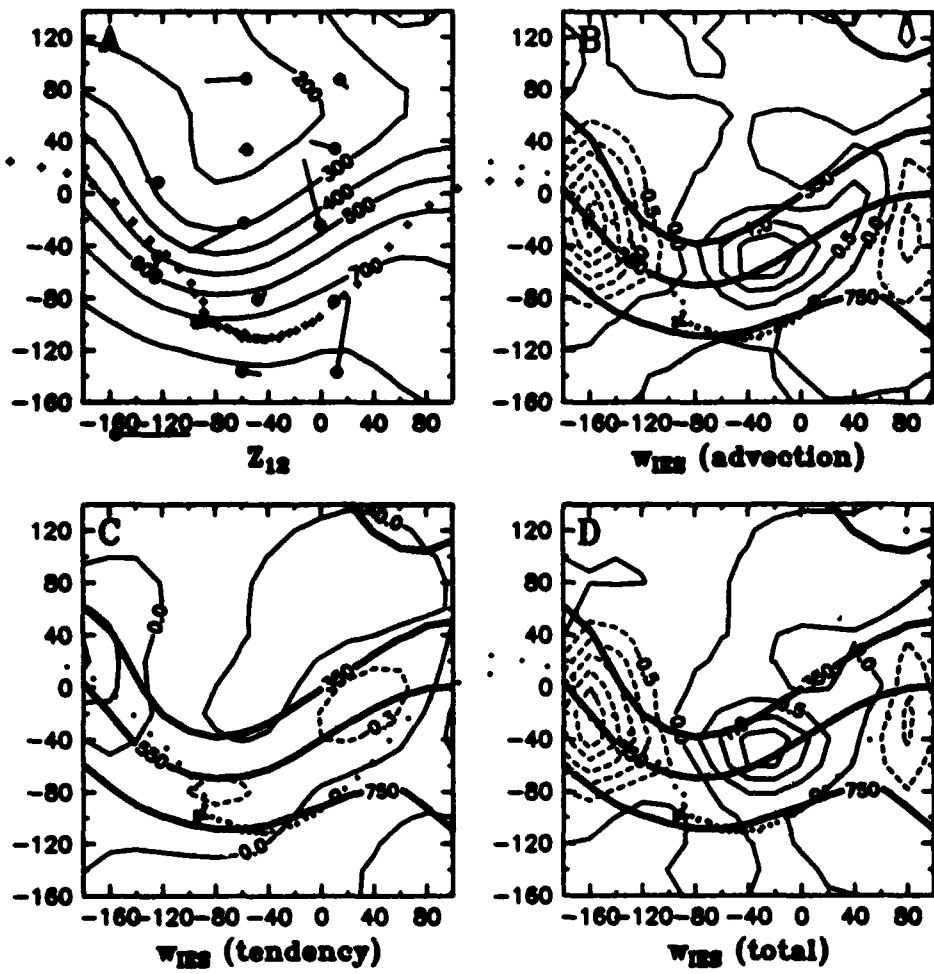
Figure 6: As in Figure 5, except for 1600 UTC 23 September 1988.

Figure 7: As in Figure 3, except for CM I4 for the five days surrounding float 129's closest approaches to I4, both of which times are indicated by vertical lines.

## 3.3 Case 3: Float 136, CM I4, 8 December 1988, 1600 UTC

### 3.3.1 Overview

The Gulf Stream in the period during which float 136 (Figure 8) moved through the Central Array was characterized by a succession of crests and meanders. Float 136 initially moved fairly slowly through the Central Array along the southern edge of the stream. Halfway through the array, however, the float accelerated to the northeast, apparently influenced by an approaching propagating trough (Figure 9).



Figure 8: As in Figure 1, but for float 136. The three closest RAFOS fixes to CM I4 are boxed. Launch date: 0921 UTC, 19 November 1988.

### 3.3.2 Vertical motion results

$w_{RAF} = 0.81$ mm s$^{-1}$ , $w_{CM} = 0.43$ mm s$^{-1}$ , $w_{IES} = 0.17$ mm s$^{-1}$

Float 136 moved from 669 to 668 to 622 db during the time it was closest to CM I4 (Figure 8), reflecting the acceleration up and northeastward out of a meander trough. CM data

14

Figure 9: As in Figure 2, except for 1600 UTC 8 December 1988. The track of float 136 is indicated by dots, and the location of CM I4 is marked by a circle.

at the same time show currents that are veering with decreasing depth, suggesting upward motion (Figure 10a,c,e). At the same time, CM temperatures are steady (Figure 10b); the majority of vertical motion diagnosed from CM data is related to the change of the current vector with height. Vertical motion determined from IES data shows weak upward motion forced by vorticity advection (Figure 9b), and weaker still downward motion related to the vorticity tendency (Figure 9c); the net motion (Figure 10d) is upward.
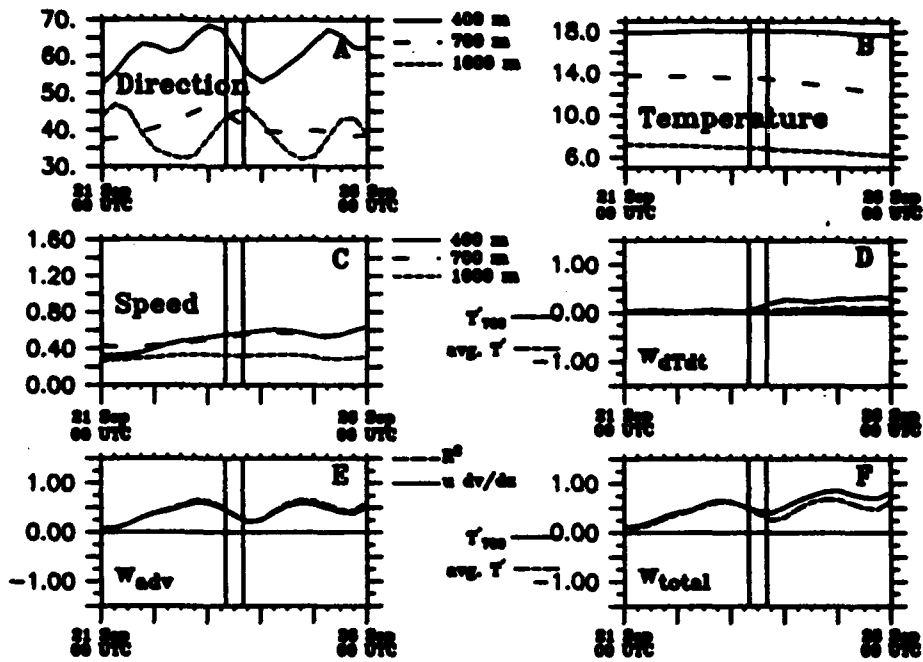
Figure 10: As in Figure 3, except for CM I4 for the five days surrounding float 136's closest approaches to I4, which time is indicated by vertical line.

## 3.4 Case 4: Float 141, CM I4, 2 November 1988, 1600 UTC

### 3.4.1 Overview

RAFOS float 141 (Figure 11) moved steadily through the Central Array at a time during which flow was from the northwest to the southeast, suggesting a large ridge upstream of the Central Array. However, there are wiggles in the float path suggesting smaller-scale crests and troughs are propagating through the larger-scale ridge, and this view is confirmed by the IES $z_{12}$ topography (Figure 12).
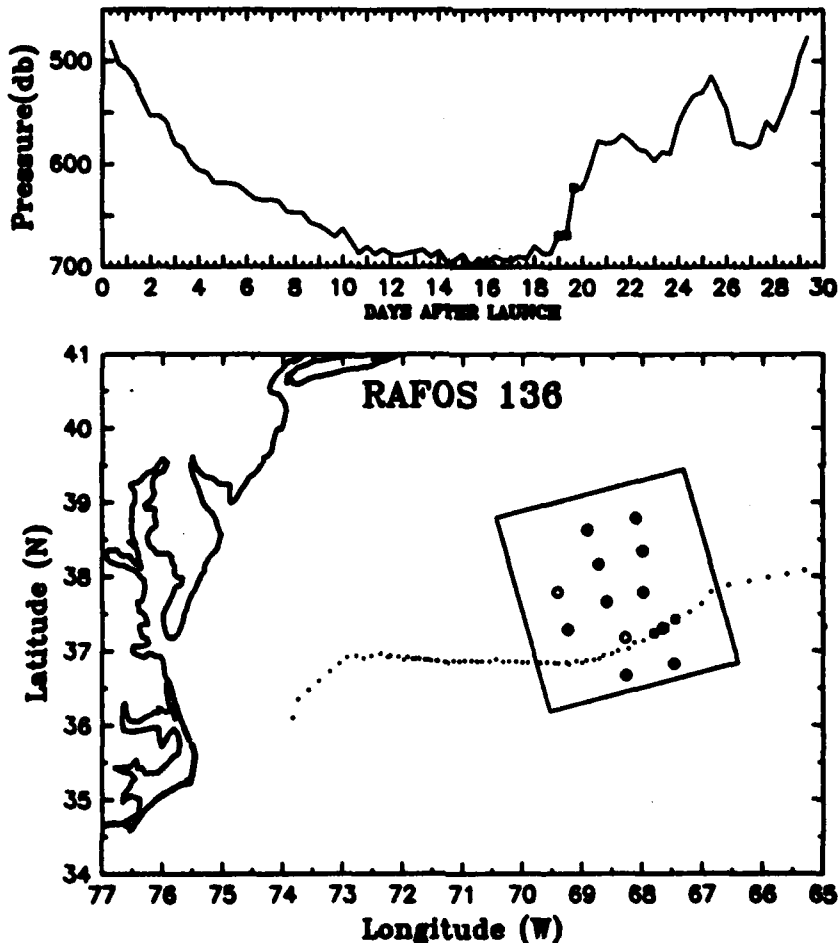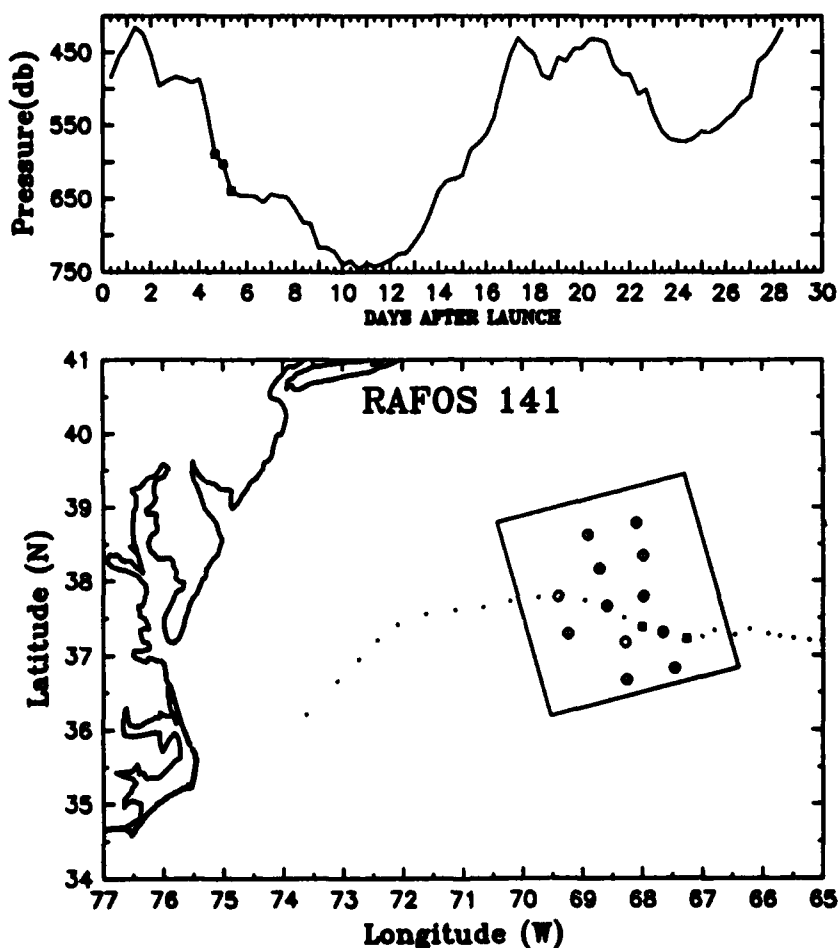


Figure 11: As in Figure 1, but for float 141. The three closest RAFOS fixes to CM I4 are boxed. Launch date: 0921 UTC, 28 October 1988.

### 3.4.2 Vertical motion results

$w_{RAF} = -0.87$ mm s$^{-1}$ , $w_{CM} = -0.94$ mm s$^{-1}$ , $w_{IES} = -0.43$ mm s$^{-1}$.

RAFOS float 141 downwelled from 589 to 603 to 639 db (Figure 11) in the period closest to CM I4, which is a mean motion of $-.87$ mm s$^{-1}$ . CM data for the time of closest ap-
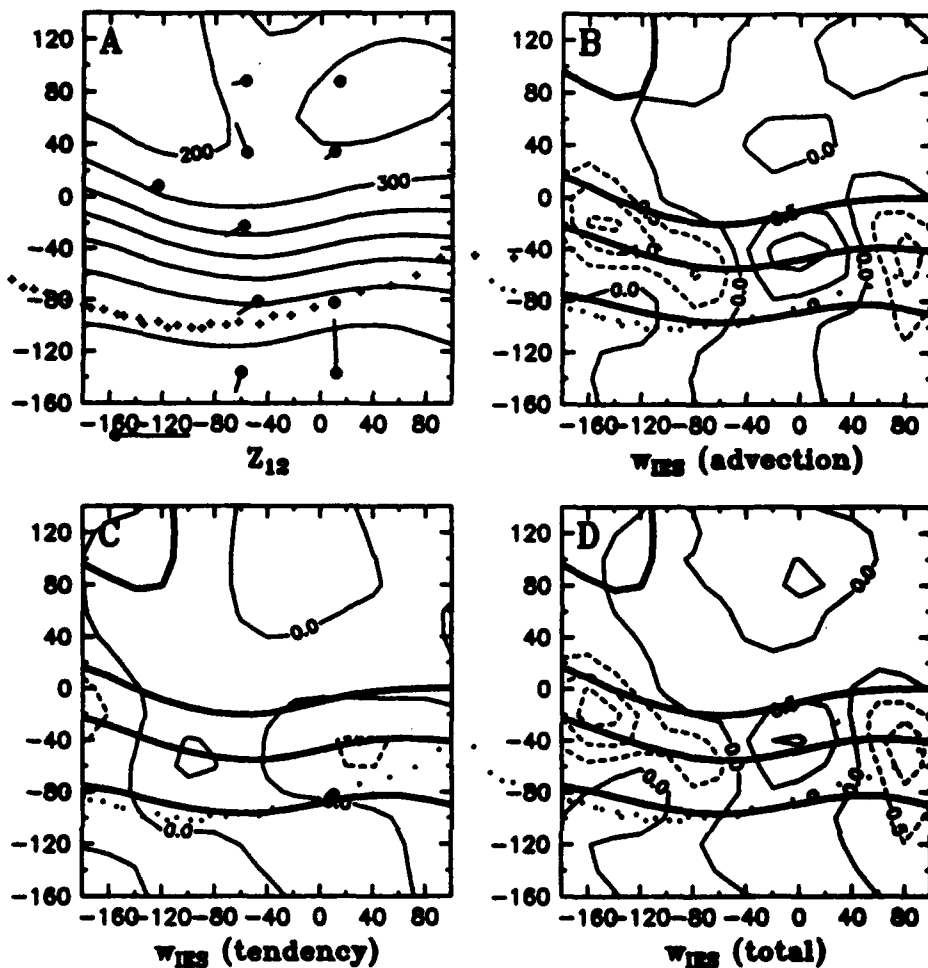
17

Figure 12: As in Figure 2, except for 1600 UTC 2 November 1988. The track of float 141 is indicated by dots, and the location of CM I4 is marked by a circle.

proach also suggests downwelling; although the currents are veering, suggesting upwelling (Figures 13a,c,e), temperatures are warming rapidly enough that the accompanying down-welling dominates (Figures 13b,d,f). Note that here, again, using the average of 400 and 1000 temperature tendencies to predict the tendency at 700 m leads to an underprediction of the magnitude of the vertical motion caused by the local temperature tendency, and hence a sign error in the resultant total vertical motion (Figures 13d,f). IES data shows that CM I4 is downstream of a crest; anticyclonic vorticity advection associated with this crest is forcing downward motion (Figure 12).
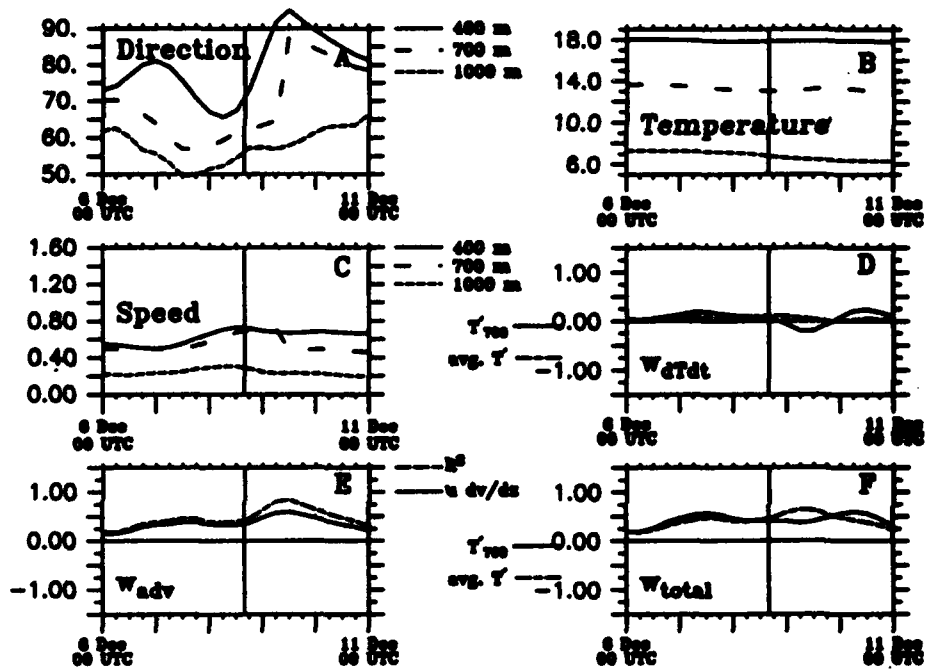
Figure 13: As in Figure 3, except for CM I4 for the five days surrounding float 141's closest approaches to I4, which time is indicated by vertical line.

## 3.5    Case 5: Float 175, CM I4, 20 January 1989, 1600 UTC

### 3.5.1    Overview

As was the case for float 141, RAFOS float 175 traversed the Central Array moving from northeast to southwest on a track consistent with an upstream crest (Figure 14). There were wiggles in the track that suggest smaller scale features propagating through the larger scale crest. This is confirmed by the map of $z_{12}$ (Figure 15).

Figure 14: As in Figure 1, but for float 175. The three closest RAFOS fixes to CM I4 are boxed. Launch date: 1005 UTC, 14 January 1989.

### 3.5.2    Vertical motion results

$w_{RAF} = -0.56$ mm s$^{-1}$ , $w_{CM} = -0.05$ mm s$^{-1}$ , $w_{IES} = -0.63$ mm s$^{-1}$

RAFOS float 175 moved in the vertical from 328 to 364 to 361 db during the time when it was closest to CM I4 (Figure 14), a mean downwelling of $-0.56$ mm s$^{-1}$ . Note that the float is near the bottom of a trough and is about to commence upwelling downstream of it.
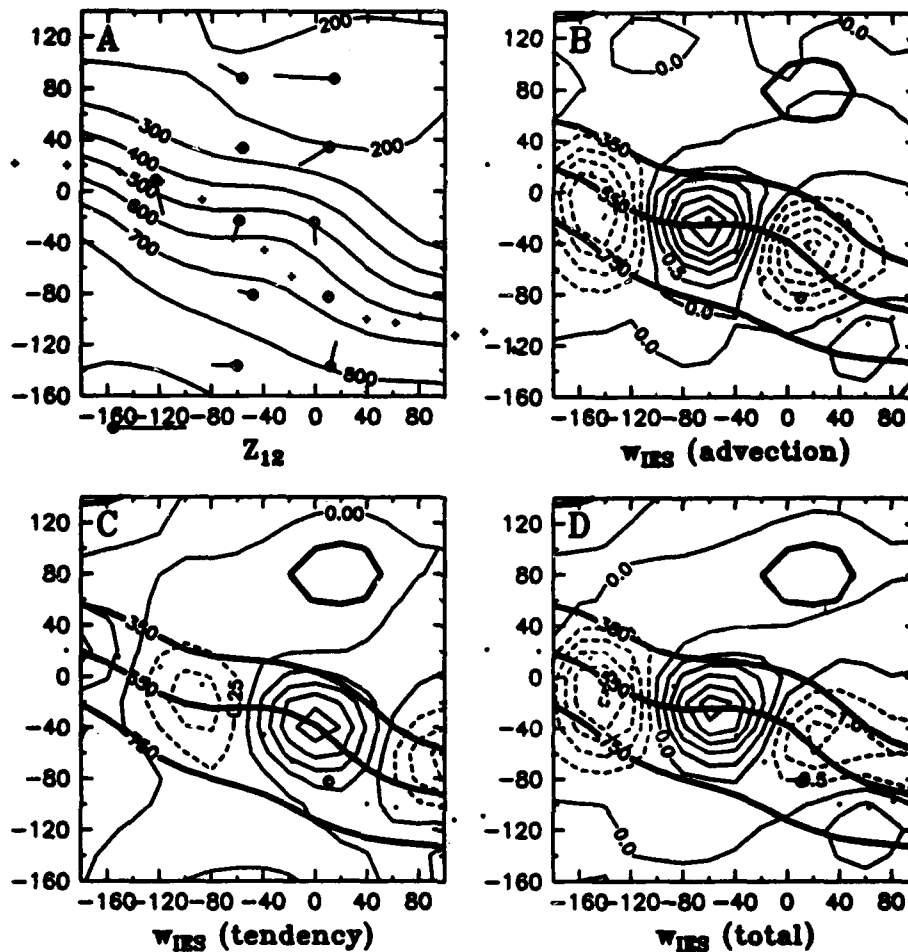
20

Figure 15: As in Figure 2, except for 1600 UTC 21 January 1989. The track of float 175 is indicated by dots, and the location of CM I4 is marked by a circle.

CM vertical motion is also flipping sign (Figure 16) as the float passes by I4, reflecting the propagation of the meander crest. Vertical motion is still slightly downward, however, as measured by the CM when the float is close by. Vertical motion as diagnosed by vertical stretching data at 400 m is also downward; CM I4 is downstream of a crest (Figure 15).
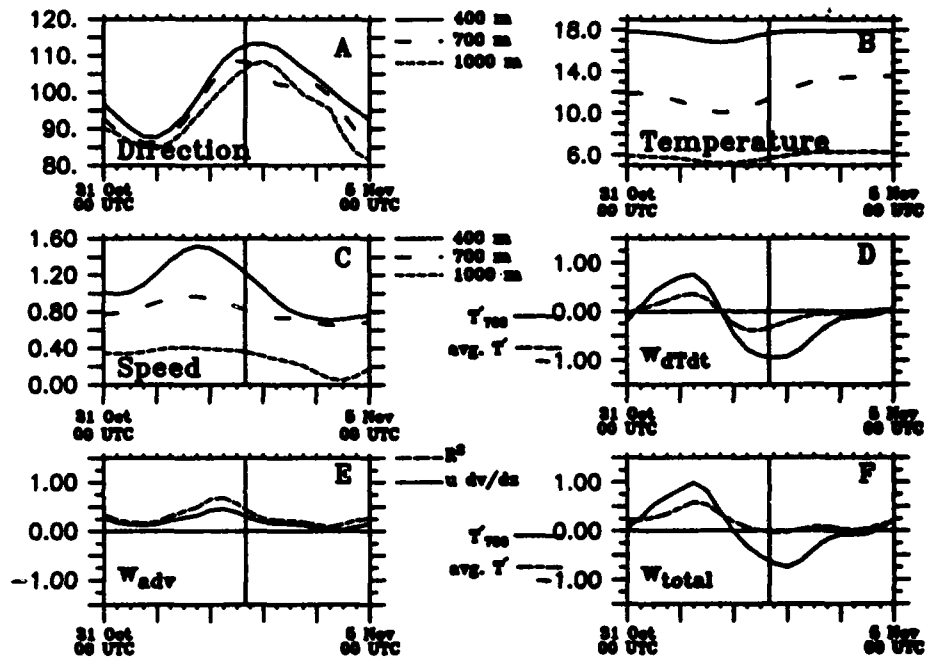
Figure 16: As in Figure 3, except for CM I4 for the five days surrounding float 175's closest approaches to I4, which time is indicated by vertical line.

## 3.6 Case 6: Float 176, CM I5, 7 February 1989, 0000 UTC – 8 February 1989, 0000 UTC

### 3.6.1 Overview

Float 176 moved slowly through the Central Array at first (Figure 17), tracing out an anticyclonic path, before being expelled from the stream, after which time it drifted very slowly southward. IES data (Figures 18- 21) show the crest on the eastern edge of the Central Array, and also suggests a sharp southern edge to the stream: float 176 is moving very slowly in a region that is close to the main part of the Gulf Stream.
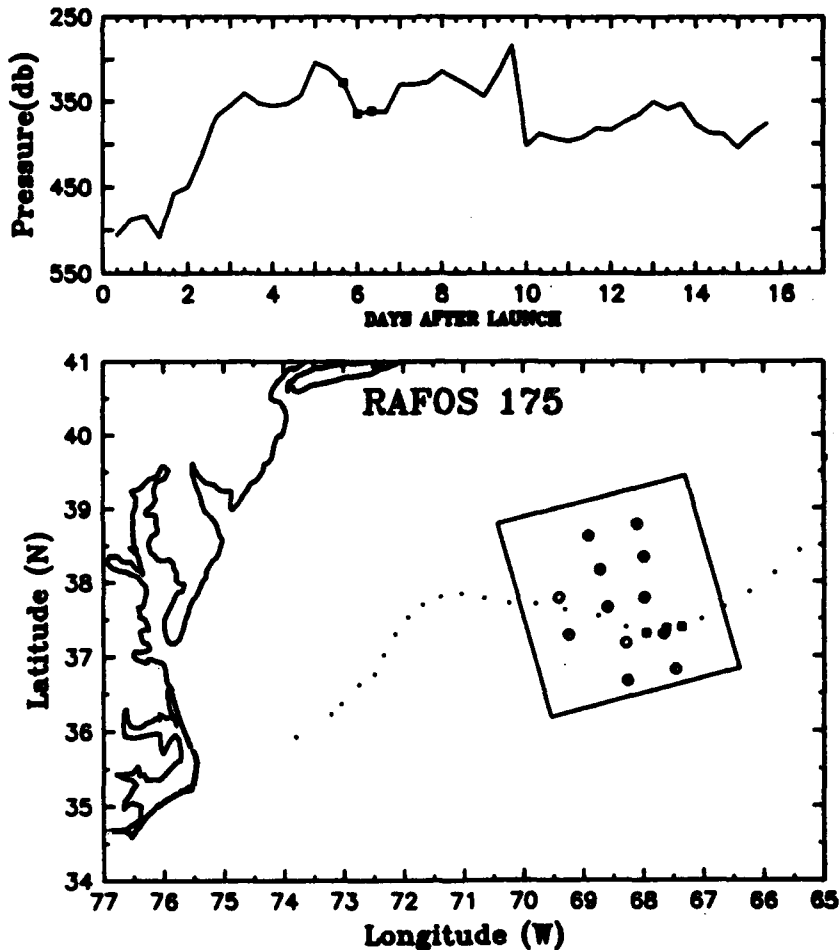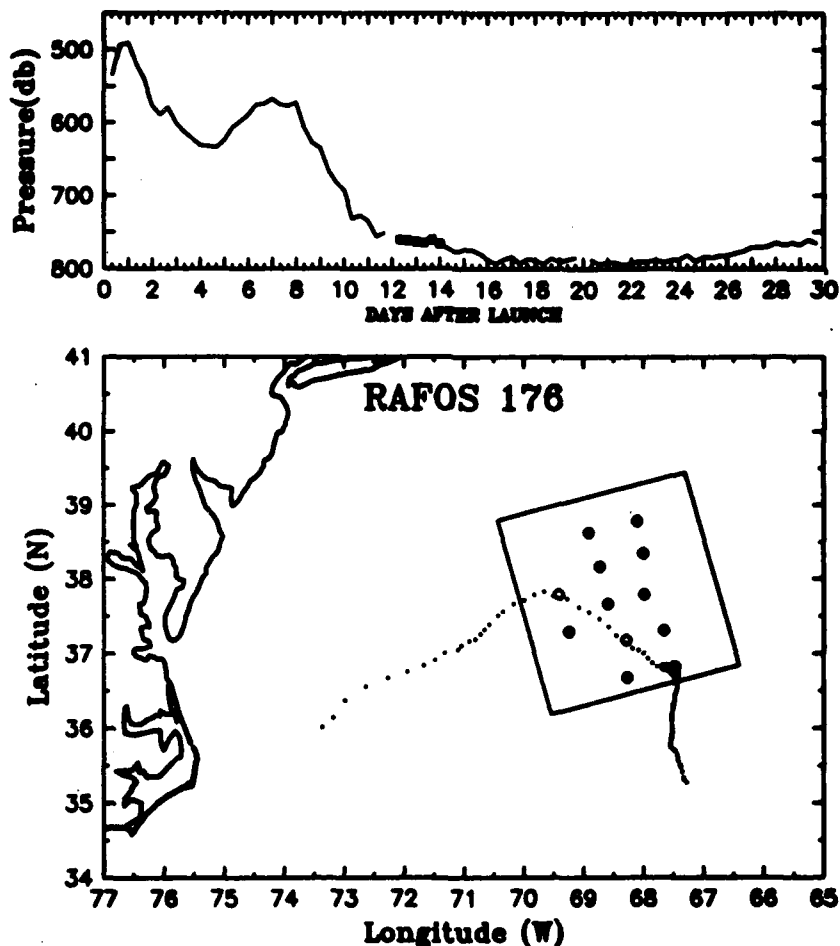


Figure 17: As in Figure 1, but for float 176. The seven closest RAFOS fixes to CM I5 are boxed. Launch date: 1131 UTC, 25 January 1989.

### 3.6.2 Vertical motion results

$w_{RAF} = -0.04$ mm s$^{-1}$ , $w_{CM} = 0.02$ mm s$^{-1}$ , $w_{IES} = 0.25$ mm s$^{-1}$ (0000 UTC 7 February)
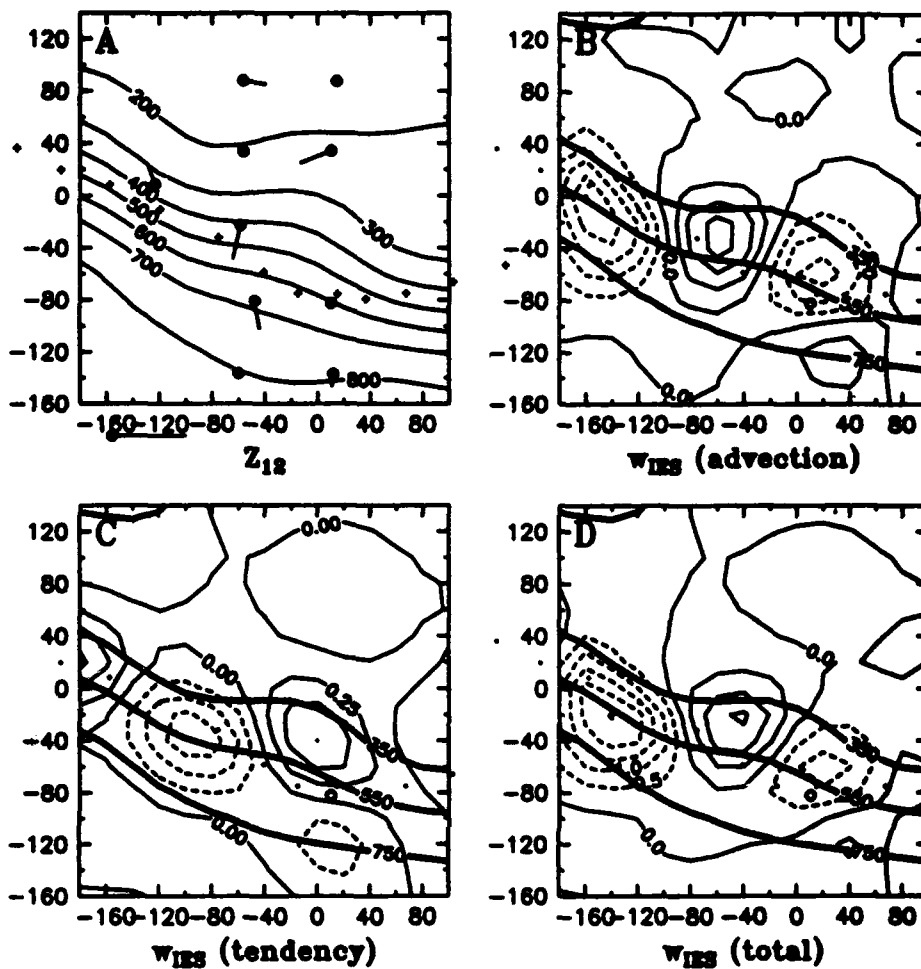
23
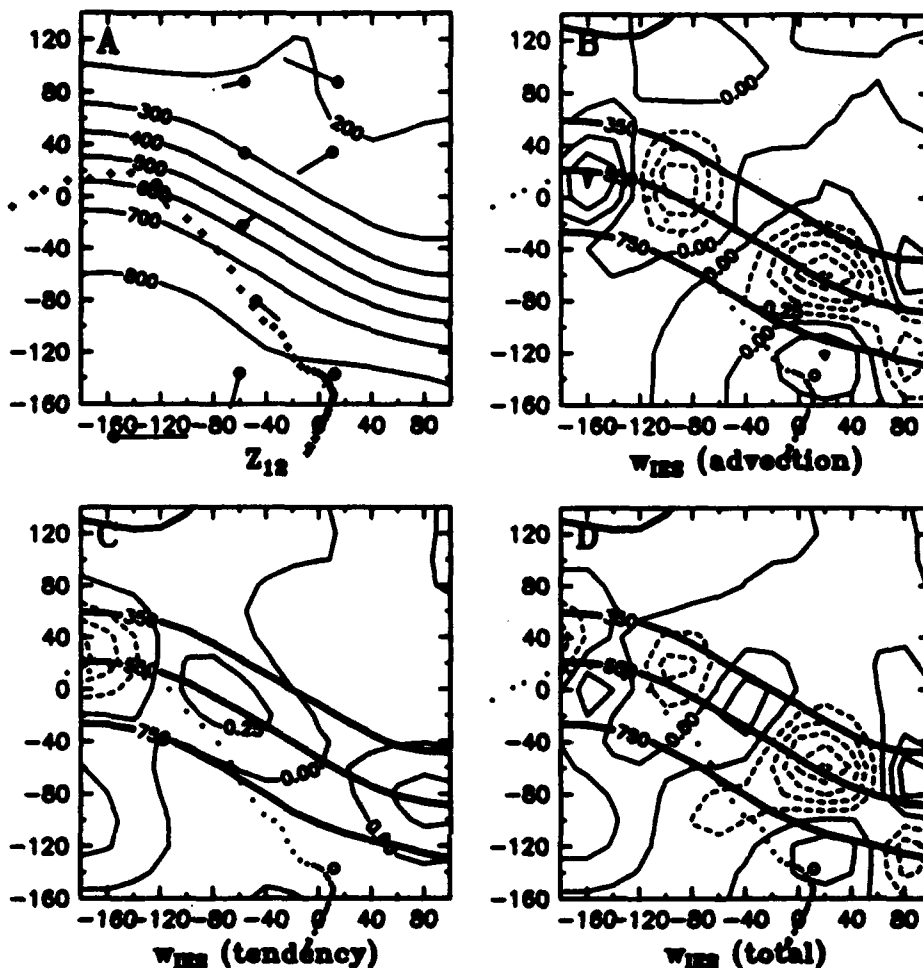
Figure 18: As in Figure 2, except for 0800 UTC 7 February 1989. The track of float 176 is indicated by dots, and the location of CM I5 is marked by a circle.

$w_{RAF} = -0.05$ mm s$^{-1}$ , $w_{CM} = 0.03$ mm s$^{-1}$ , $w_{IES} = 0.26$ mm s$^{-1}$ (0800 UTC 7 February)

$w_{RAF} = 0.04$ mm s$^{-1}$ , $w_{CM} = 0.02$ mm s$^{-1}$ , $w_{IES} = 0.27$ mm s$^{-1}$ (1600 UTC 7 February)

$w_{RAF} = -0.03$ mm s$^{-1}$ , $w_{CM} = -0.05$ mm s$^{-1}$ , $w_{IES} = 0.26$ mm s$^{-1}$ (0000 UTC 8 February)

As the RAFOS float drifts southward in the vicinity of CM I5 (it remains within 10 km of I5 for a day), it stays between 761 and 766 db (Figure 17), so vertical motion is negligible. In addition, CM data diagnoses small vertical motion (Figure 22); there is veering and backing of currents, but the currents are extremely weak. Similarly, local temperature changes are very small. IES data (Figures 18- 21), however, diagnoses upward vertical motion forced by cyclonic vorticity advection (local tendency of vorticity is near zero). $w_{IES}$ is nearly 0.25 mm s$^{-1}$ for the daylong period when the float is close to I5; however, I5 is near the edge of the IES mapping region, and the derivatives required to compute vorticity and its advection

24

Figure 19: As in Figure 18, except for 1600 UTC 7 February 1989.

may not be accurate.
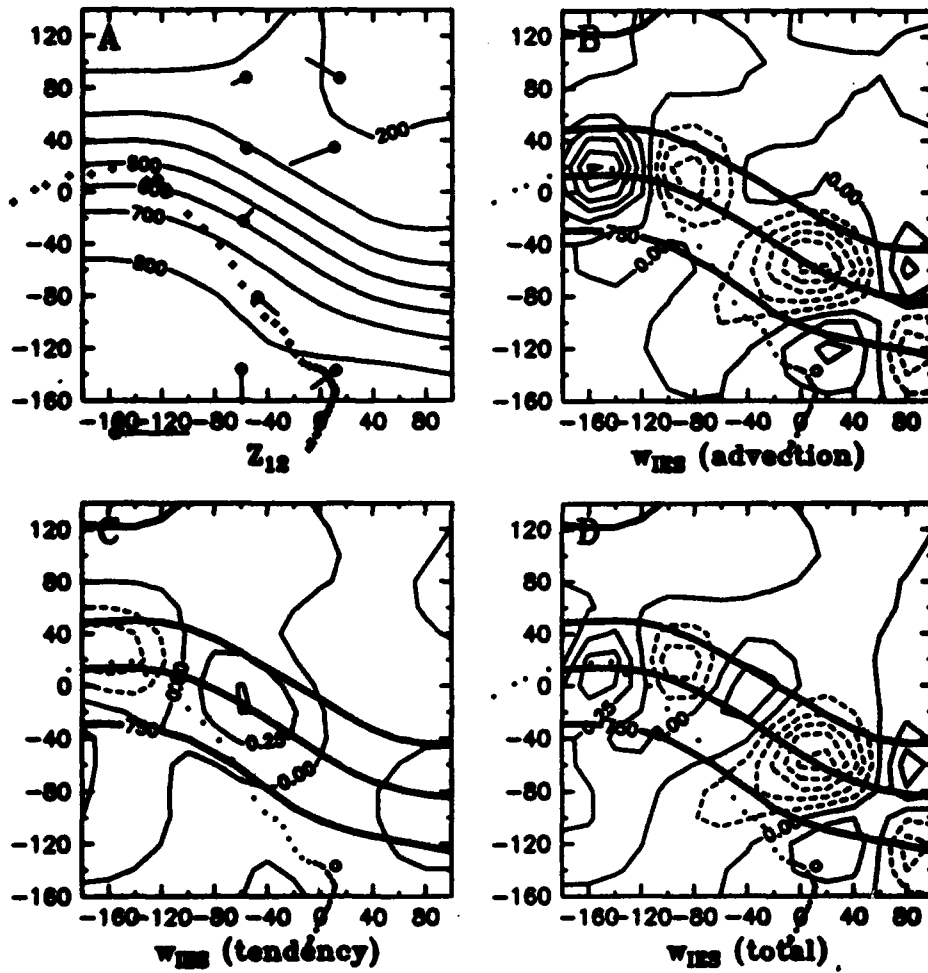
Figure 20: As in Figure 18, except for 0000 UTC 8 February 1989.

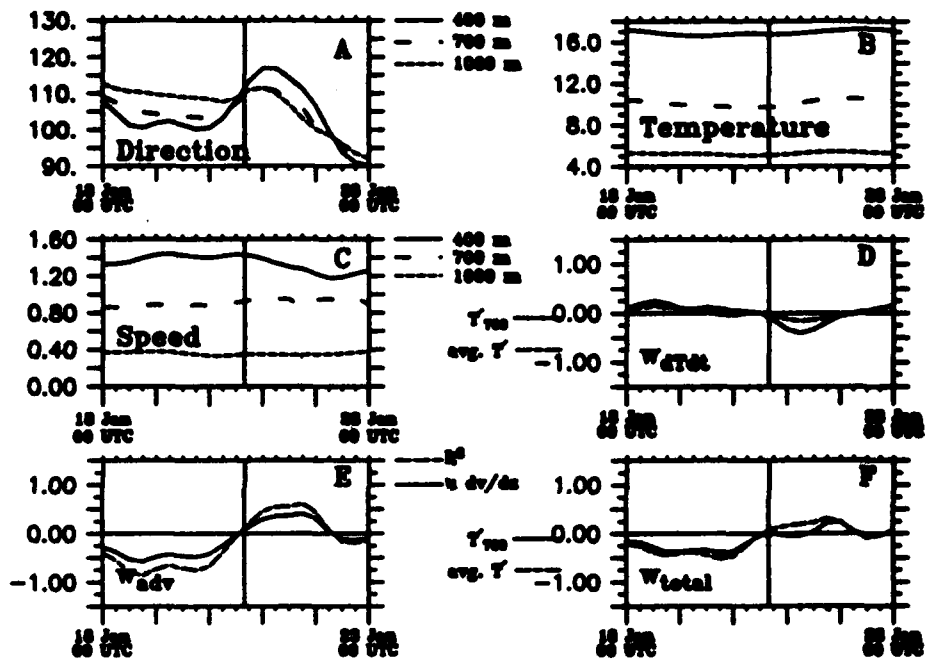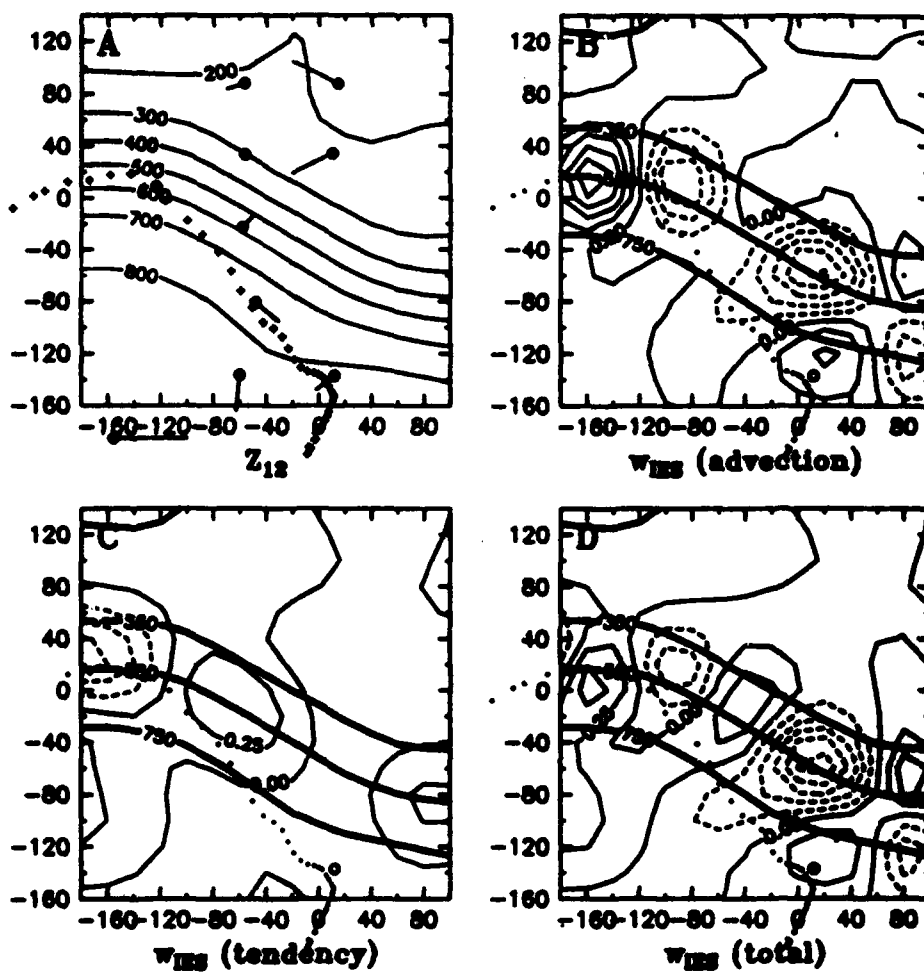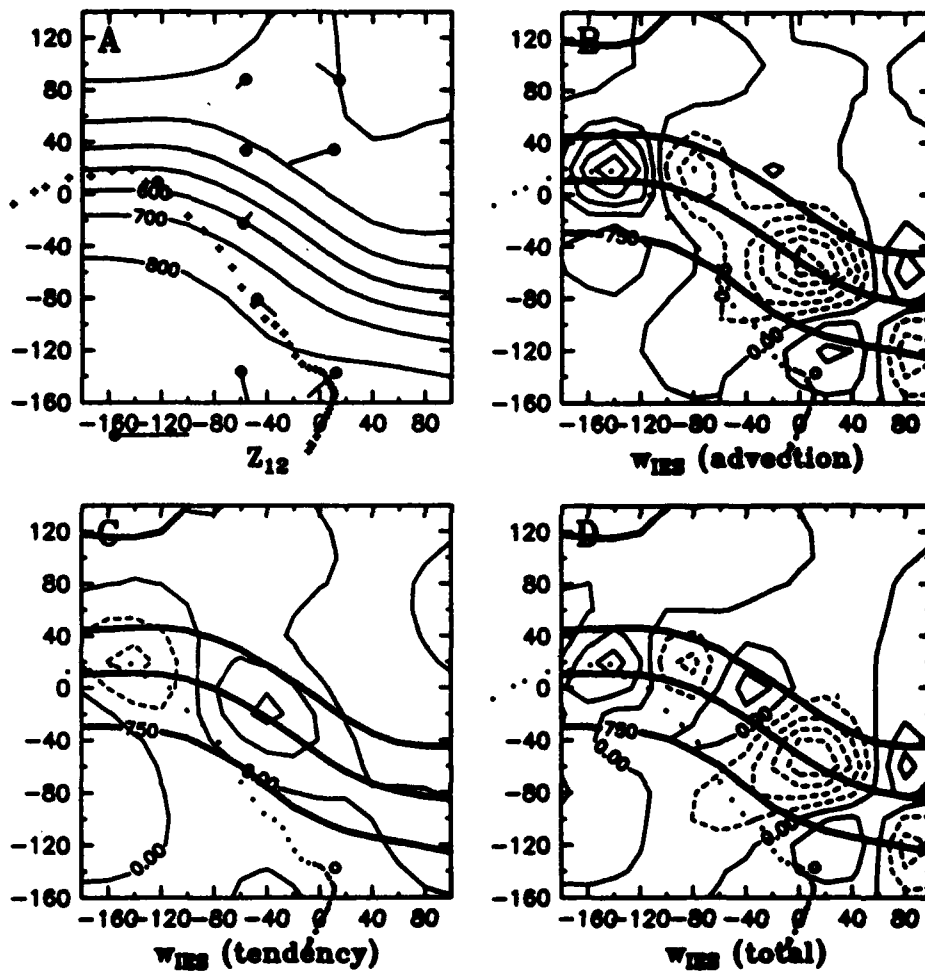Figure 21: As in Figure 18, except for 0800 UTC 8 February 1989.

Figure 22: As in Figure 3, except for CM I5 for the five days surrounding float 176's closest approaches to I5, which times are indicated by vertical lines.

## 3.7 Case 7: Float 194, CM I5, 15 November 1989, 0000 UTC

### 3.7.1 Overview

RAFOS float 194 moved through the central array during a time of significant stream-ring interaction. This is reflected in its unusual south-to-north path through the array (Figure 23), moving around a cyclonic cold eddy in the southern part of the domain, and around a crest in the northern part of the domain (Figure 24).



Figure 23: As in Figure 1, but for float 194. The three closest RAFOS fixes to CM I5 are boxed. Launch date: 1843 UTC, 5 November 1989.

### 3.7.2 Vertical motion results

$w_{RAF} = 0.71$ mm s$^{-1}$ , $w_{CM} = 0.23$ mm s$^{-1}$ , $w_{IES} = -0.22$ mm s$^{-1}$

As float 194 moved around the cold eddy past I5, it upwelled from 663 to 662 to 622 db (Figure 23), a mean value of .71 mm s$^{-1}$ . This is just as expected from the work of Bower(1989); the float has emerged from a trough and is moving towards a crest. The path

29

Figure 24: As in Figure 2, except for 0000 UTC 15 November 1989. The track of float 194 is indicated by dots, and the location of CM I5 is marked by a circle.

is more convoluted than normal, however. CM data at the same time at I5 also suggest upwelling (Figure 25): Currents are veering, and temperatures are cooling slightly. Both of these will force upward vertical motion. IES data (Figure 24) for this time, however, suggests downward motion. Both vorticity advection and local tendency are forcing downward motion. A possible cause for the discrepancy in diagnosed vertical motion is discussed in the next section.
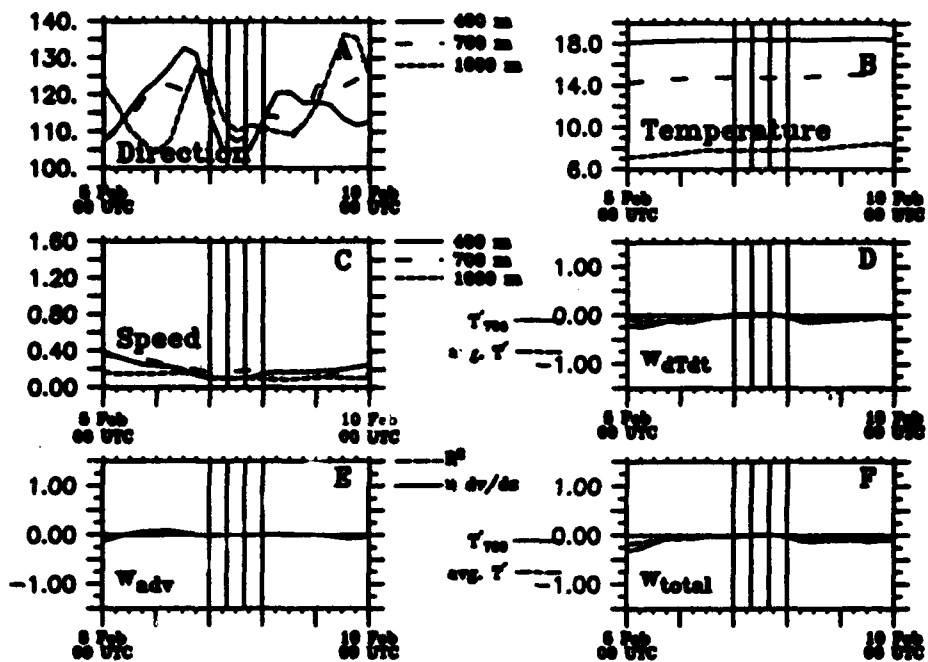
Figure 25: As in Figure 3, except for CM I5 for the five days surrounding float 194's closest approaches to I5, which time is indicated by vertical line.

31

## 3.8 Case 8: Float 194, CM I4, 16 November 1989, 0000 UTC

### 3.8.1 Overview

RAFOS float 194's unusual path (Figure 26) south to north from ring to crest (Figure 27) is described in Section 3.7.
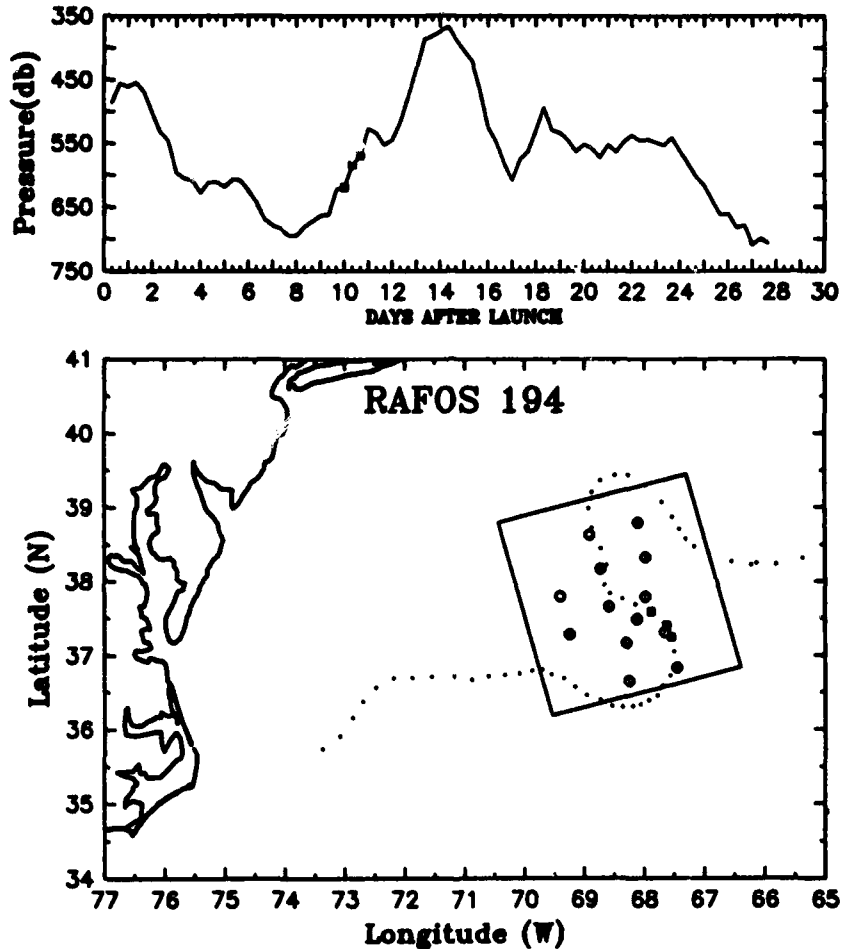

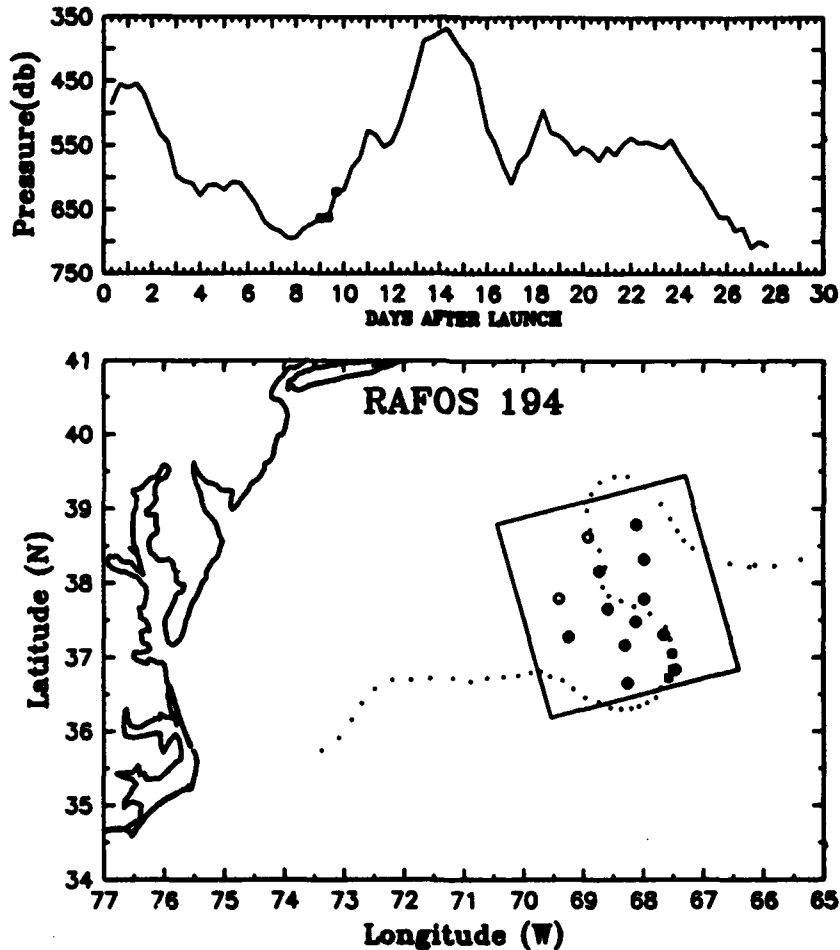
Figure 26: As in Figure 23. The three closest RAFOS fixes to CM I4 are boxed. Launch date: 1843 UTC, 5 November 1989.

### 3.8.2 Vertical motion results

$w_{RAF} = 0.86$ mm s$^{-1}$ , $w_{CM} = 1.20$ mm s$^{-1}$ , $w_{IES} = -1.06$ mm s$^{-1}$

Float 194 continued upwelling as it passed CM I4, moving from 619 to 584 to 570 db (Figure 26). This is a mean upwelling of 0.86 mm s$^{-1}$ . CM data at I4 also diagnosed upward motion (Figure 28), forced mostly by strong cooling observed at the current meter site (Figure 28b,d). Vertical motion caused by currents veering with height is smaller in size. In contrast to the upwelling measured by the float and diagnosed by the CM, IES data
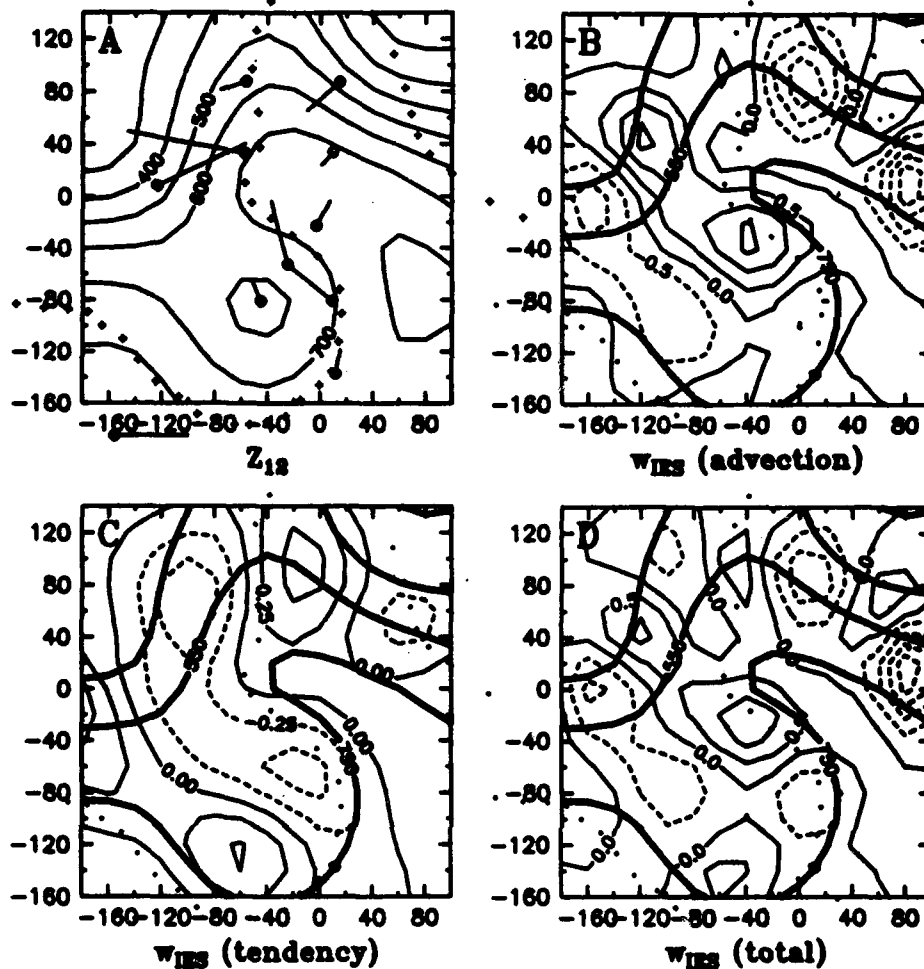
32

Figure 27: As in Figure 24, except for 0000 UTC 16 November 1989. The track of float 194 is indicated by dots, and the location of CM I4 is marked by a circle.

(Figure 27) suggests downwelling. Weak downwelling is being forced by vorticity advection, supplementing the stronger downwelling forced by the local change in the vorticity. This considerable disagreement between $w_{IES}$ and the other two methods is discussed in the next section.
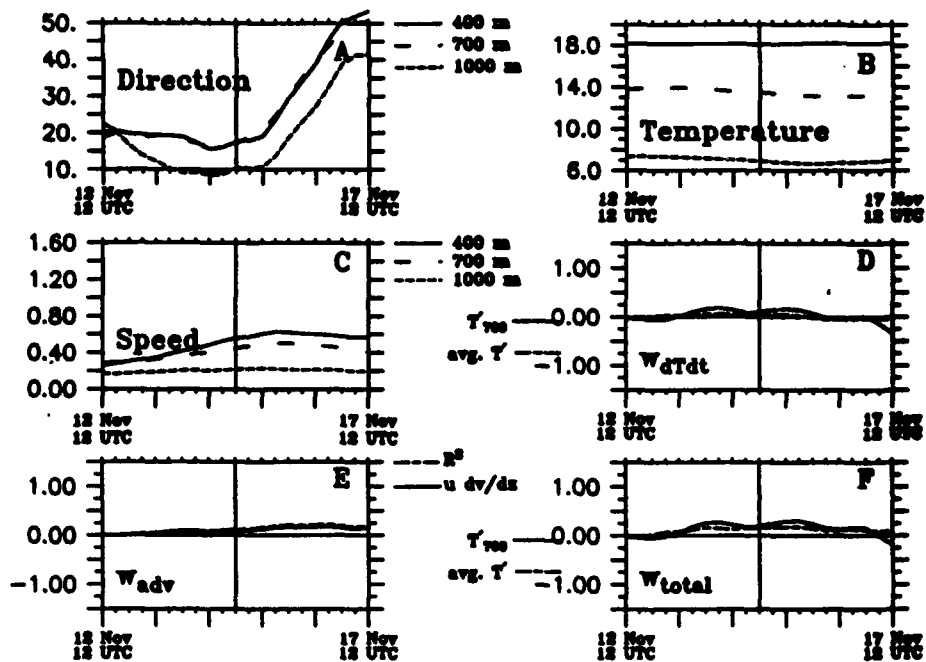
Figure 28: As in Figure 3, except for CM I4 for the five days surrounding float 194's closest approaches to I4, which time is indicated by vertical line.

## 3.9 Case 9: Float 199, CM I5, 23 November 1989, 0000 UTC

### 3.9.1 Overview

The circuitous path that RAFOS float 199 (Figure 29) took through the Central Array was unique for SYNOP floats. The thermocline topography (Figure 30) shows two distinct features: an east-to-west Gulf Stream to the north of a cyclonic cold eddy. Float 199 left the stream and was entrained into the cold eddy, circling three times before being expelled.
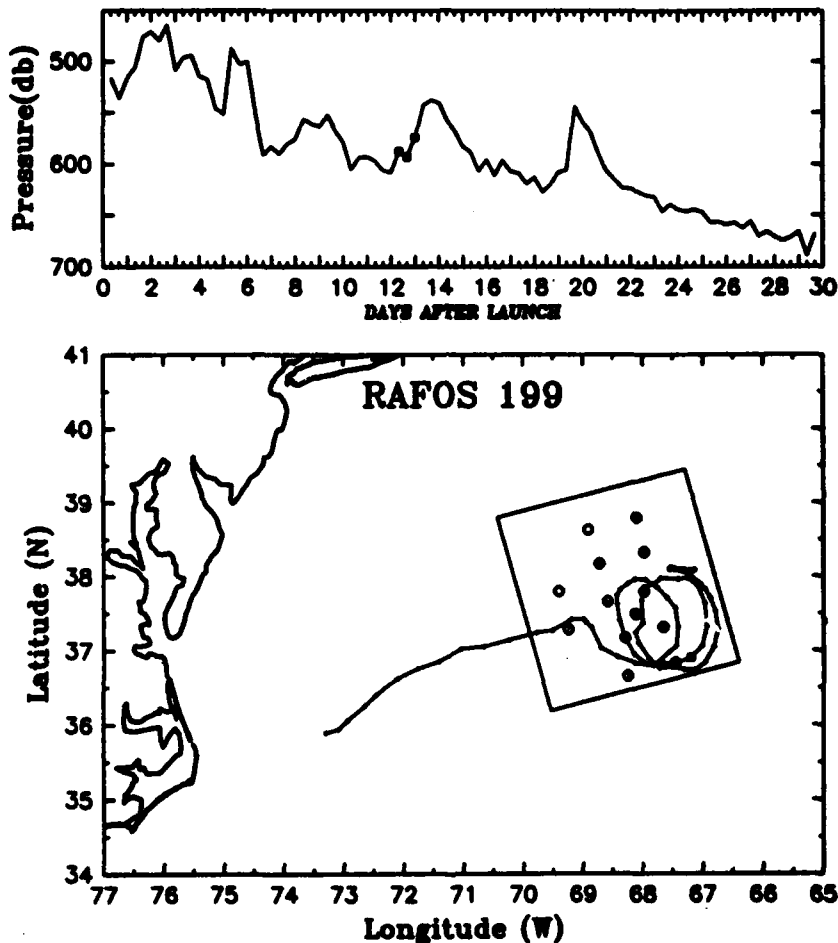


Figure 29: As in Figure 1, but for float 199. The three closest RAFOS fixes to CM I5 (first approach) are boxed. Launch date: 1258 UTC, 10 November 1989.

### 3.9.2 Vertical motion results

$w_{RAF} = 0.24$ mm s$^{-1}$ , $w_{CM} = 0.23$ mm s$^{-1}$ , $w_{IES} = -0.13$ mm s$^{-1}$

As float 199 circled the cold eddy and passed close to I5 (the first time), it was moved from 588 to 593 to 574 db, a mean upwelling of 0.24 mm s$^{-1}$ (Figure 29); at this time, the float was in the middle of a vertical displacement of some 70 m. CM data (Figure 31) for
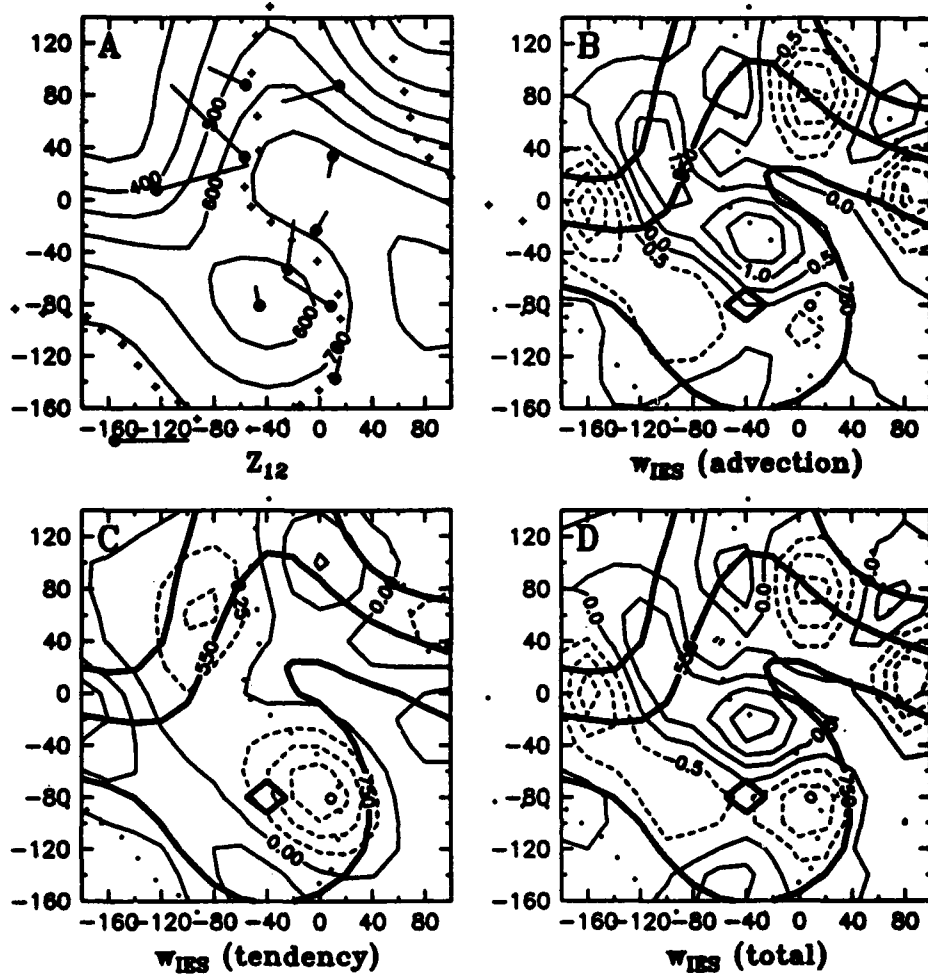
35
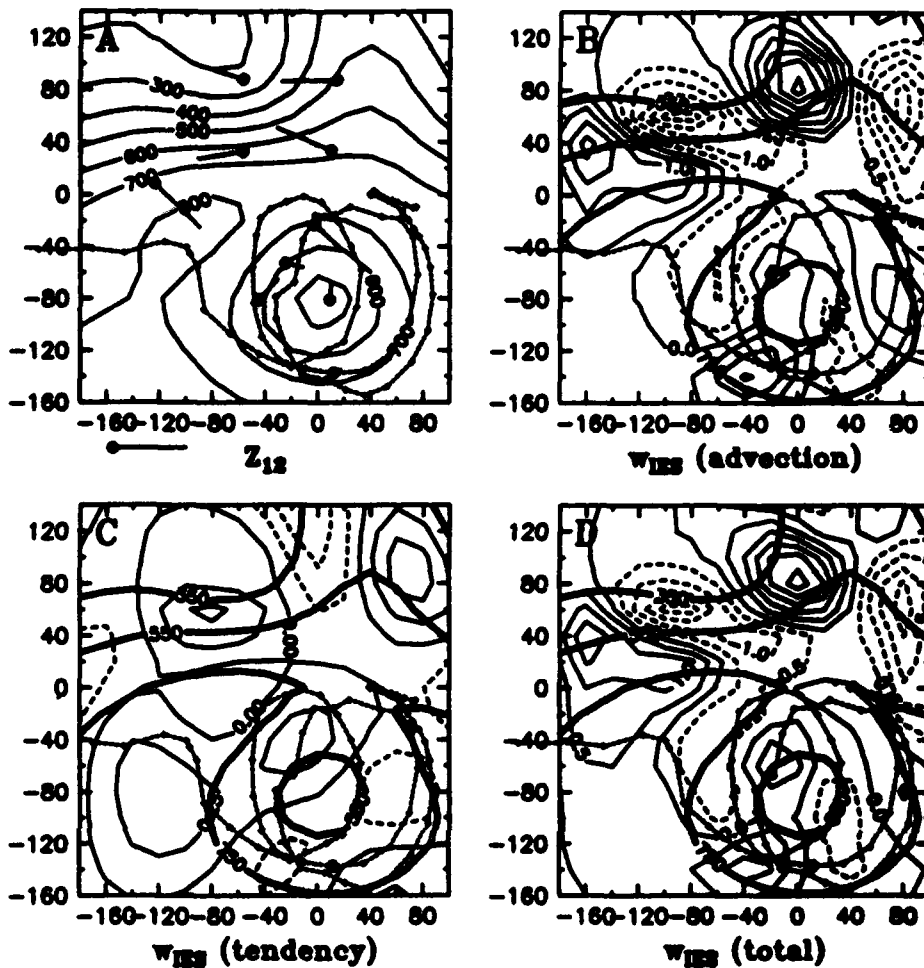
Figure 30: As in Figure 2, except for 0000 UTC 23 November 1989. The track of float 199 is indicated by dots, and the location of CM I5 is marked by a circle.

the same time also suggests upward vertical motion: although currents are backing with decreasing depth (suggestive of downwelling) (Figure 31a,c,e), there is a simultaneous decrease in temperature associated with a rise in isothermal surfaces that overwhelms this descent (Figure 31b,d,f). Vertical motion as diagnosed from IES data (Figure 30), however, suggests weak downwelling as a result of both local vorticity tendency and vorticity advection.
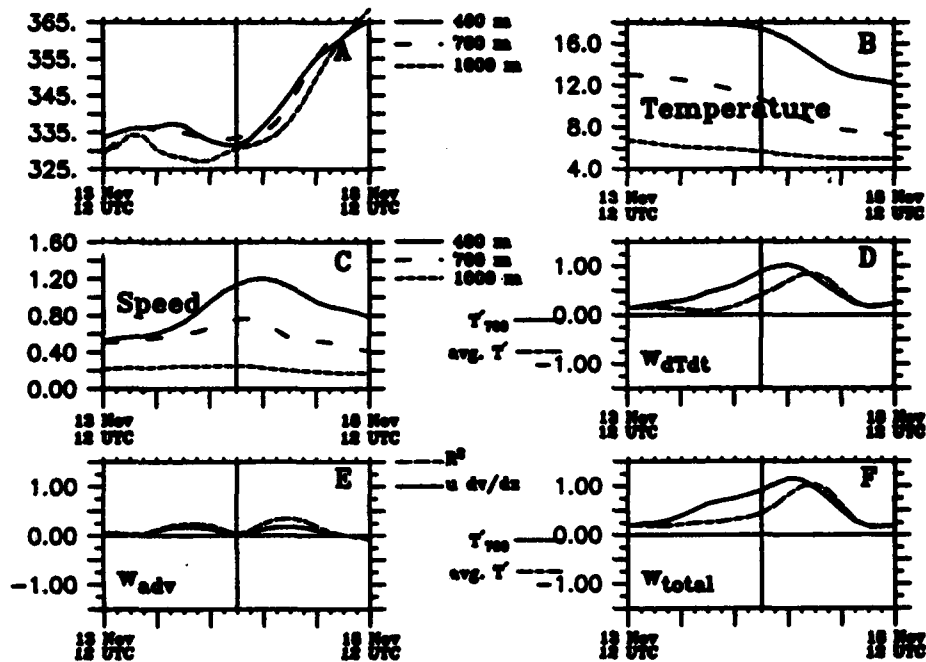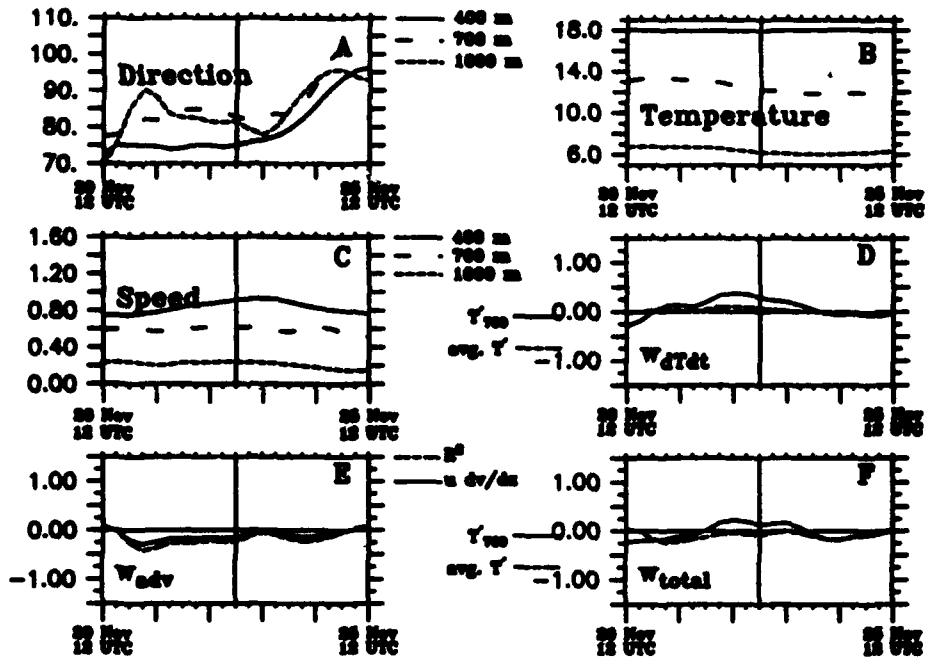
Figure 31: As in Figure 3, except for CM I5 for the five days surrounding float 199's closest (first) approach to I5, which time is indicated by vertical line.

### 3.10 Case 10: Float 199, CM I5, 28 November 1989, 1600 UTC

#### 3.10.1 Overview

See Case 9. At this time, the float is still circling around the cold eddy (Figure 32) that figures prominently in the IES topography (Figure 33).
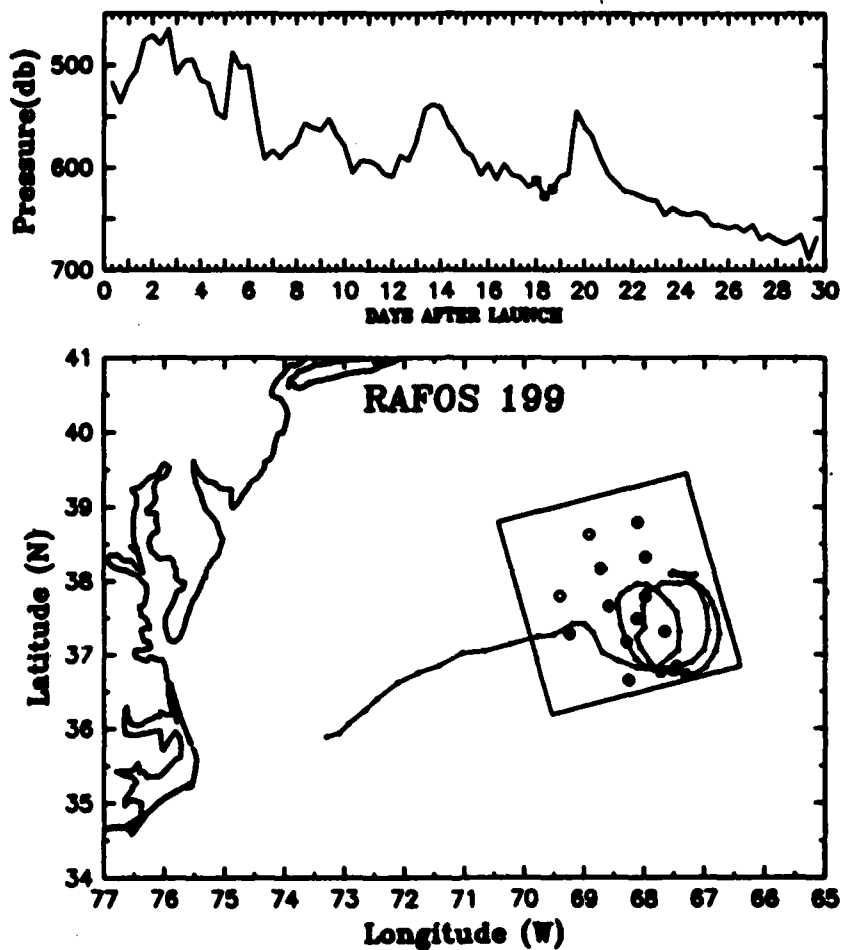


Figure 32: As in Figure 29, but for second close approach.

#### 3.10.2 Vertical motion results

$w_{RAF} = -0.13$ mm s$^{-1}$ , $w_{CM} = 0.04$ mm s$^{-1}$ , $w_{IES} = 0.54$ mm s$^{-1}$

As RAFOS float 199 passed by CM I5 for the second time, it moved from 613 to 627 to 621 db (Figure 32), a mean downwelling of $-0.13$ mm s$^{-1}$ ; however, immediately after passing I5, the float upwelled about 75 m in 2 days. CM data (Figure 34) shows upwelling, caused mostly by local temperature changes (Figure 34b,d,f); currents are switching between backing and veering when the float passed by, so vertical motion from this effect was near

38
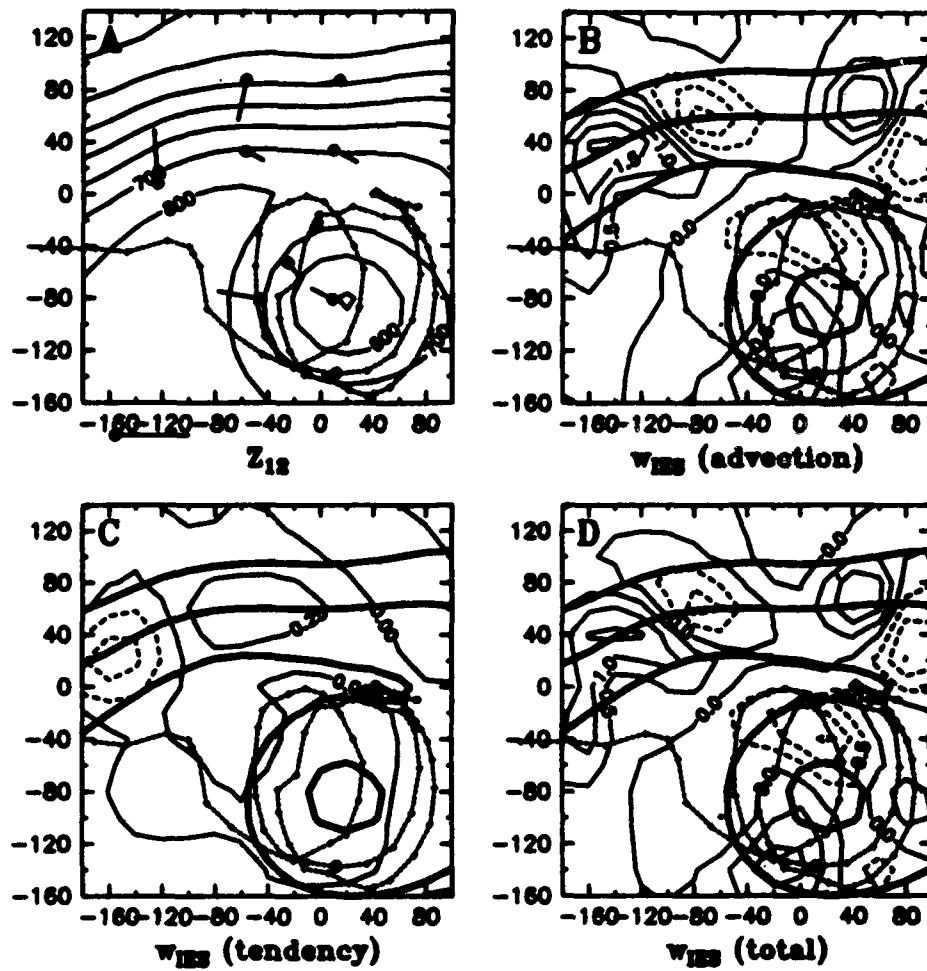
Figure 33: As in Figure 30, except for 1600 UTC 28 November 1989.

zero (Figure 34a,c,e). IES vertical motion (Figure 33) at the same time suggested upward motion (0.54 mm s$^{-1}$ ) forced mostly by cyclonic vorticity advection.
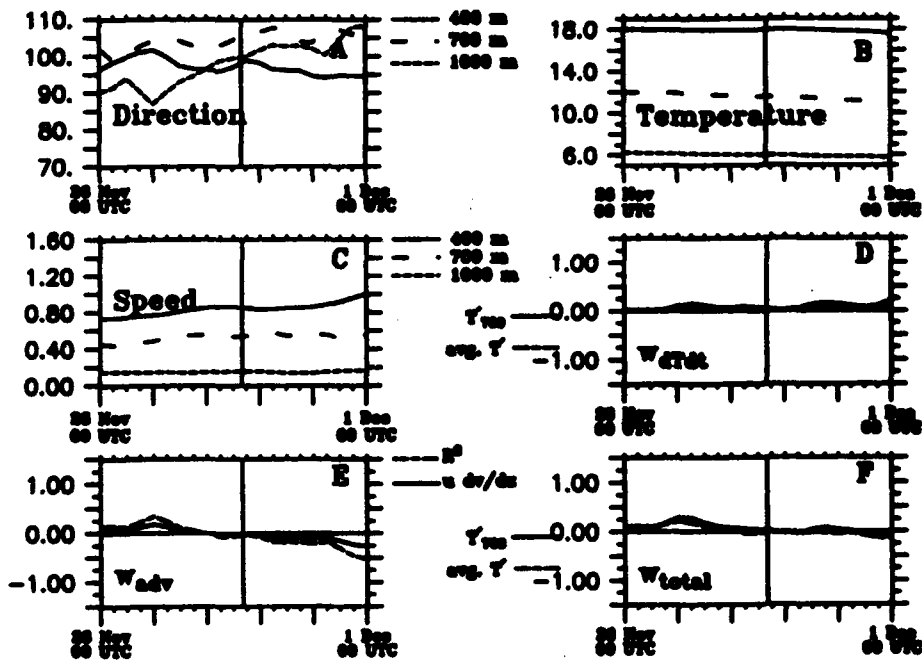
Figure 34: As in Figure 31, except for the second close approach by float 199 to I5, which time is indicated by vertical line.

## 3.11 Case 11: Float 201, CM I1, 23 November 1989, 0800 UTC

### 3.11.1 Overview

Float 201 moved though the northern part of the Central Array (Figure 35) at a time when the thermocline topography (Figure 36) indicated a vigorous cold ring in the southern part of the array (In fact, float 199 was circling this eddy as float 201 moved through the array). $z_{12}$ data also show the sharp trough in the center of the Central Array which float 201 passed just before being expelled from the stream to the north of the Central Array.



Figure 35: As in Figure 1, but for float 201. The three closest RAFOS fixes to CM I1 are boxed. Launch date: 1550 UTC, 15 November 1989.

### 3.11.2 Vertical motion results

$w_{RAF} = 0.97$ mm s$^{-1}$ , $w_{CM} = 1.51$ mm s$^{-1}$ , $w_{IES} = 1.66$ mm s$^{-1}$

As float 201 passed by CM I1, it was just beginning an ascent that would take the float from 600 db up to 150 db (Figure 35). For the three times that the float was closest to I1,

41

Figure 36: As in Figure 2, except for 0800 UTC 23 November 1989. The track of float 201 is indicated by dots, and the location of CM I1 is marked by a circle.

it moved from 575 to 560 to 519 db, a mean upwelling of 0.97 mm $s^{-1}$ . CM data for this time also suggest strong upward motion (Figure 37). Not only are temperatures cooling significantly (suggestive of strong upwelling), but there is also significant veering. Note that this is a case where the computation of $w_{CM}$ using $R^2 \frac{\partial \phi}{\partial z}$ leads to an (assumed) erroneously large component of vertical motion due to backing and veering currents (Figure 37a,c,e) that does not occur if $w_{CM}$ is computed using $v\frac{\partial u}{\partial z} - u\frac{\partial v}{\partial z}$. IES topography also suggests strong upward motion, forced entirely by the cyclonic vorticity advection downstream of the sharp trough at $x = -40$ (Figure 36b,d).

Figure 37: As in Figure 3, except for closest approach by float 201 to I1, which time is indicated by vertical line.

## 3.12 Case 12: Float 207, CM I2, 4 September 1989, 0800 UTC

### 3.12.1 Overview

During float 207's lengthy passage through the Central Array (Figure 38), the Central Array was characterized by unusually intense eddy activity (Figure 39). As a result, the float followed a complex route, entering the Central Array four times, twice from the eastern edge. At the time of passing I2, the float was moving *to the west* on the southern edge of an anticyclonic (warm) eddy.
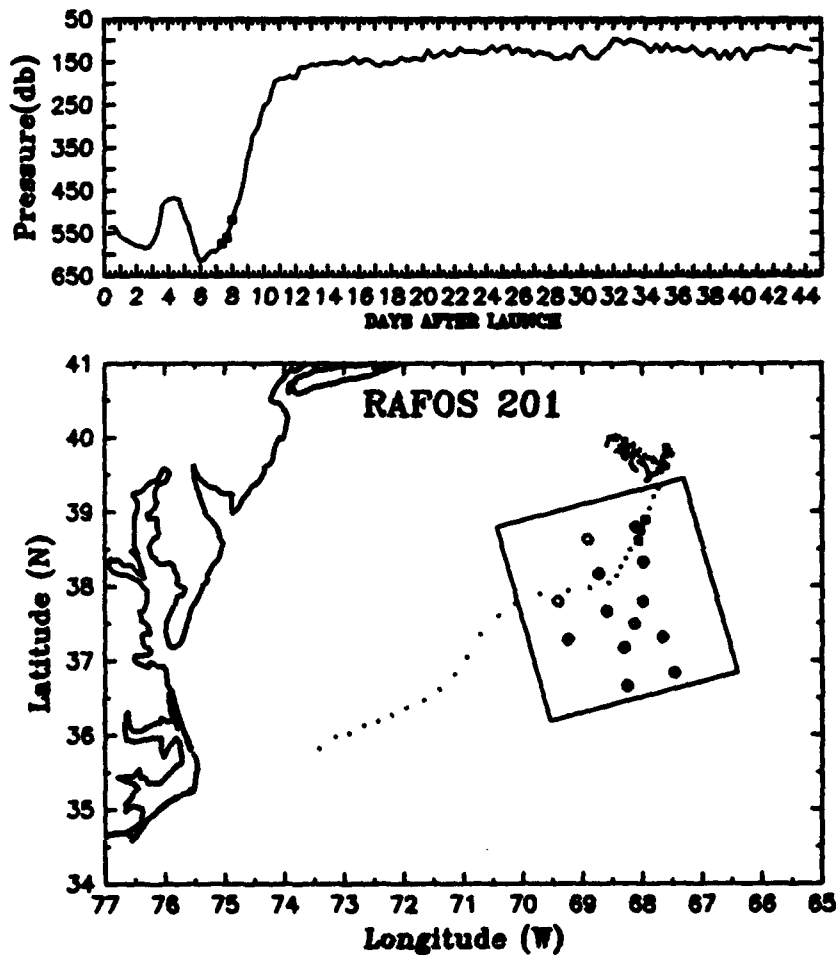


Figure 38: As in Figure 1, but for float 207. The three closest RAFOS fixes to CM I2 are boxed. Launch date: 1858 UTC, 23 August 1989.

### 3.12.2 Vertical motion results

$w_{RAF} = -0.25$ mm s$^{-1}$ , $w_{CM} = -0.06$ mm s$^{-1}$ , $w_{IES} = -0.24$ mm s$^{-1}$

Float 207 (Figure 38) moved from 158 to 164 to 172 db during the time it was closest to CM I2, at a level in the ocean that was the shallowest of all the RAFOS floats considered in
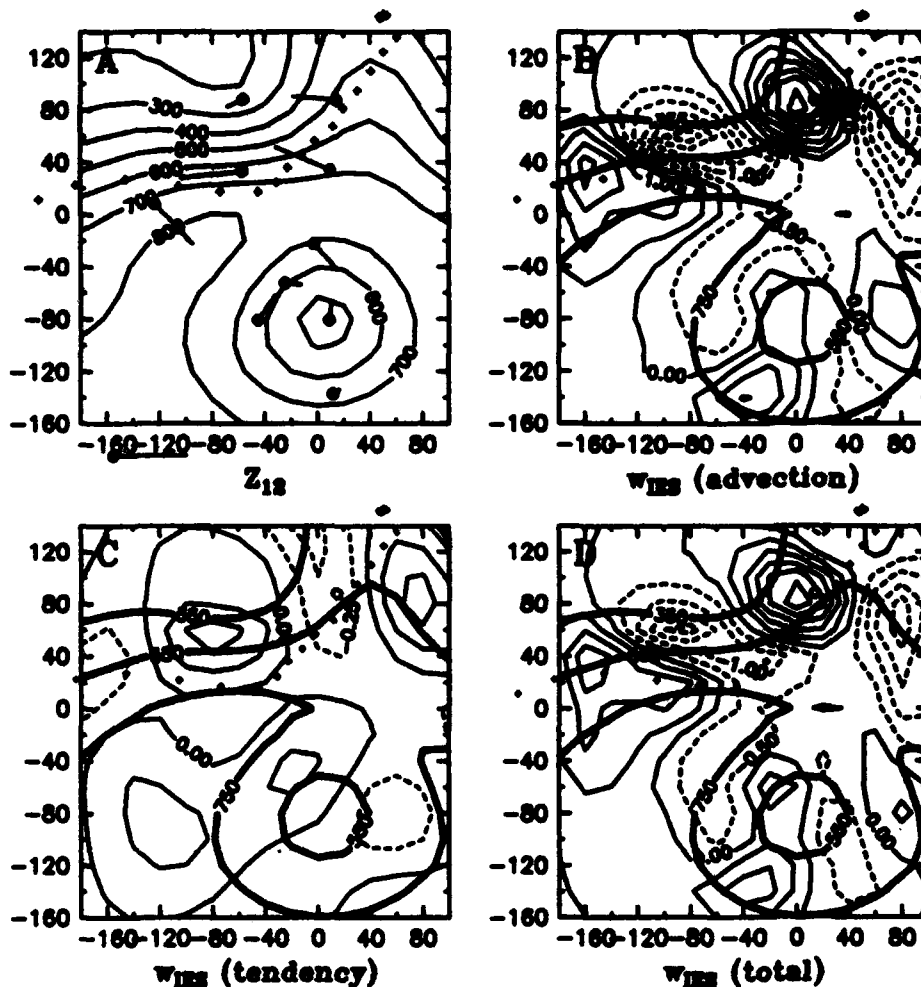
44

Figure 39: As in Figure 2, except for 0800 UTC 4 September 1989. The track of float 207 is indicated by dots, and the location of CM I2 is marked by a circle.

this report (Float 201 moved to a shallower level after exiting the Central Array, however). Current meter data at the same time also suggested downwelling — albeit very weak — (Figure 40), forced by backing currents. The effect of the backing currents dominates upwelling diagnosed as a result of cooling temperatures. IES data suggests downwelling forced mostly by local vorticity changes (Figure 39c).
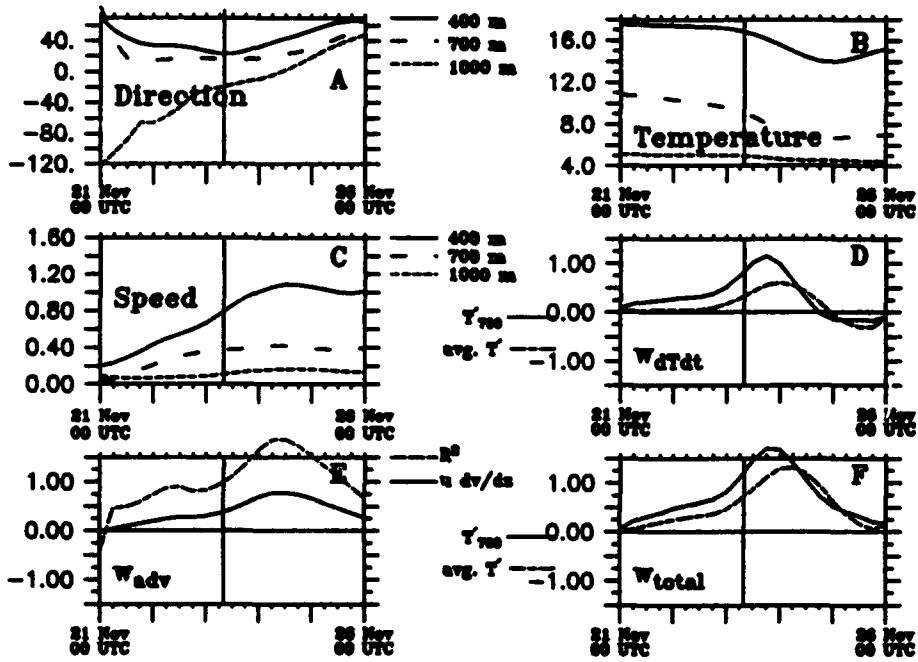
45

Figure 40: As in Figure 3, except for closest approach by float 207 to I2, which time is indicated by vertical line.

### 3.13 Case 13: Float 209, CM I5, 13 September 1989, 0800 UTC

#### 3.13.1 Overview

RAFOS float 209 moved steadily through the Central Array (Figure 41) on a path that suggests the float moved around a large meander trough in the eastern part of the array. This trough is obvious as well in the $z_{12}$ topography (Figure 42), which also shows a warm eddy moving through the slope waters to the north of the stream.
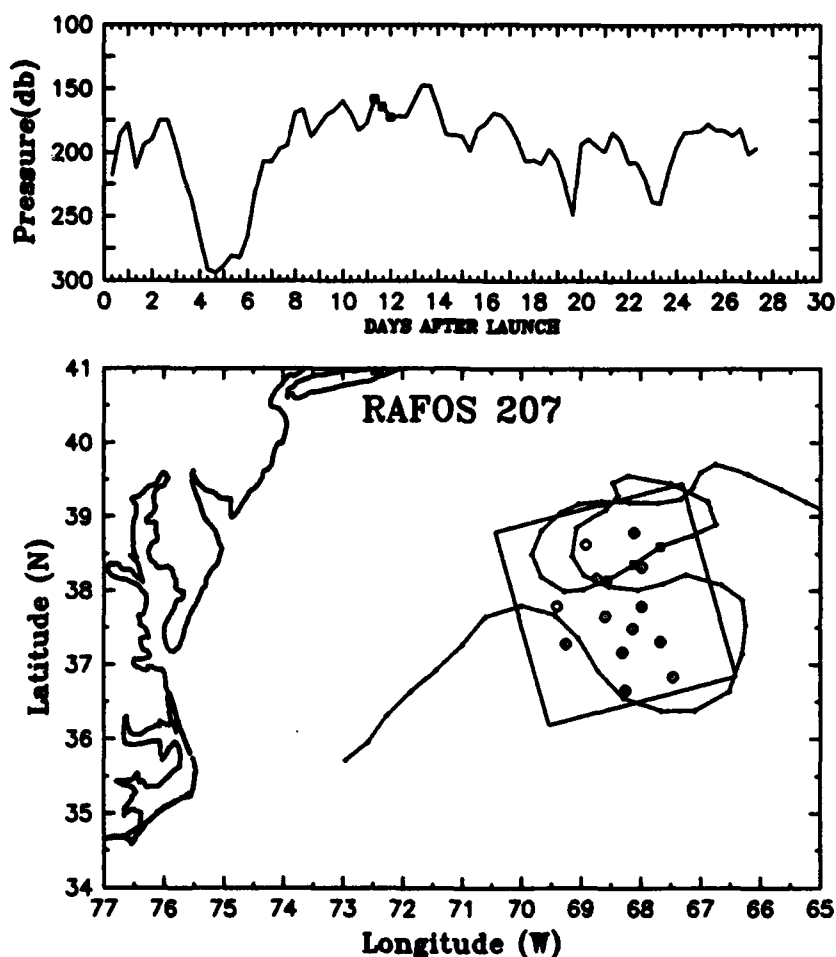


Figure 41: As in Figure 1, but for float 209. The three closest RAFOS fixes to CM I5 are boxed. Launch date: 1034 UTC, 7 September 1989.

#### 3.13.2 Vertical motion results

$$w_{RAF} = -1.53 \text{ mm s}^{-1} \, , \, w_{CM} = -2.14 \text{ mm s}^{-1} \, , \, w_{IES} = 0.22 \text{ mm s}^{-1}$$

Float 209 (Figure 41) moved from 584 to 629 to 672 db as it moved closest to CM I5. The mean downwelling from this motion is among the largest observed in the Central Array. At the same time, CM data (Figure 43) shows currents are backing, which is consistent with
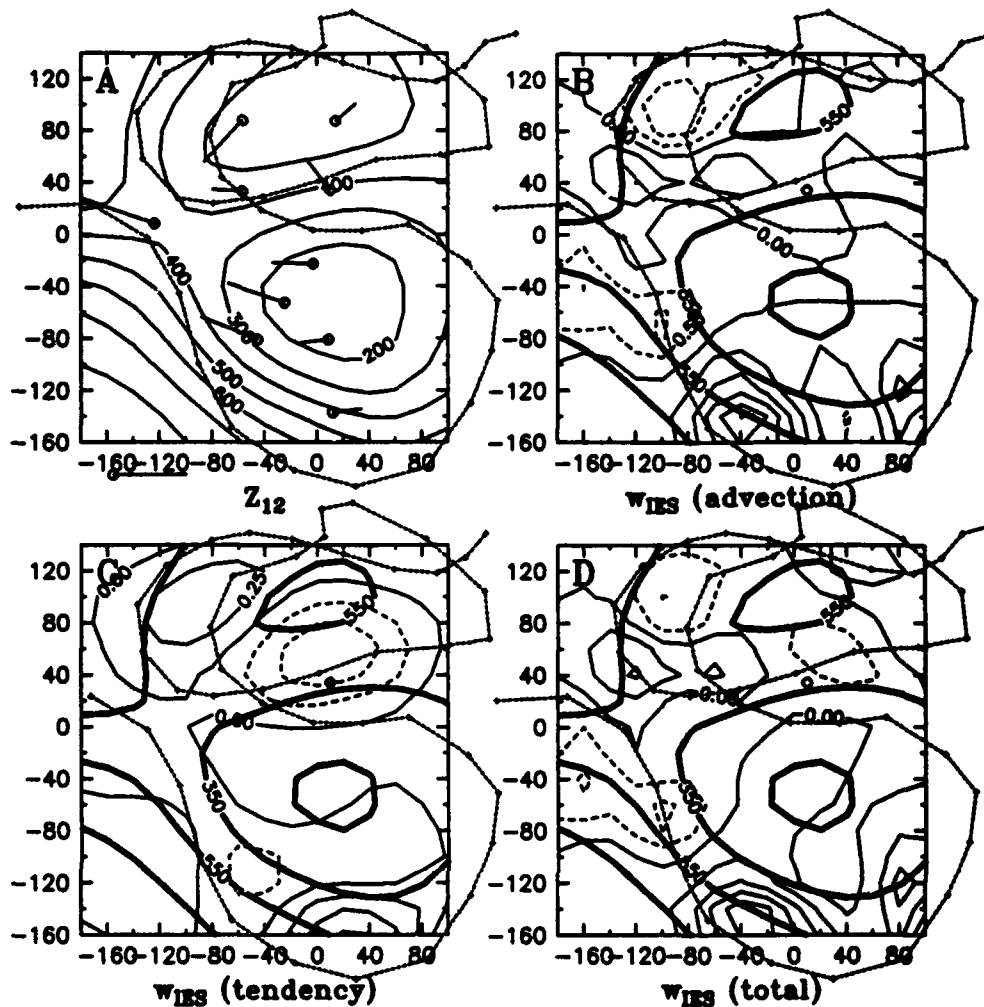
47

Figure 42: As in Figure 2, except for 0800 UTC 13 September 1989. The track of float 209 is indicated by dots, and the location of CM I5 is marked by a circle.

the strong downward motion. Furthermore, isotherms are descending (Figure 43d), also suggesting downward motion. IES data (Figure 42) for this time, however, suggests weak upward motion, a result of cyclonic vorticity advection and local tendency. Site I5 is near the edge of the IES mapping region; the derivatives of the $z_{12}$ field necessary to compute vorticity and vorticity advection may not be accurately estimated. A second possible reason for the startling disagreement is considered in Section 4.
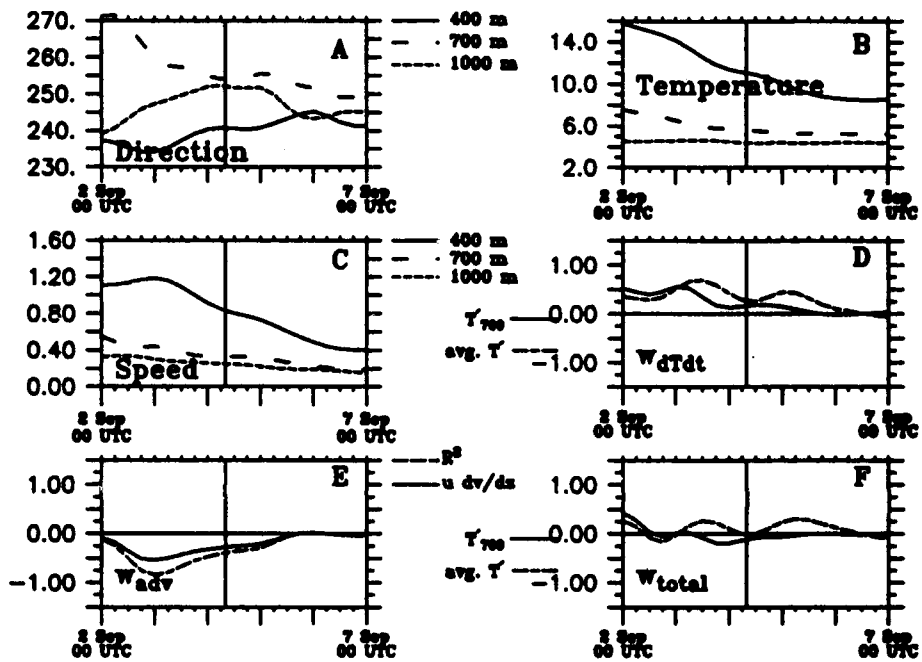
Figure 43: As in Figure 3, except for closest approach by float 209 to I5, which time is indicated by vertical line.

## 3.14 Case 14: Float 210, CM H4, 6 October 1989, 0800 UTC

### 3.14.1 Overview

Float 210 passed through the Central Array twice, suggesting significant interaction with nearby rings (Figure 44). Indeed, $z_{12}$ data (Figure 45) suggests that float 210 is circling a developing ring.
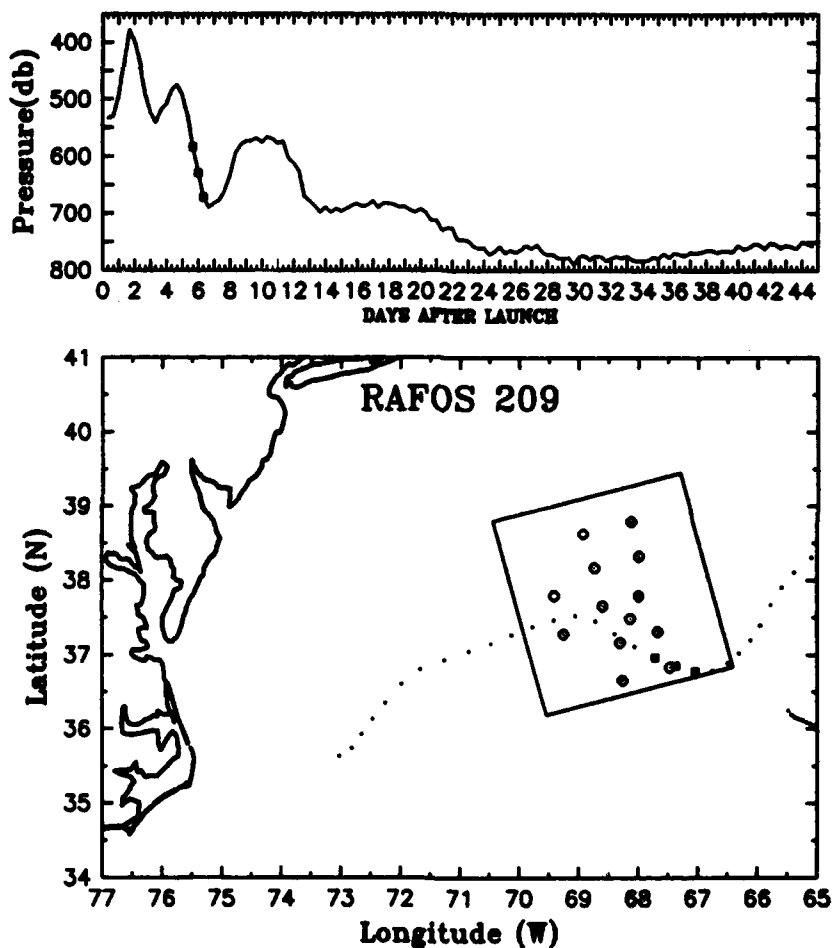


Figure 44: As in Figure 1, but for float 210. The three closest RAFOS fixes to CM H4 are boxed. Launch date: 1326 UTC, 26 September 1989.

### 3.14.2 Vertical motion results

$w_{RAF} = -0.02$ mm s$^{-1}$ , $w_{CM} = -0.19$ mm s$^{-1}$ , $w_{IES} = -0.84$ mm s$^{-1}$

As float 210 moved by CM H4 (Figure 44), it moved only from 636 to 644 to 637 db, despite the anticyclonic curvature to the path that might suggest strong downwelling. Current meter data at the same time also reflects the slight downward motion (Figure 46). Temperatures are warming, which suggests downwelling of isotherms, but this motion is
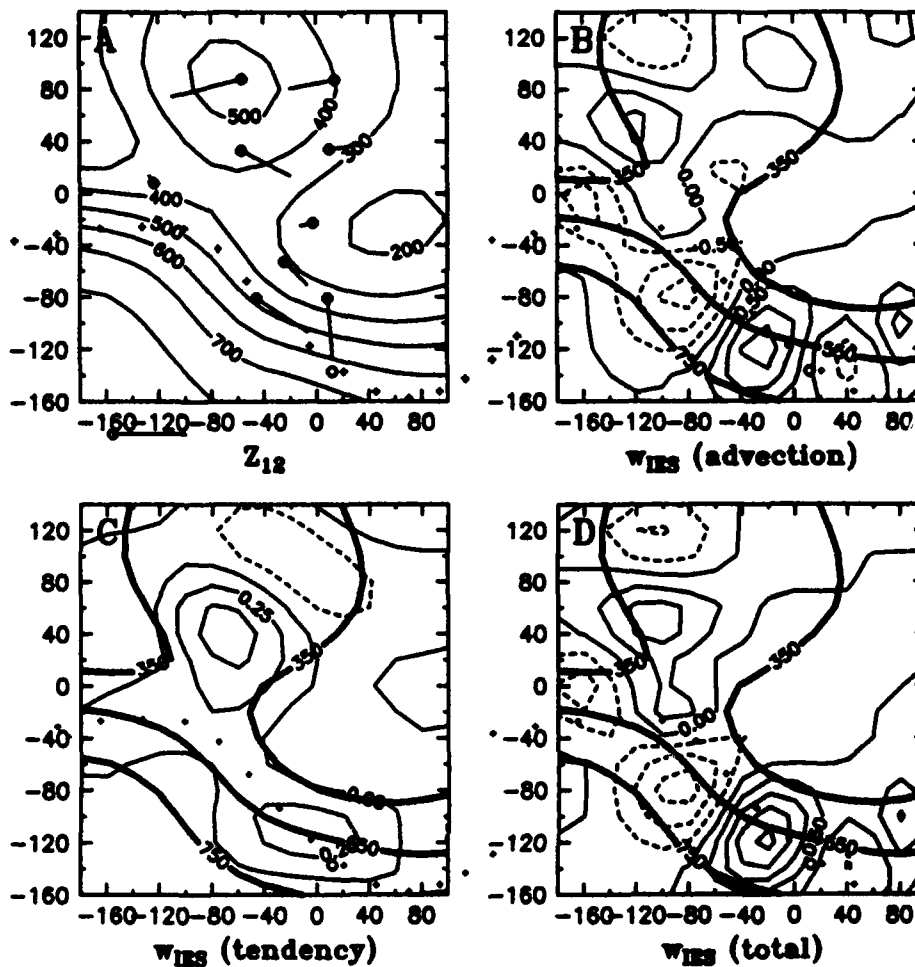
50

Figure 45: As in Figure 2, except for 0800 UTC 6 October 1989. The track of float 210 is indicated by dots, and the location of CM H4 is marked by a circle.

mostly offset by the veering current. $z_{12}$ data suggests descent forced by vorticity advection (Figure 46).
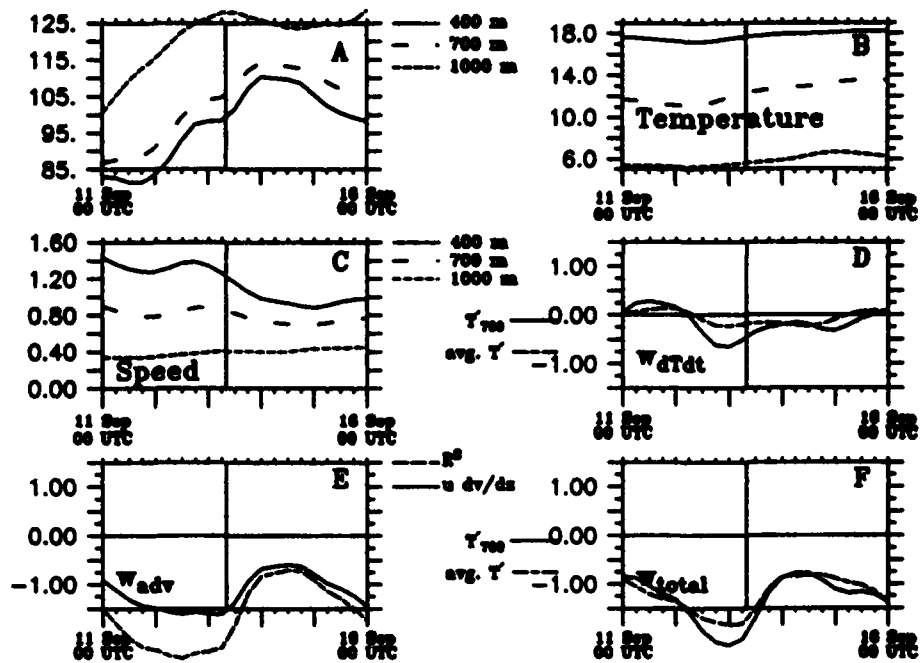
Figure 46: As in Figure 3, except for closest approach by float 210 to H4, which time is indicated by vertical line.

### 3.15 Case 15: Float 210, CM I5, 21 October 1989, 0000 UTC

#### 3.15.1 Overview

Float 210's second passage through the central array occurred as the float (Figure 47), circulating around a cold eddy (Figure 48), entered the southern edge of the Central Array and then turned to the west.
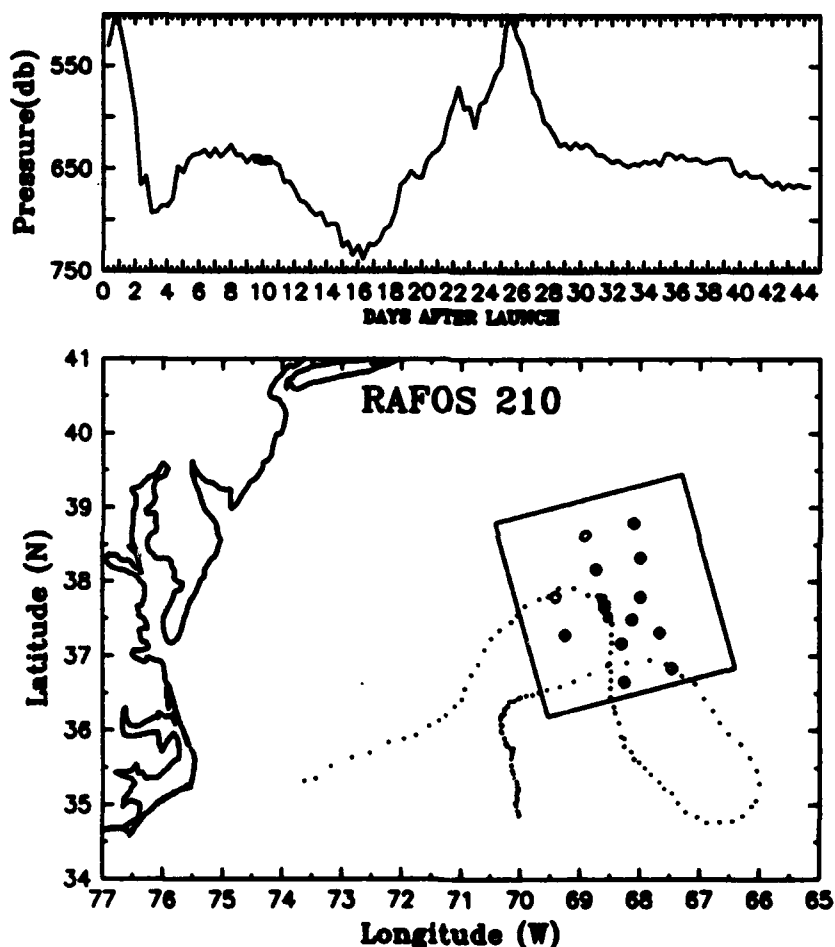


Figure 47: As in Figure 44. The three closest RAFOS fixes to CM I5 are boxed. Launch date: 1326 UTC, 26 September 1989.

#### 3.15.2 Vertical motion results

$$w_{RAF} = 0.36 \text{ mm s}^{-1} \text{ , } w_{CM} = 1.07 \text{ mm s}^{-1} \text{ , } w_{IES} = -0.33 \text{ mm s}^{-1}$$

As float 210 passed by CM I5, the float upwelled from 571 to 557 to 550 db, (Figure 47) consistent with the float's cyclonically curved path. Indeed, the float was in the middle of a three-day upward excursion of 100 m as it passed I5. CM data also suggest strong upwelling (Figure 49): there is significant veering to the currents and isotherms are rising, as indicated

53

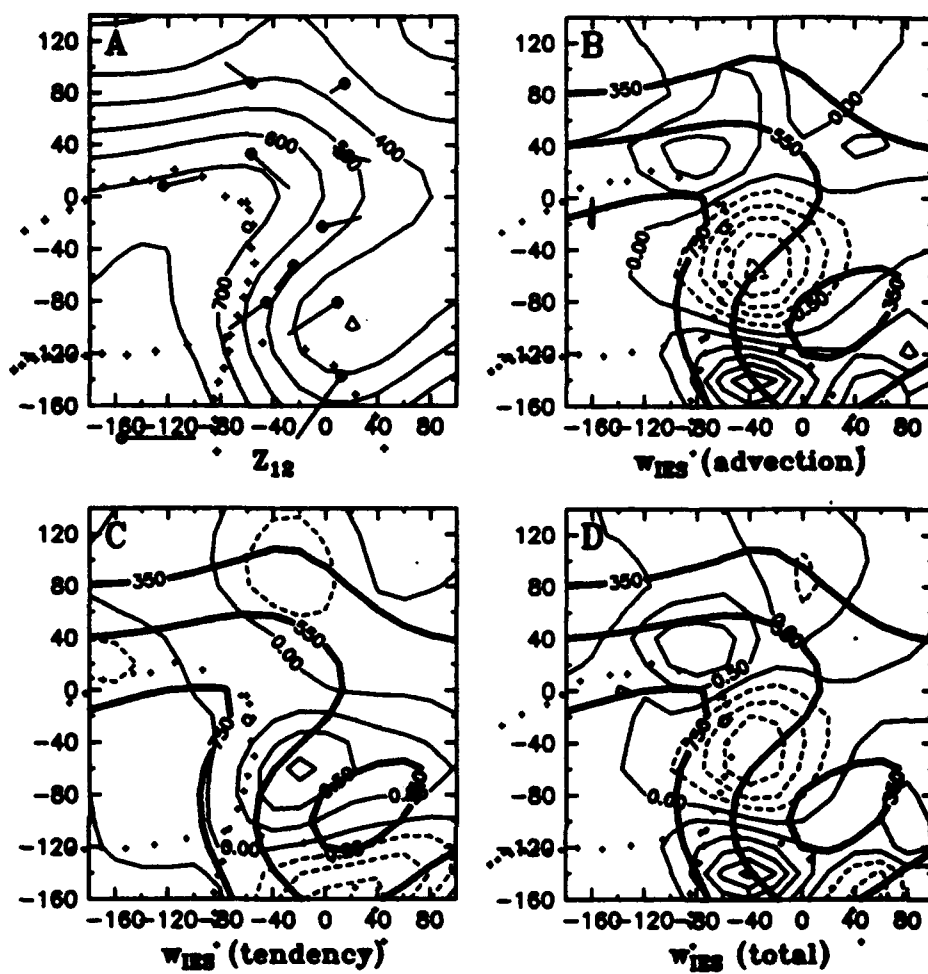Figure 48: As in Figure 2, except for 0000 UTC 21 October 1989. The track of float 210 is indicated by dots, and the location of CM I5 is marked by a circle.

by the decreasing temperatures (Figure 49b). IES data, however, show downwelling, forced both by anticyclonic vorticity advection and by local tendency (Figure 48). We note again that site I5 is not well located for $w_{IES}$ computations.
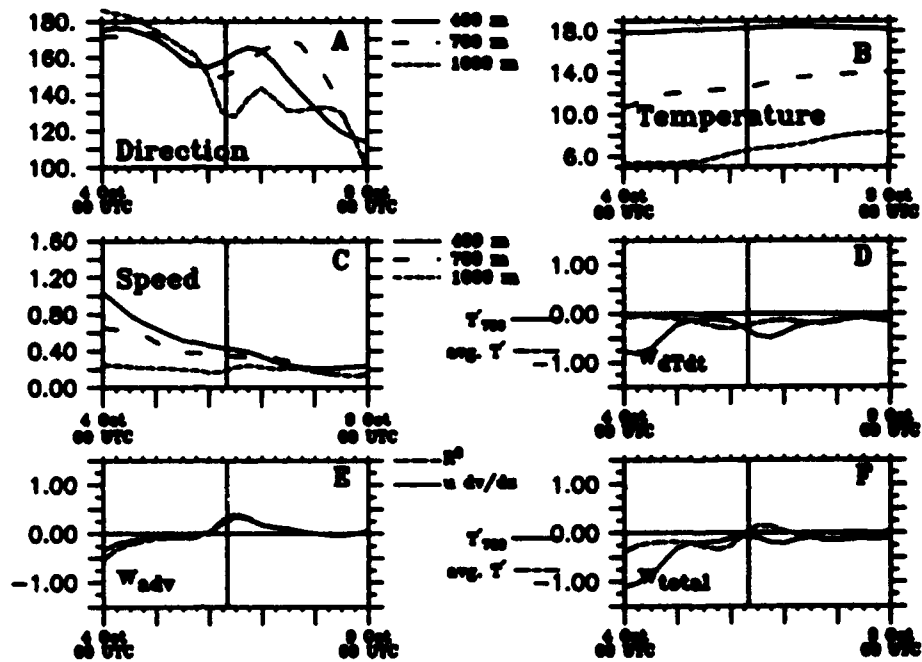
Figure 49: As in Figure 3, except for closest approach by float 210 to I5, which time is indicated by vertical line.

## 3.16 Case 16: Float 211, CM M13, 8 October 1989, 0000 UTC

### 3.16.1 Overview

Float 211 (Figure 50) moved on an anticyclonically curved path the entire time it was within the Central Array. This was because of a crest/trough structure in the $z_{12}$ topography (Figure 51) that was directing the main Gulf Stream flow out the southern Central Array border.
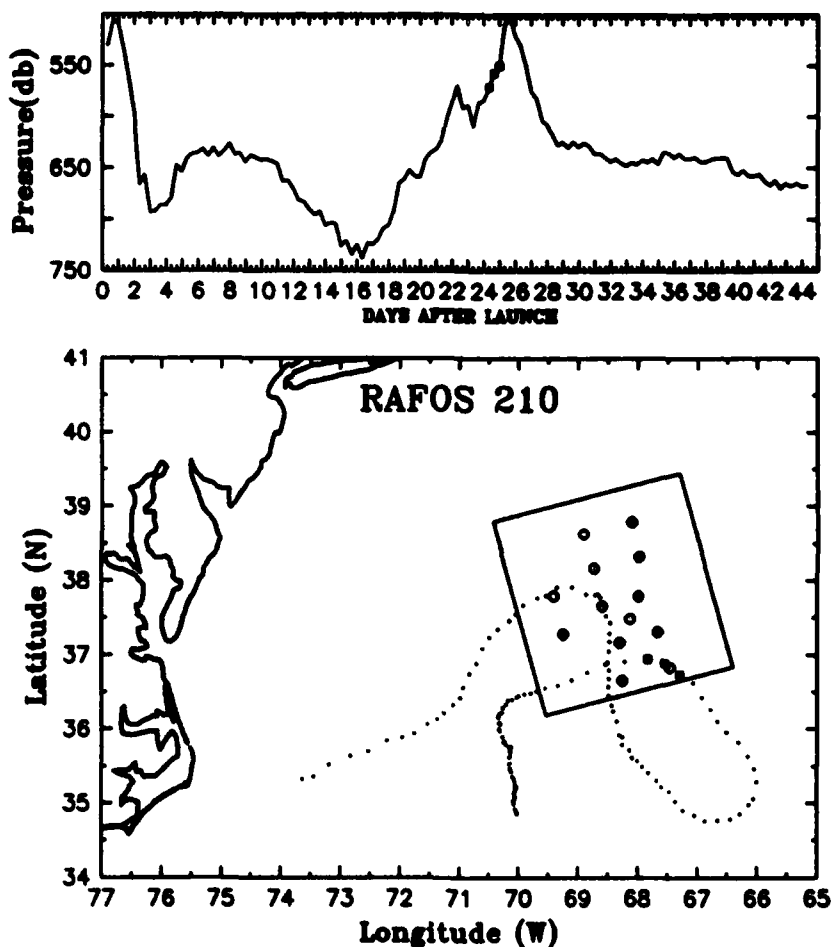


Figure 50: As in Figure 1. The three closest RAFOS fixes to CM M13 are boxed. Launch date: 1243 UTC, 30 September 1989.

### 3.16.2 Vertical motion results

$w_{RAF} = -0.44$ mm s$^{-1}$ , $w_{CM} = -0.68$ mm s$^{-1}$ , $w_{IES} = -0.78$ mm s$^{-1}$

During the three closest positions to CM M13, RAFOS float 211 was at pressure levels 613, 659, and 638 db, for a mean downward motion of $-0.44$ mm s$^{-1}$ (Figure 50). CM data (Figure 52) also suggested downward motion: temperatures at M13 were increasing,

56

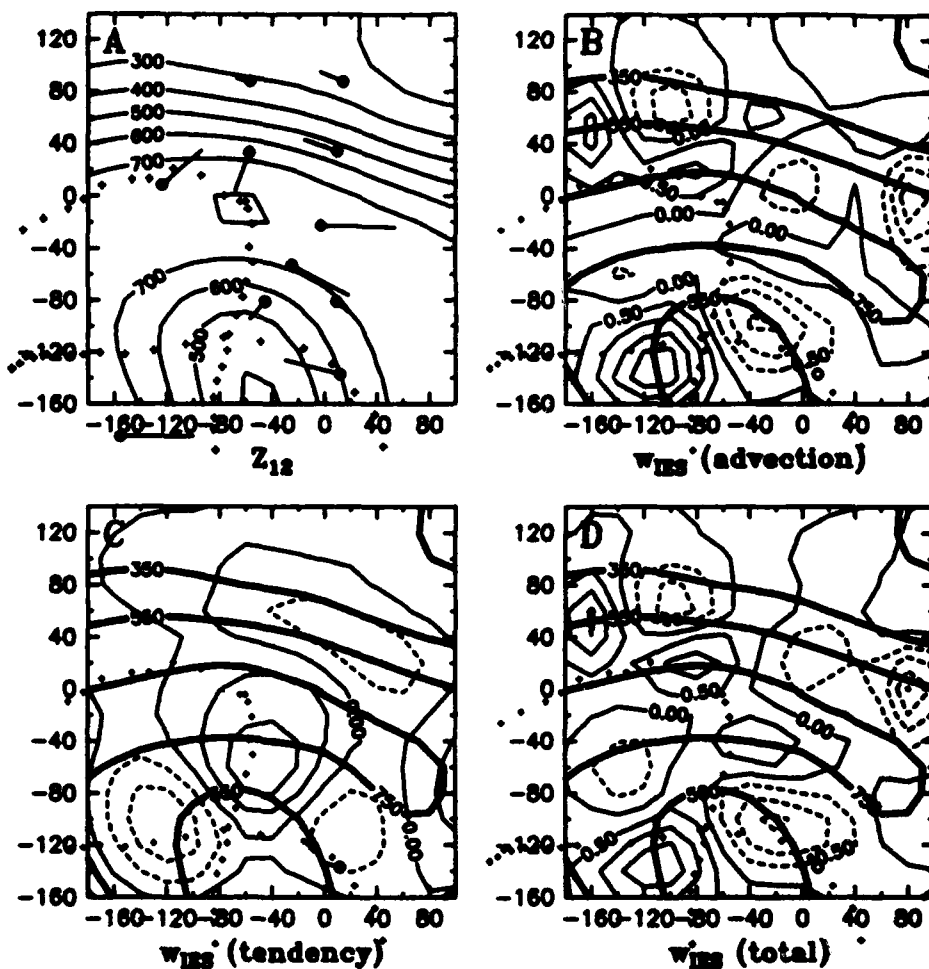Figure 51: As in Figure 2, except for 0000 UTC 8 October 1989. The track of float 211 is indicated by dots, and the location of CM M13 is marked by a circle.

reflecting downward-moving isotherms, which dominated the vertical motion diagnosed by the veering currents at M13. IES data also suggests downward motion (Figure 51), as should be expected given the strong anticyclonic vorticity advection over the site.
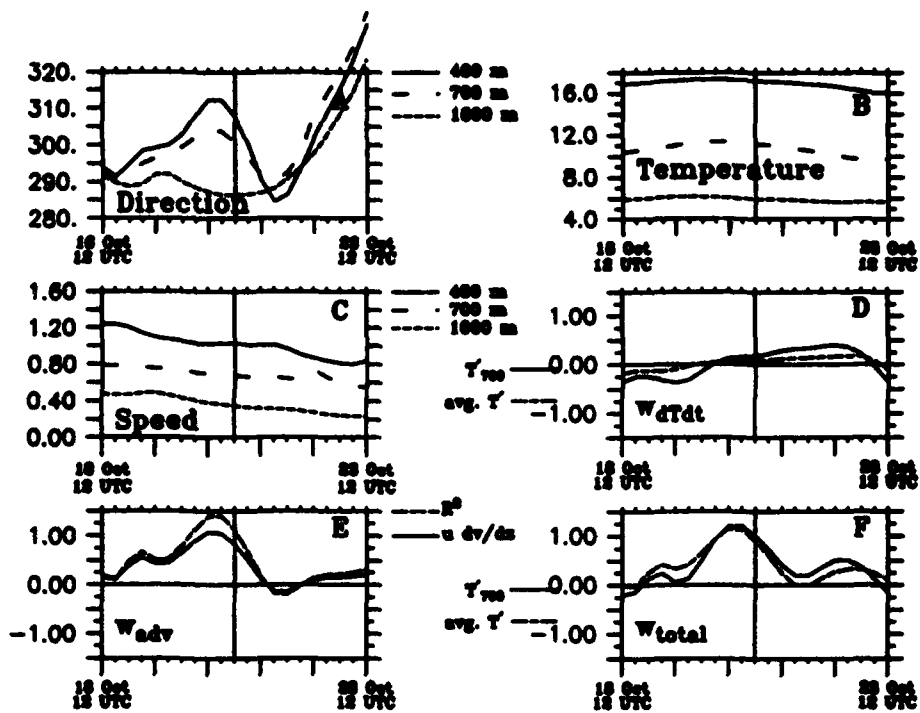
Figure 52: As in Figure 3, except for closest approach by float 211 to M13, which time is indicated by vertical line.

## 3.17 Case 17: Float 216, CM I1, 26 November 1989, 0000 UTC

### 3.17.1 Overview

Float 216 (Figure 53) moved through the Central Array at a time when a cold eddy was in the southeast corner of the array (Figure 54); however, the float's motion through the array was evidently unaffected by this cold ring.
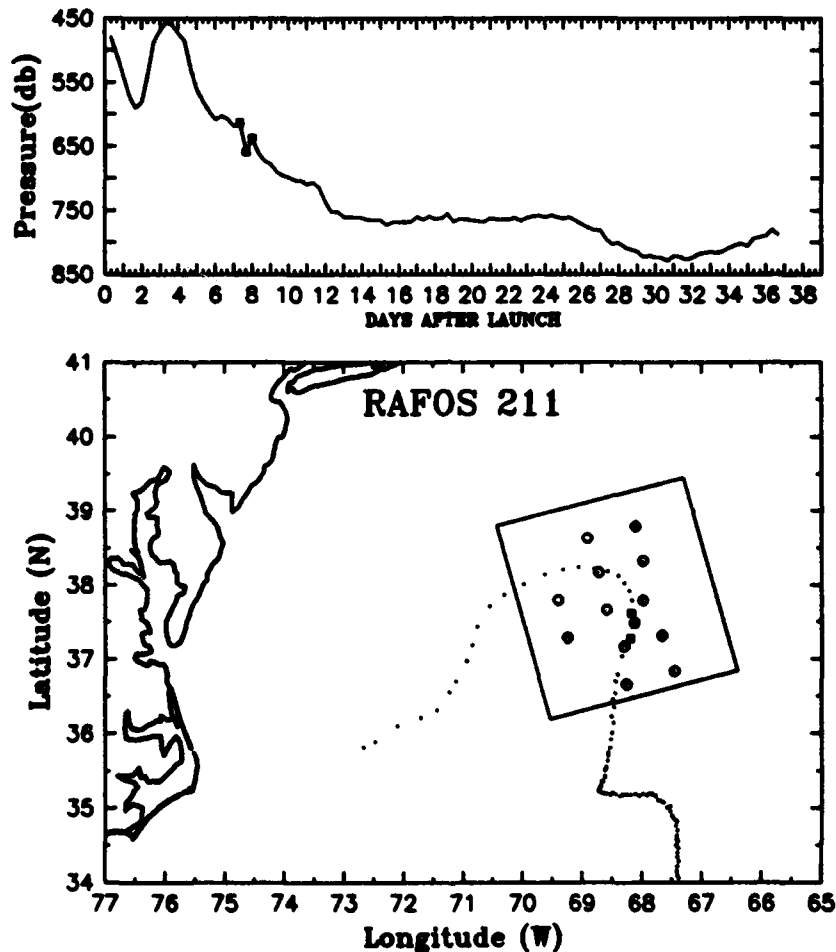


Figure 53: As in Figure 1. The three closest RAFOS fixes to CM I1 are boxed. Launch date: 1034 UTC, 18 November 1989.

### 3.17.2 Vertical motion results

$w_{RAF} = -0.02$ mm s$^{-1}$ , $w_{CM} = 0.14$ mm s$^{-1}$ , $w_{IES} = 0.86$ mm s$^{-1}$

Float 216 passed by CM I1 just before downwelling more than 200 m in a week (Figure 53). Close to I1, however, the float moved from 567 to 576 to 568 db on a path the trajectory of which was straight. IES data (Figure 54) shows significant curvature to the $z_{12}$ field, however, with cyclonic vorticity advection forcing upward motion at I1 (in fact, the
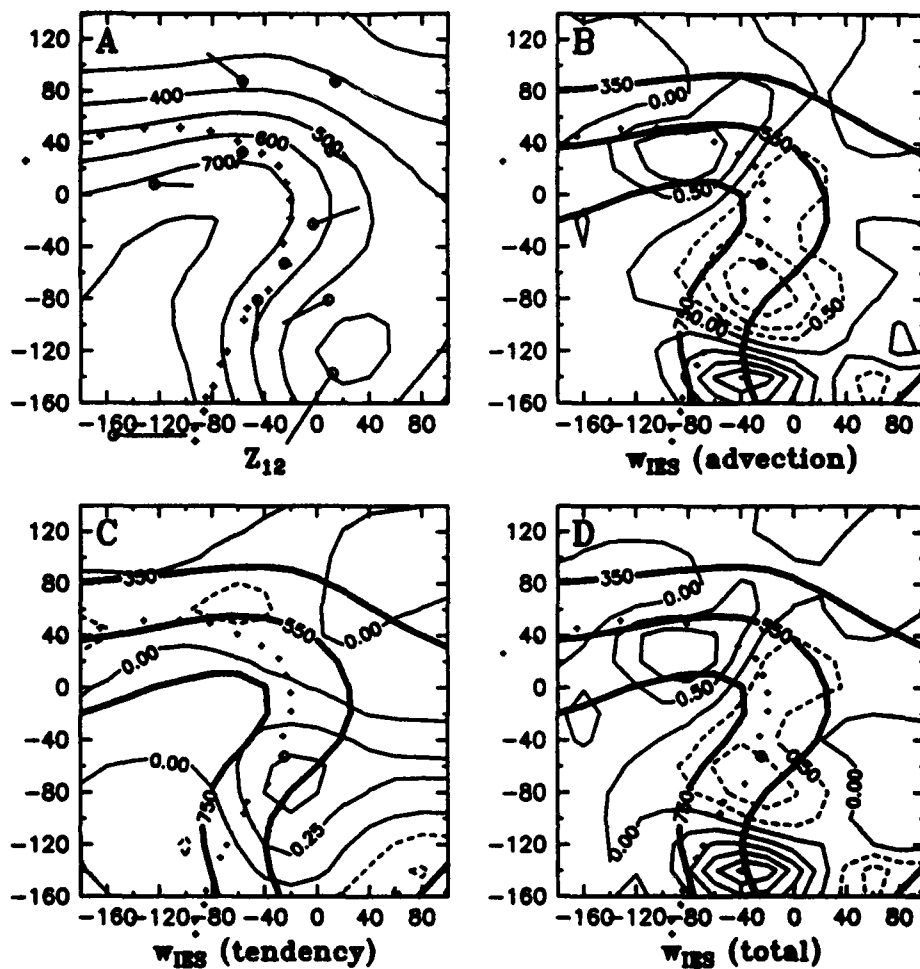
Figure 54: As in Figure 2, except for 0000 UTC 26 November 1989. The track of float 216 is indicated by dots, and the location of CM I1 is marked by a circle.

fields look very similar to those associated with float 201). CM data for the same time also suggest a Gulf Stream that is not straight (there is time variability in the direction (Figure 55a)). Upward motion is forced by veering currents, overwhelming the weak downward motion associated with the isotherm's descent (Figure 55b,d).
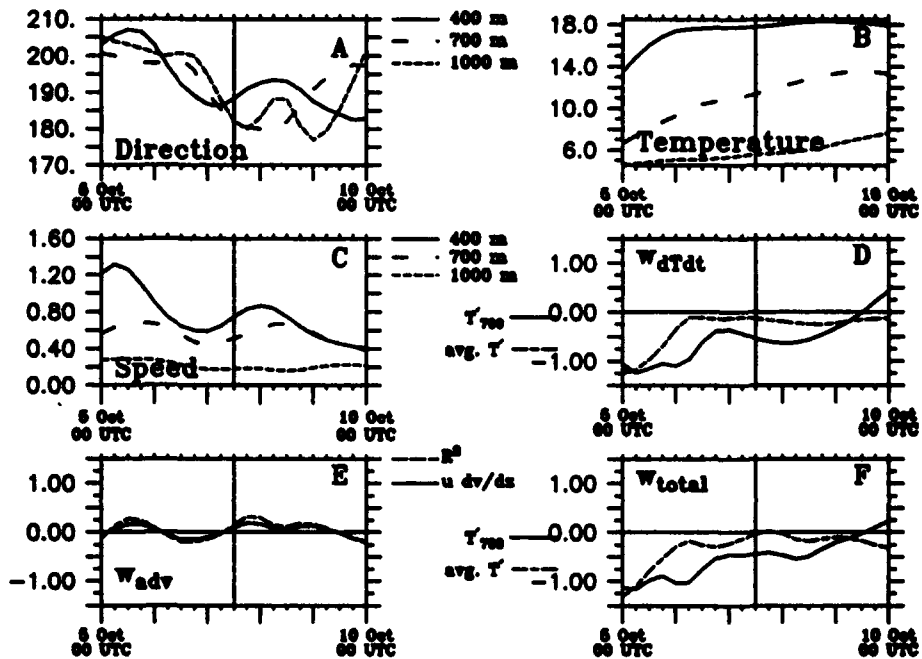
Figure 55: As in Figure 3, except for closest approach by float 216 to I1, which time is indicated by vertical line.

## 3.18   Case 18: Float 221, CM I2, 6 January 1990, 0800 UTC

### 3.18.1   Overview

Float 221 (Figure 56) moved quickly through the Central Array on a straight path. $z_{12}$ data (Figure 57) also shows a mostly straight Gulf Stream path (in which are embedded minor troughs/crests) with a cold eddy far to the south of the stream.
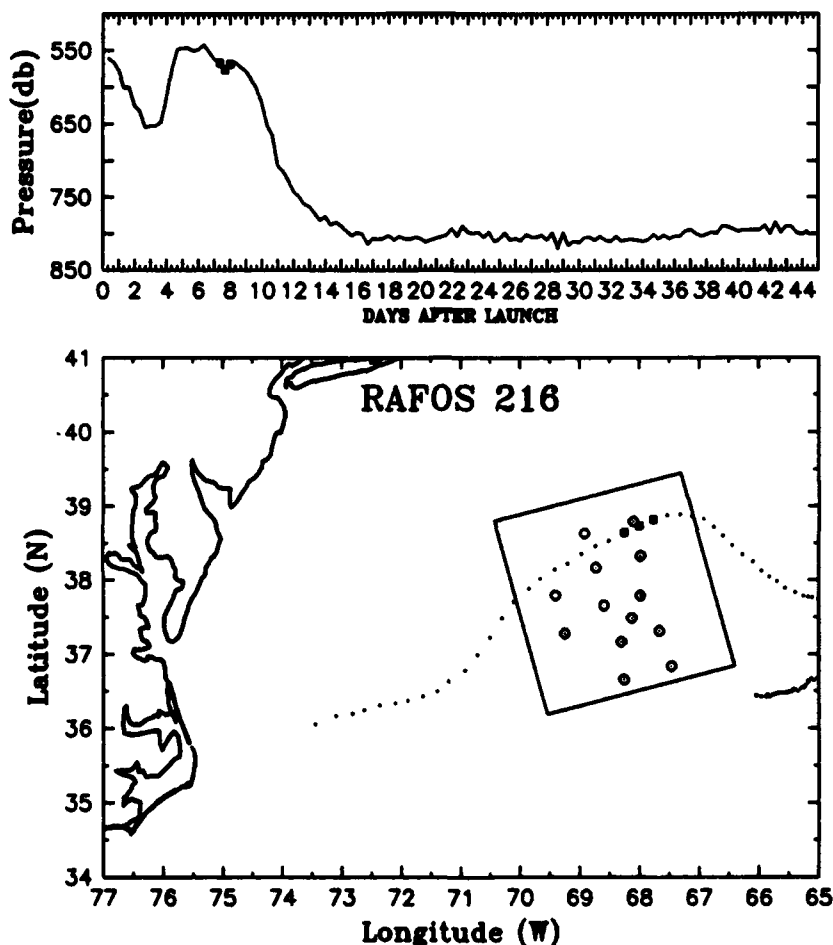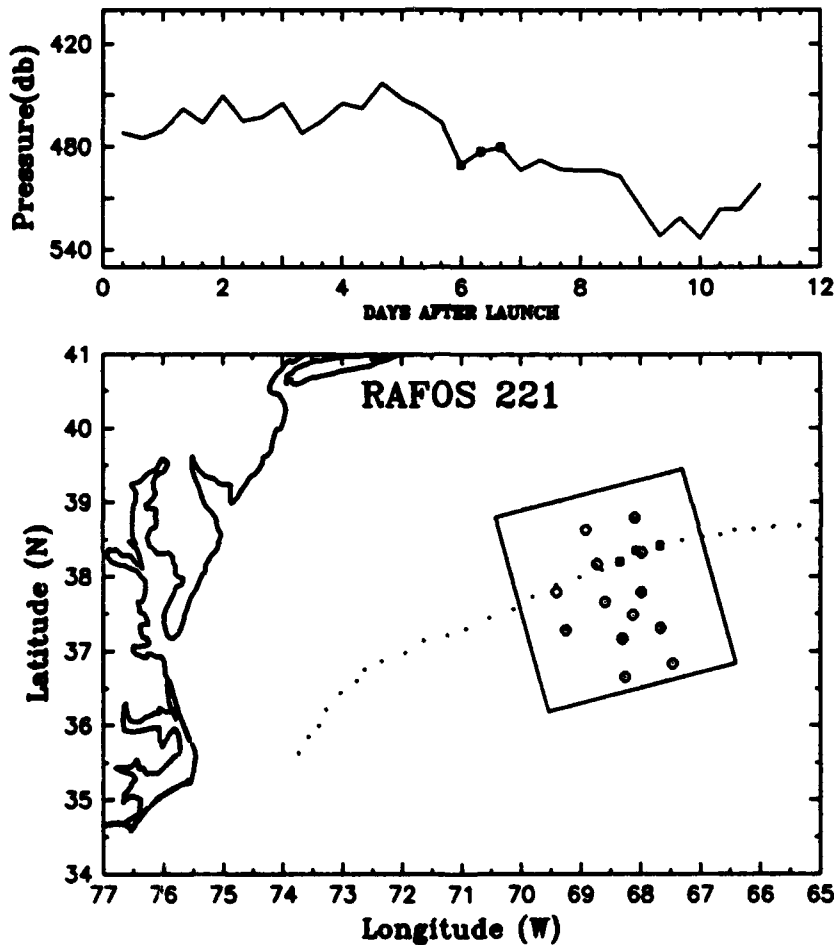


Figure 56: As in Figure 1. The three closest RAFOS fixes to CM I2 are boxed. Launch date: 0253 UTC, 30 December 1989.

### 3.18.2   Vertical motion results

$w_{RAF} = 0.18$ mm s$^{-1}$ , $w_{CM} = 0.21$ mm s$^{-1}$ , $w_{IES} = 0.45$ mm s$^{-1}$

Float 221 moved from 490 to 483 to 480 db in the time surrounding its closest passage to CM I2 (Figure 56). IES data suggest this upward ascent is forced both by cyclonic vorticity advection and by local vorticity tendencies (Figure 57). CM data (Figure 58) also reflect the upward motions, as there is significant veering motion and slight cooling.
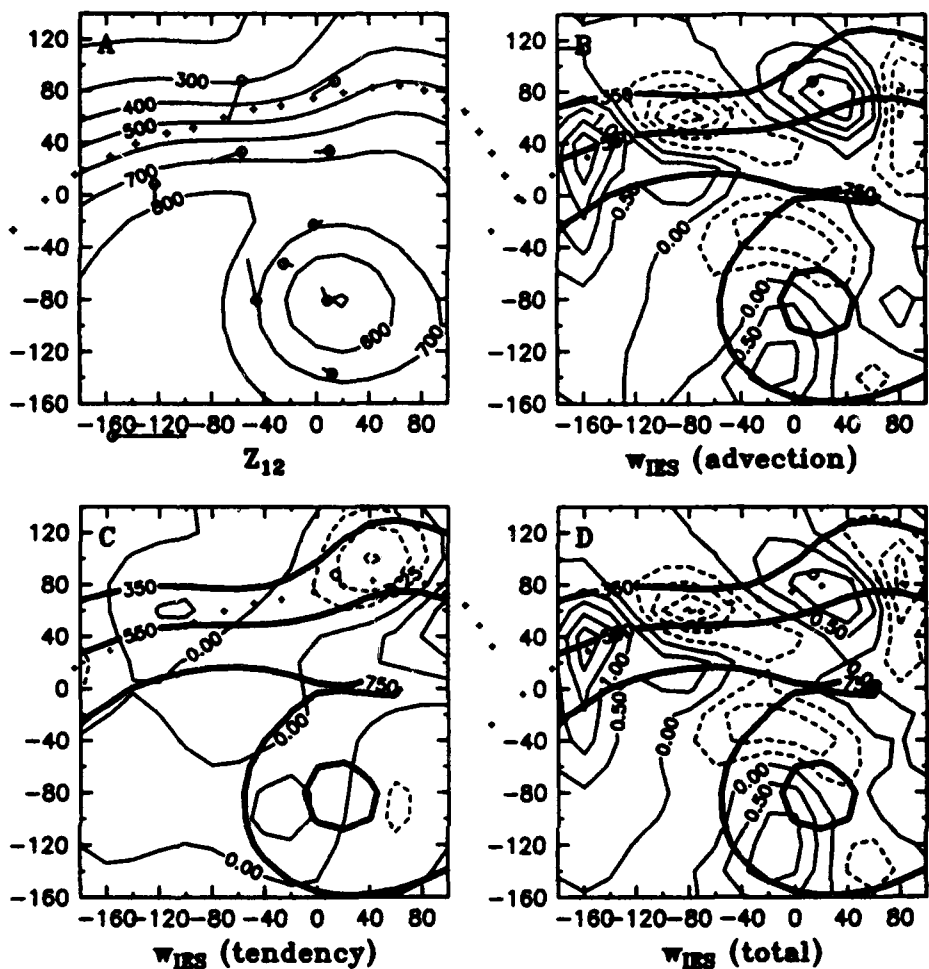
62
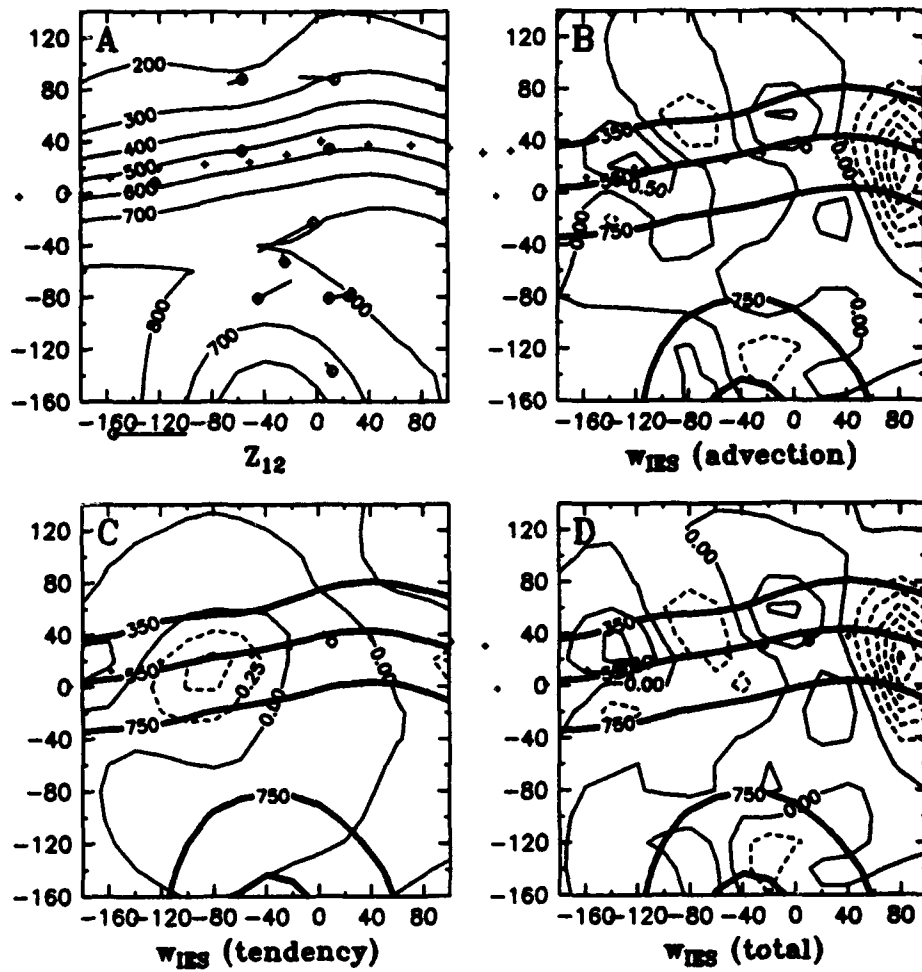
Figure 57: As in Figure 2, except for 0800 UTC 6 January 1990. The track of float 221 is indicated by dots, and the location of CM I2 is marked by a circle.
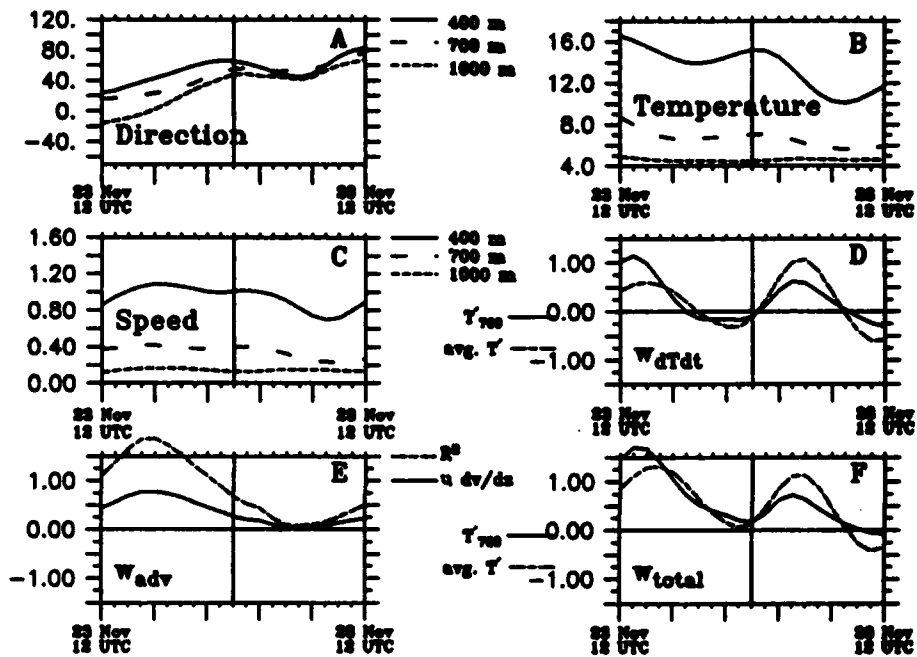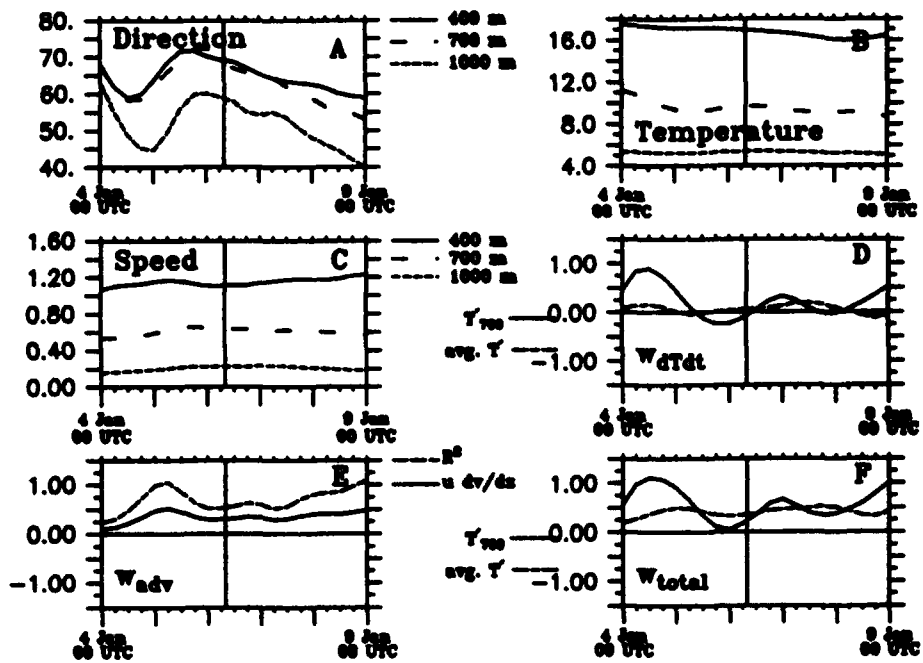
Figure 58: As in Figure 3, except for closest approach by float 221 to I2, which time is indicated by vertical line.

## 3.19 Case 19: Float 224, CM H4, 20 January 1990, 0800 UTC

### 3.19.1 Overview

Float 224 (Figure 59) passes through the Central Array at a time when a cold eddy is apparently interacting with the Gulf Stream (Figure 60). This interaction, however, does not seem to affect the float.
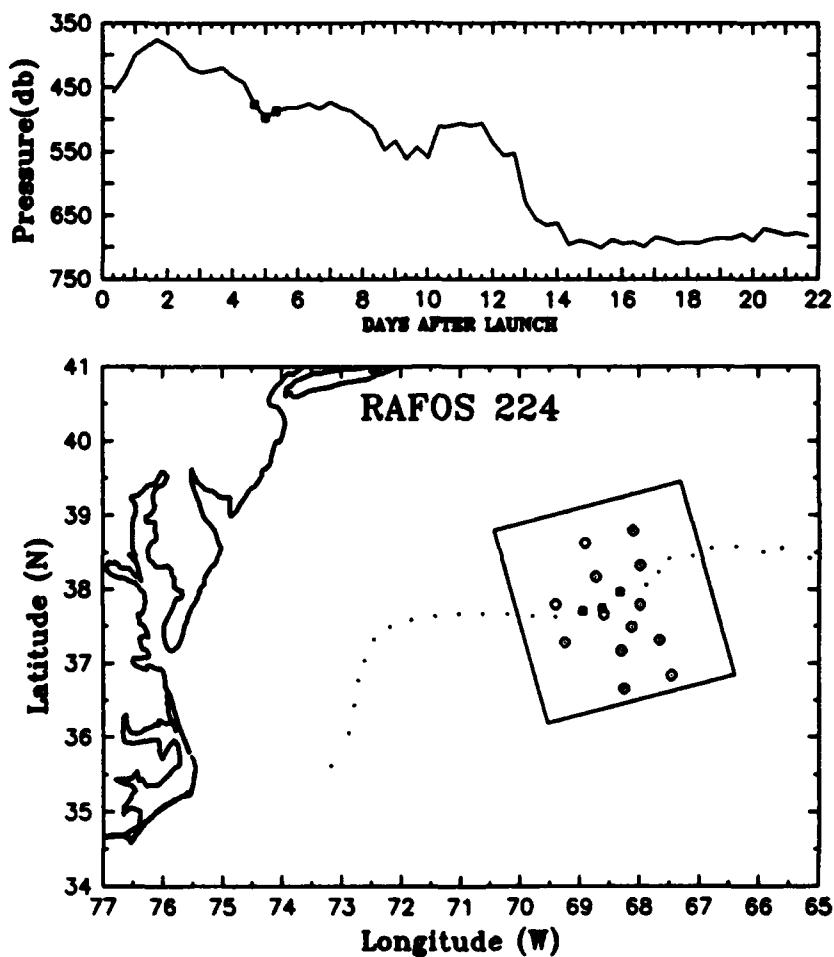
Figure 59: As in Figure 1. The three closest RAFOS fixes to CM H4 are boxed. Launch date: 1200 UTC, 15 January 1990.

### 3.19.2 Vertical motion results

$$w_{RAF} = -0.18 \text{ mm s}^{-1} \quad w_{CM} = -0.10 \text{ mm s}^{-1} \quad w_{IES} = -0.30 \text{ mm s}^{-1}$$

As it passed close to CM H4, float 224 moved from 477 to 497 to 487 db. The pressure trace (Figure 59) suggests that the float downwelled until 0800 UTC 20 January 1990 (when it was closest to H4), and then it leveled off, or upwelled slightly. IES data suggests this may also be true; although downwelling is diagnosed in the vicinity of H4, upwelling is

65
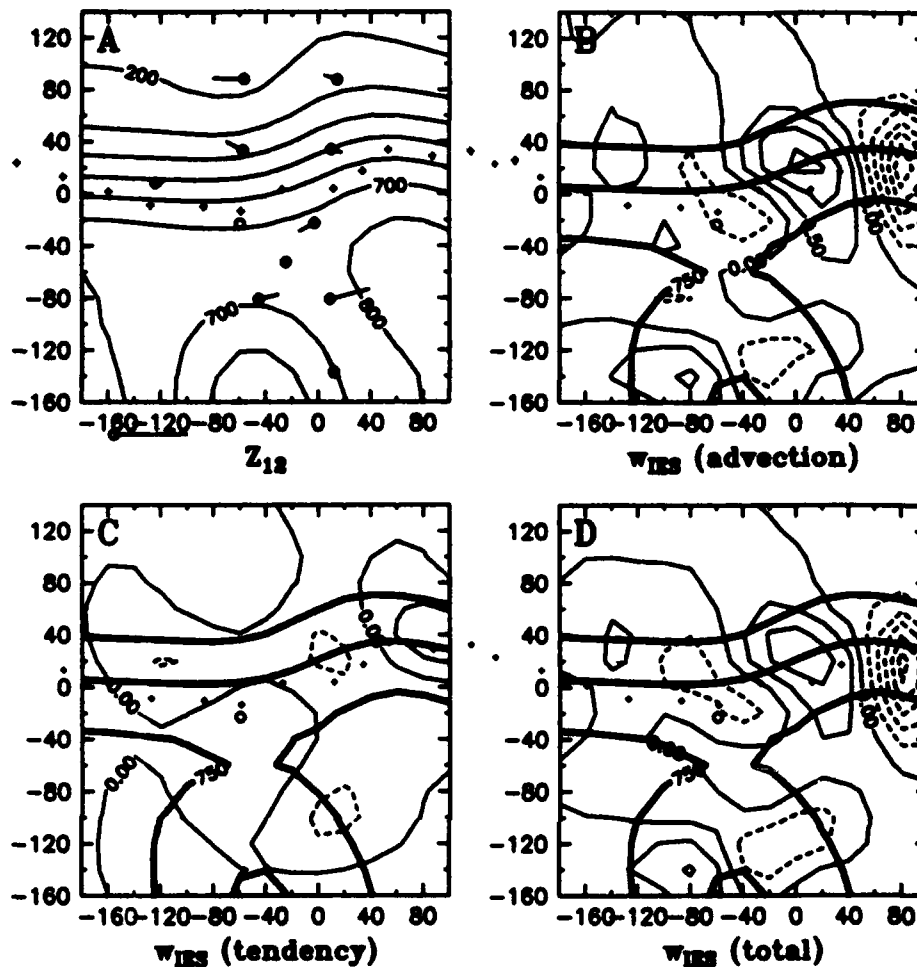
Figure 60: As in Figure 2, except for 0800 UTC 20 January 1990. The track of float 224 is indicated by dots, and the location of CM H4 is marked by a circle.

occurring just downstream, both forced primarily by vorticity advection (Figure 60). CM data also suggest downwelling; veering currents are forcing upward motion (Figure 61a,c,e) that is offset by the greater downward motion associated with local warming/descending isotherm (Figure 61b,d,f). This is another example where the temperature tendency at 700 m is much stronger than the average of the 400 m and 1000 m tendencies. The 1000 m and 400 m sensors are respectively below and above the main thermocline.
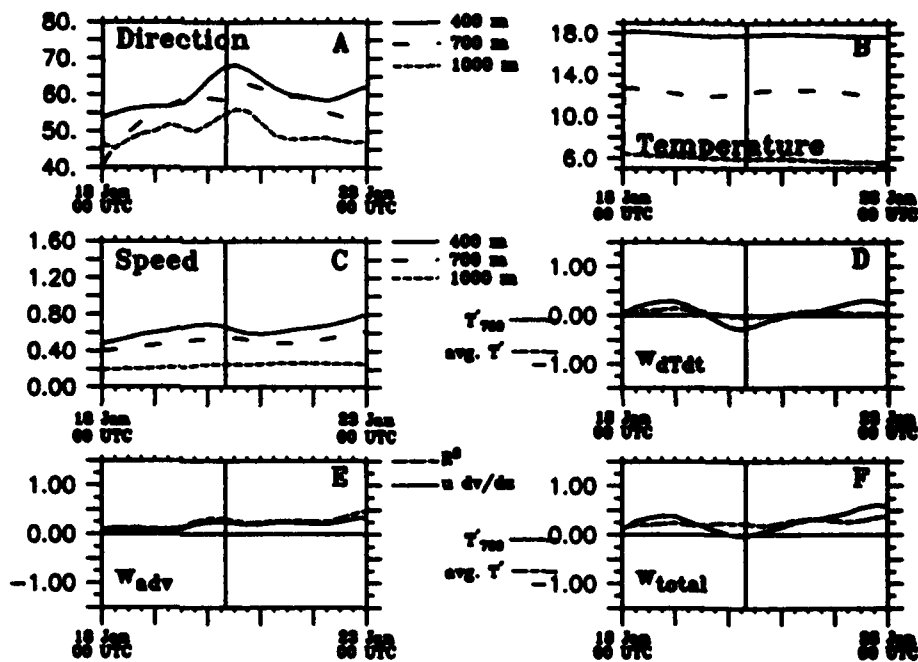
Figure 61: As in Figure 3, except for closest approach by float 224 to H4, which time is indicated by vertical line.

# 4 Comparing the three different methods

## 4.1 Statistics

What are the general statistics of vertical motion in the Central Array from the three data sources? Table 1 shows the means, standard deviations, maxima, minima, and the number of observations for the two-year period for each data source. All data sources indicate mean downwelling, which is consistent with expectations from quasi-geostrophic motion and the time average of equation (7) given the the observed crest just upstream of the Central Array (near the Gulf Stream 'node' at 70° W) and a trough near the eastern boundary of the array in the mean. The larger mean value of $w_{RAF}$ may reflect a sampling bias: floats remained mostly within the strongly baroclinic structure of the central Gulf Stream when traversing the Central Array, whereas CM and IES measured vertical motions throughout the region spanning also the Slope and Sargasso waters where large-scale vertical motions are smaller. Note that $w_{RAF}$ downwelling averaged over all tracks, including those that escaped the Gulf Stream, is an order of magnitude smaller than within the Central Array. We are examining a segment of the Gulf Stream that, for these 26 months at least, experienced mean downwelling.

Table 1: Vertical Motion Statistics: Mean, maximum, and minimum vertical motion (in mm s$^{-1}$) with standard deviation and number of (not all independent) observations for CM, IES, RAFOS floats in the Central Array only, and for all RAFOS floats

| Source | Mean | Std. Deviation | Maximum | Minimum | # obs |
|---|---|---|---|---|---|
| Current Meters | −0.015 | 0.347 | 3.676 | −2.297 | 25419 |
| Mapped IES | −0.027 | 0.440 | 4.006 | −3.794 | 188640 |
| RAFOS in central array | −0.048 | 0.617 | 2.10 | −2.66 | 947 |
| All RAFOS | −0.006 | 0.532 | 3.30 | −3.34 | 5939 |

To test the statistical significance of mean downwelling in Table 1, we computed the uncertainty of the mean for timeseries of $w_{CM}$ at each CM site, and at the ten extrema in the mean $w_{IES}$ field in Figure 62 using techniques in Bendat and Piersol (1973) and Dewar and Bane (1985). For each of the ten $w_{IES}$ extrema, the mean value differed from zero by at least one standard deviation (and usually two). Mean values of $w_{CM}$ also were usually at least one standard deviation from zero, except for several sites where $w_{CM}$ was very nearly zero. The mean downwelling is associated with the fact that the IES instruments preferentially sampled a crest-to-trough segment of the Gulf Stream. It follows from the work of Bower (1989) that downwelling should occur. How representative of the long-term mean are our results? Lee (1993) shows a trough in the Central Array for 6 out 8 years using infrared satellite data. We do believe the values for mean vertical motion in Table I have some statistical significance.

## 4.2 Case Studies

We now present several Figures that give evidence that the vertical motion determined from all three data sources is consistent. Figure 63 shows two time-series of $w_{CM}$ and $w_{IES}$ at two unrelated sites and times, G2 and I1. There are clear similarities between $w_{CM}$ and $w_{IES}$: both show events of up- and downwelling that develop and pass coherently with some high-frequency noise, extrema are approximately colocated, signal strength is similar in the
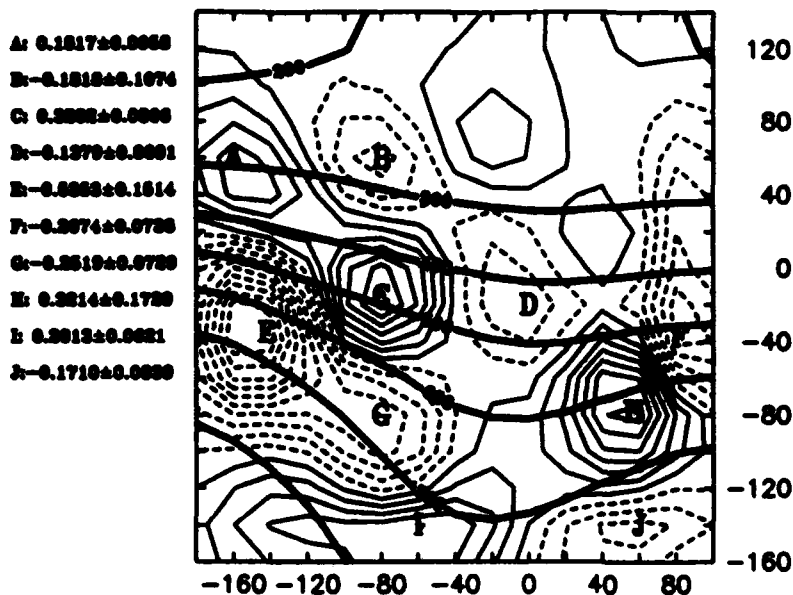
Figure 62: Mean $z_{12}$ topography (bold lines, contoured every 100 m) and mean vertical motion from (7) (thin lines contoured every 0.05 mm s$^{-1}$, negative values dashed) for the period 15 June 1988 – 7 August 1990 within the Central Array. Point values ($\pm$ standard deviation) of extrema as indicated. $x-$ and $y-$ axis labels are in kilometers.

two lines, and the episodic nature is obvious. We have made a similar comparison for all CM sites in the two-year deployment period; the similarity evident in Figure 63 characterizes all sites: large vertical motion in one data source usually has a corresponding extremum in the other; however, some counterexamples will be shown. Examples of the $w$ records along the 'G' line of current meters (G2 and G3 for both Year 1 and Year 2), along the 'H' line (H2, H3, H4, and H6 for both Year 1 and Year 2, H5 for only Year 1), along the 'I' line (I1, I2, I3, I4, I5 for both Year 1 and Year 2), and at M13 (Year 2) are shown in Figures 64— 76. In each of these time series, the characteristics highlighted in Figure 63 are evident. In each time series, a large peak in vertical motion in one method generally has a corresponding peak in the other method, although some time series (e.g., Figure 69) are better than others (Figure 75). There is inter-time series variability as well. Compare, for instance, Year 1 in Figure 68, which shows little coherence, with Year 2, which shows considerably more. Despite occasional short-period discrepancies between methods, we show below that time series of $w_{C_M}$ and $w_{I_{ES}}$ are coherent at periods longer than 12 days.
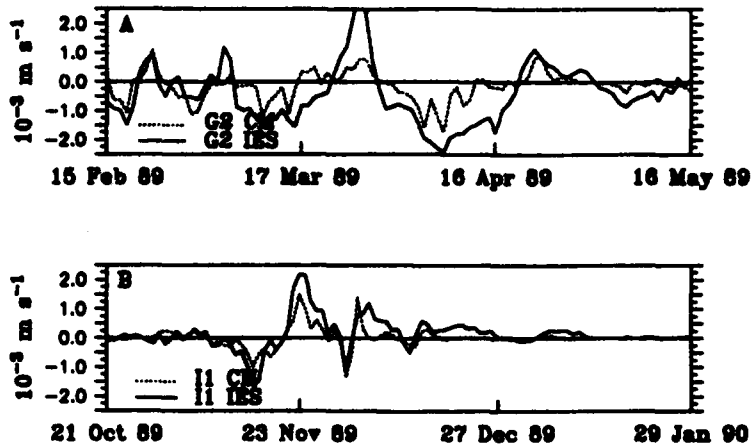
Figure 63: Time series of vertical motion. (A) CM G2 and (B) CM I1 with dates as indicated on the $x$-axis. Vertical motion from CM data ($w_{CM}$) using equation (4) in indicated with the dotted line; that from IES data ($w_{IES}$) and equation (7) is indicated with the solid line.
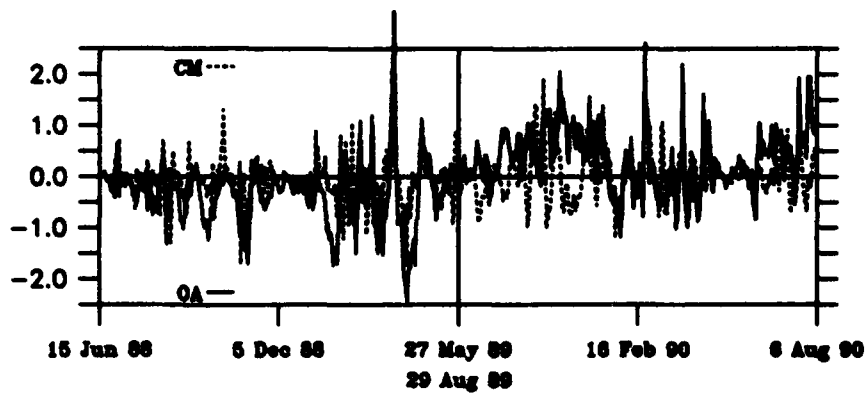


Figure 64: Time series of $w_{IES}$ (solid line) and $w_{CM}$ (dashed line) for CM G2 for Year 1 and Year 2.

70
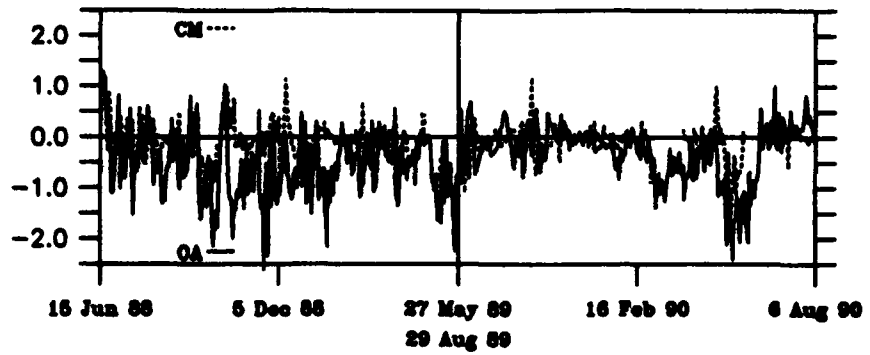
Figure 65: As in Figure 64, but for G3.
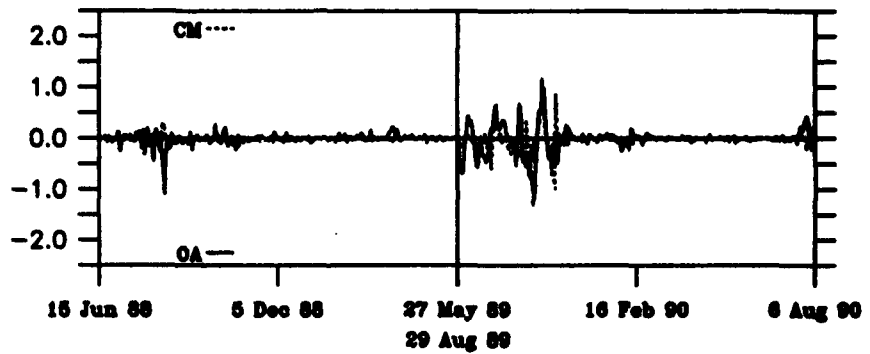


Figure 66: As in Figure 64, but for H2.
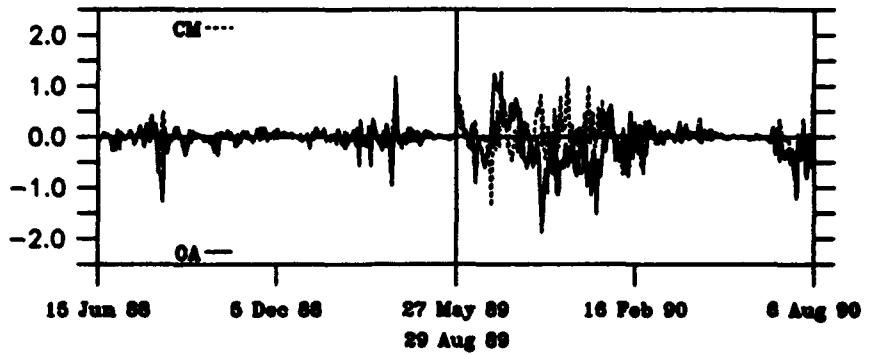


Figure 67: As in Figure 64, but for H3.

71
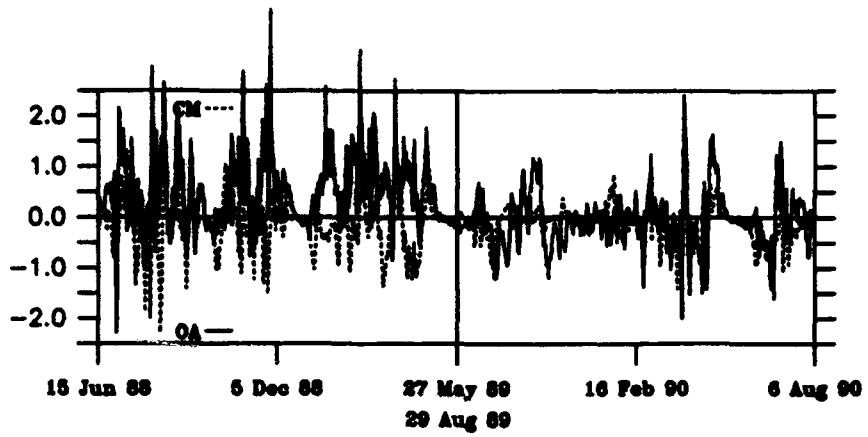
Figure 68: As in Figure 64, but for H4.
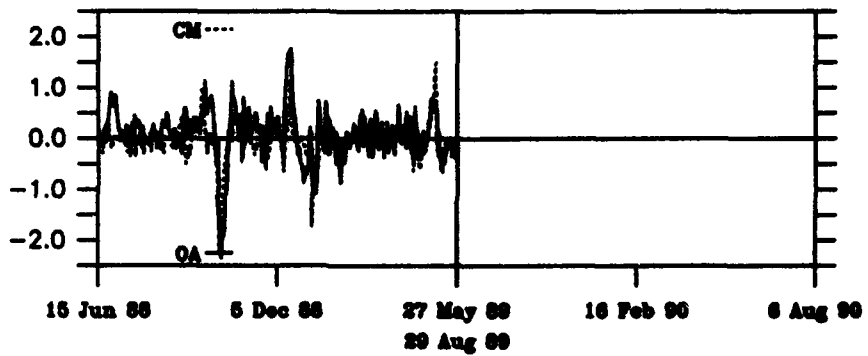


Figure 69: As in Figure 64, but for H5, Year 1 only.
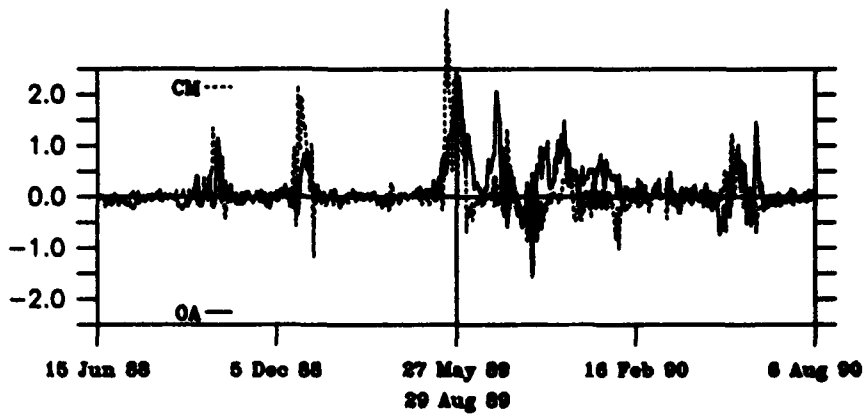


Figure 70: As in Figure 64, but for H6.

72
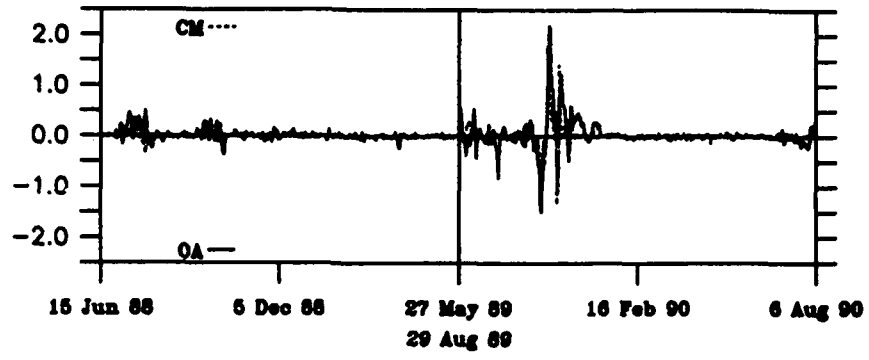
Figure 71: As in Figure 64, but for I1.



Figure 72: As in Figure 64, but for I2.



Figure 73: As in Figure 64, but for I3.

Figure 74: As in Figure 64, but for I4.



Figure 75: As in Figure 64, but for I5.



Figure 76: As in Figure 64, but for M13, Year 2 only.

74

Table 2 presents comparisons of vertical motion for all 23 cases in which a float passed within 10 $km$ of a CM mooring with working instrumentation at 400, 700, and 1000 m. These are the cases discussed in Section 3. Figure 77a is a scatterplot of RAFOS vertical motions versus CM vertical motions, with data taken from Table 2. A linear relationship is clearly evident with correlation $r^2 = 0.82$. That the slope of the line is greater than unity could arise from our choices of values for $\alpha_o$ or $\frac{d\theta_o}{dz}$, or from $w_{RAF}$ being biased low. However, the plot underscores the excellent agreement between $w_{RAF}$ and $w_{CM}$.
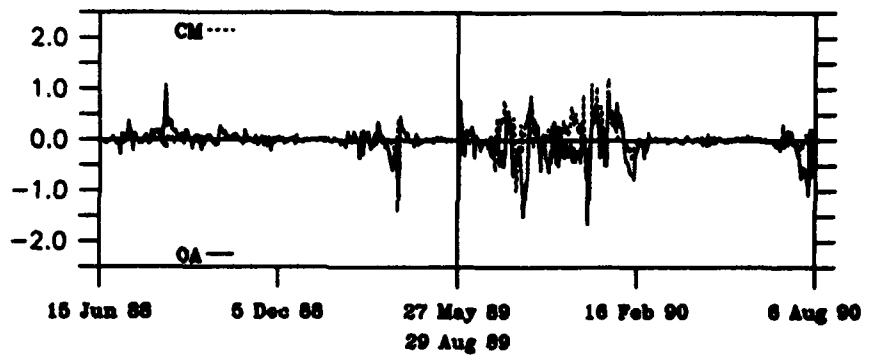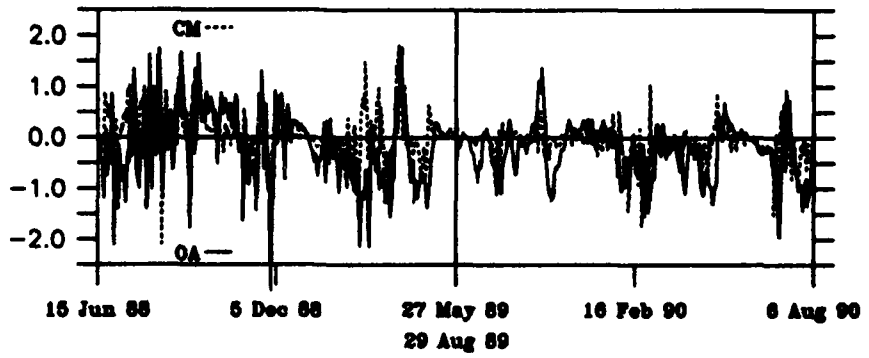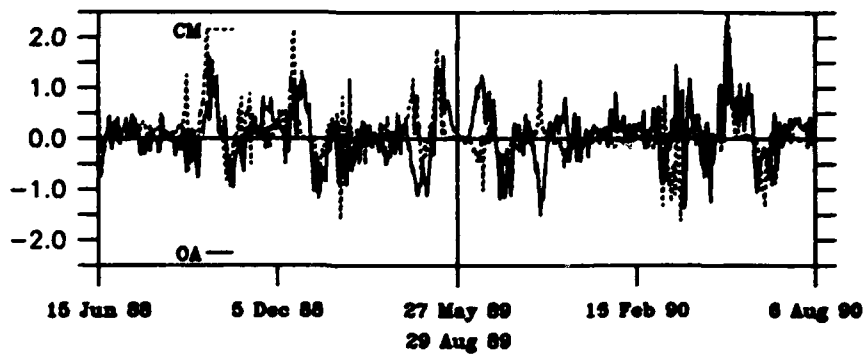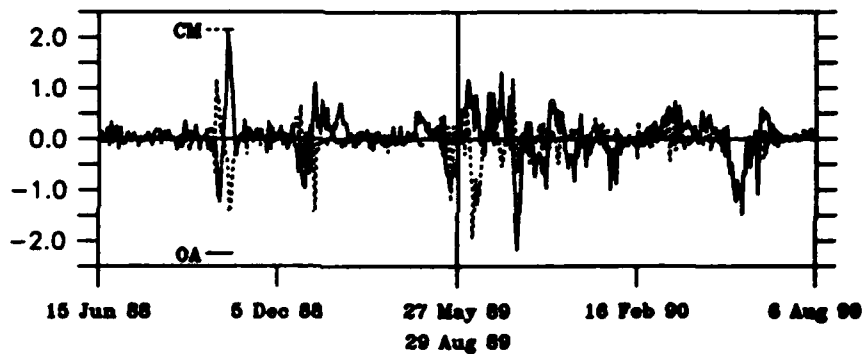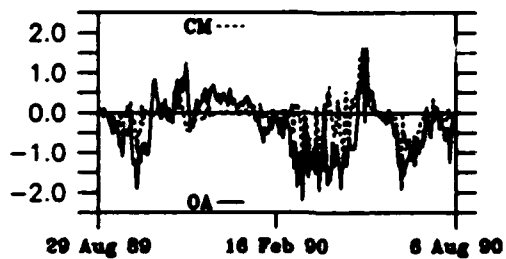
Table 2: Vertical Motion Comparisons: Vertical motions from RAFOS float, CM, and IES data ($w_{RAF}$, $w_{CM}$, and $w_{IES}$, respectively), with units of mm s$^{-1}$ for date/time shown and for RAFOS float and CM indicated. Depth of the RAFOS float at the comparison time (in meters) is also shown.

| Float | CM | date/time | $w_{RAF}$ | $w_{CM}$ | $w_{IES}$ | Depth |
|---|---|---|---|---|---|---|
| RAF123 | H4 | 4Jul88/00z | −0.58 | −0.98 | −1.42 | 550.3 m |
| RAF129 | I4 | 23Sep88/08z | 0.19 | 0.53 | 0.04 | 710.7 m |
| RAF129 | I4 | 23Sep88/16z | 0.72 | 0.48 | 0.05 | 706.4 m |
| RAF136 | I4 | 8Dec88/16z | 0.81 | 0.43 | 0.17 | 668.4 m |
| RAF141 | I4 | 2Nov88/16z | −0.87 | −0.94 | −0.43 | 603.0 m |
| RAF175 | I4 | 20Jan89/16z | −0.56 | −0.05 | −0.63 | 363.7 m |
| RAF176 | I5 | 7Feb89/00z | −0.04 | 0.02 | 0.25 | 761.5 m |
| RAF176 | I5 | 7Feb89/08z | −0.05 | 0.03 | 0.26 | 763.0 m |
| RAF176 | I5 | 7Feb89/16z | 0.04 | 0.02 | 0.27 | 764.5 m |
| RAF176 | I5 | 8Feb89/00z | −0.03 | −0.05 | 0.26 | 760.7 m |
| RAF194 | I5 | 15Nov89/00z | 0.71 | 0.23 | −0.22 | 662.2 m |
| RAF194 | I4 | 16Nov89/00z | 0.86 | 1.20 | −1.06 | 584.3 m |
| RAF199 | I5 | 23Nov89/00z | 0.24 | 0.23 | −0.13 | 593.2 m |
| RAF199 | I5 | 28Nov89/16z | −0.13 | 0.04 | 0.54 | 627.4 m |
| RAF201 | I1 | 23Nov89/08z | 0.97 | 1.51 | 1.66 | 560.4 m |
| RAF207 | I2 | 4Sep89/08z | −0.25 | −0.06 | −0.24 | 164.0 m |
| RAF209 | I5 | 13Sep89/08z | −1.53 | −2.14 | 0.22 | 629.2 m |
| RAF210 | H4 | 6Oct89/08z | −0.02 | −0.19 | −0.84 | 642.4 m |
| RAF210 | I5 | 21Oct89/00z | 0.36 | 1.07 | −0.33 | 557.4 m |
| RAF211 | M13 | 8Oct89/00z | −0.44 | −0.68 | −0.78 | 658.9 m |
| RAF216 | I1 | 26Nov89/00z | −0.02 | 0.14 | 0.86 | 576.2 m |
| RAF221 | I2 | 6Jan90/08z | 0.18 | 0.21 | 0.45 | 482.9 m |
| RAF224 | H4 | 20Jan90/08z | −0.18 | −0.10 | −0.30 | 496.7 m |

The comparison between $w_{RAF}$ and $w_{IES}$ for the same 23 cases (Figure 77b) shows more scatter, in part because the cases were selected for floats passing CM sites; several of these cases are not in the best IES mapping region. Nevertheless, after excluding the two obvious outliers that are discussed below, the correlation $r^2 = 0.32$, which is significant at a confidence level of greater than 99%. That the slope of the line is less than unity suggests there may be a bias towards underestimating $w_{IES}$ that would result from the spatial filtering of the IES maps.

Careful scrutiny of Table 2 shows that $w_{IES}$ consistently is of the wrong sign at I5. The computation of vorticity and vorticity advection at site I5 is adversely impacted by

that site's close proximity to edge of the domain. After excluding all $w_{IES}$ from site I5 in Table 2, we plot the remaining values in Figure 77c, from which we compute a correlation $r^2$ of 0.51, significant at a confidence level exceeding 90%. To understand the causes of errors in Figures 77b,c, we have closely investigated the vertical motion fields associated with the one remaining outlier in Figure 77c. Two possible error sources are discussed below.
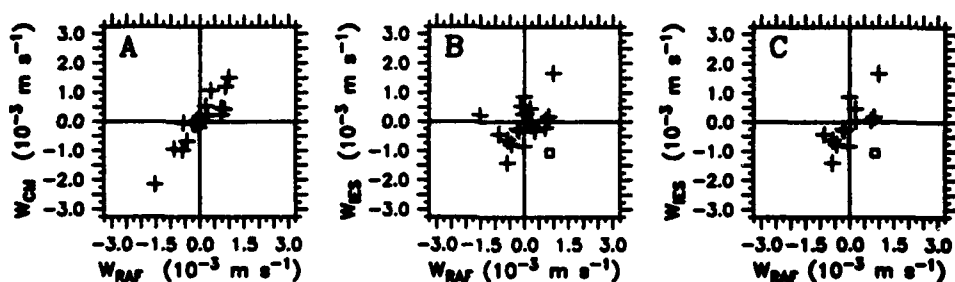


Figure 77: (A) Scatterplot of $w_{RAF}$ versus $w_{CM}$ for data as listed in Table 2. (B) Scatterplot of $w_{RAF}$ versus $w_{IES}$ as listed in Table 2. (C) As in (B), but excluding $w_{IES}$ at site I5. The box point in (B) and (C) is discussed further in text.

The point in the lower right quadrant of Figure 77b,c is from the case when RAFOS float 194 passed by CM I4 at 0000 UTC 16 November 1989 (See Section 3.8). Both CM and float vertical velocities are upward; however, $w_{IES}$ is strongly downward. This may be caused by poor IES data at site I4 during winter of Year 2, when this IES suffered from many bad data returns, necessitating frequent interpolations to compute thermocline depth at that site (Fields and Watts 1991). Such data degradation would of course have a negative impact on the computed streamfunction field and all quasigeostrophic calculations near I4 for winter of 1989-1990 data.

It is far more likely that errors were introduced into $w_{IES}$ at this time because significant currents existed at deep levels. IES measurements determine the baroclinic component of the flow only. IF there is a significant barotropic flow, then the vorticities and advections computed in (7) using only IES data will not be representative of the true flow. Figure 27 presents the IES topography and $w_{IES}$ for this time, as well as the track of float 209 as it traversed the central array. The deep currents at the CM sites are also plotted. Note the unusually strong flow at 3500 $m$ at I4. In this area, strong upward motion associated with the cyclonically curved onshore barotropic flow overwhelms the downward motion associated with the baroclinic flow. In fact, this event is associated with the strongest deep currents for the $w_{IES}$ cases plotted in Figure 77c: $|\bar{v}_{3500}| = 0.19$m s$^{-1}$, which is a value nearly two standard deviations above the mean speed at I4 during Year 2. Note that strong deep currents do not necessarily mean poor values of $w_{IES}$: Case 11 (Section 3.11) also had deep velocities in excess of 0.15 m s$^{-1}$ and there is good agreement between $w_{RAF}$ and $w_{IES}$. For this case, the deep currents flow parallel to the Gulf Stream; for the case above, the deep flow crosses under the Gulf Stream. Where the barotropic flow is significant, especially if it is spatially non-uniform, errors in $w_{IES}$ are quite likely. Because it is possible to account for the deep currents, however, (for example by combining a deep barotropic streamfunction —

measured by current meters or perhaps by electric field measurements — with the baroclinic streamfunction) we do not consider this an unbearable problem. Indeed, this is the subject of an ongoing followup study.

## 4.3   Coherence between $w_{CM}$ and $w_{IES}$

The time-series estimates of $w_{CM}$ and $w_{IES}$ (e.g., Figures 63 and  64– 76) show smoothly varying signals with varying degrees of high-frequency noise superimposed. We spectrally decomposed each pair of records and computed their statistical coherence at all sites along the central mooring H-line (whose time series are shown in Figures 66– 70) at those CM sites that had all three upper CMs functioning and that were surrounded by functioning IESs (these were H3, H5, and H6 from Year 1 and H4 and H6 from Year 2). These coherence results were averaged for the whole line and are shown in Figure 78. The average coherence between the two independent estimates of vertical motion is greater than 0.5 (at far above the 99% confidence level) throughout all periods longer than 16 days. At periods shorter than 12 days, the coherence is insignificant.   This confirms the visual impression from Figures 63– 76 that the large amplitude, low-frequency variations of $w$ from both CM and IES techniques are very consistent, while the smaller-amplitude, high-frequency variations are noise-dominated. In Figures 79– 91, we show the coherence for all of the sites, calculated separately for Year 1 and Year 2 because the instrument arrays changed between the two years. In particular, the mapping ability of the IES array to estimate terms in the vorticity equation could have changed between the two years – as it appears to have done at some sites like G2 (Figure 79) and H2 (Figure 81).
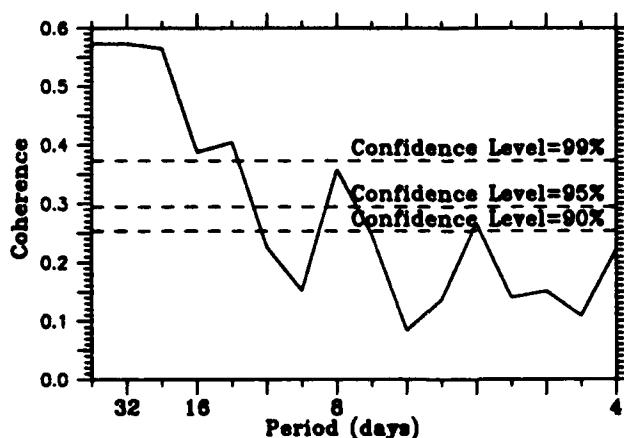


Figure 78: Coherence as a function of frequency for $w_{IES}$ and $w_{CM}$ for selected sites on the 'H' line.

Given these statistical coherences, how well can we use equations (4) and (7) to infer vertical motion using data from the CM and IES arrays that were designed for mesoscale
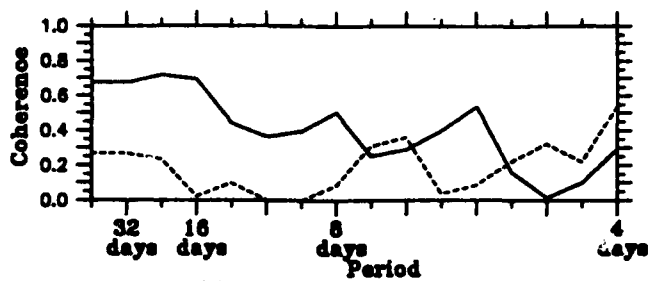
Figure 79: Coherence as a function of frequency for $w_{IES}$ and $w_{CM}$ for CM G2 Year 1 (solid line) and Year 2 (dotted line).
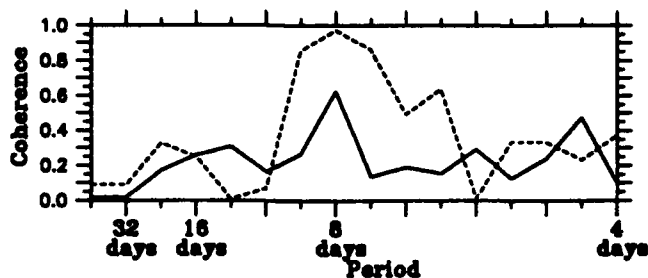


Figure 80: As in Figure 79, but for G3.

sampling? Both techniques involve temporal and spatial differentiation of measured quantities, an analysis which accentuates measurement and sampling errors. The errors in $w_{CM}$ from (4) are not dominated by measurement error but rather by submesoscale features for which the signal is incoherent between our moored $u$, $v$, $T$ sensors. Errors in $w_{IES}$ from (7) are dominated by instrument/analysis error in the streamfunction fields. The objective mapping and measurement technique filters out submesoscale features, including some that may be sampled at individual CM moorings. Nevertheless, with either technique, the major mesoscale features in $w$ are clear. The coherence between $w_{IES}$ and $w_{CM}$ shown in Figure 10 and the particularly good agreement between $w_{RAF}$ and $w_{CM}$ illustrated in Table 2 and Figure 77a, i.e. agreements between three independent techniques for measuring $w$, show that the $w_{CM}(t)$ and $w_{IES}(x, y, t)$ fields do characterize mesoscale vertical motions in the Gulf Stream.



Figure 81: As in Figure 79, but for H2.

Figure 82: As in Figure 79, but for H3.



Figure 83: As in Figure 79, but for H4.



Figure 84: As in Figure 79, but for H5 (Year 1 only).



Figure 85: As in Figure 79, but for H6.

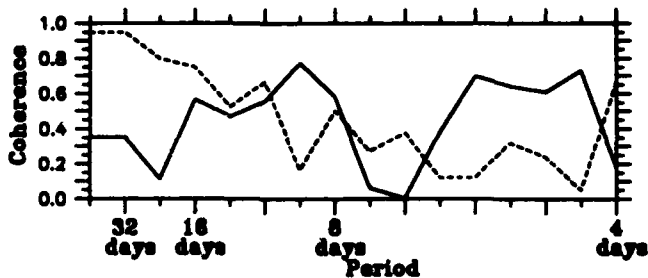Figure 86: As in Figure 79, but for I1.



Figure 87: As in Figure 79, but for I2.



Figure 88: As in Figure 79, but for I3.
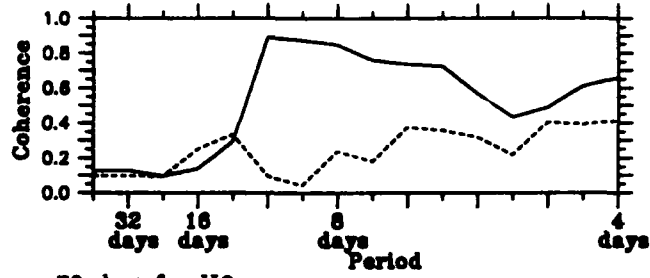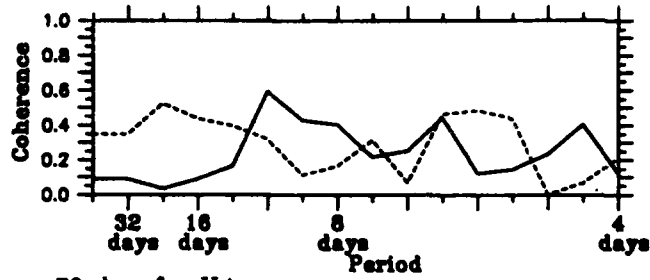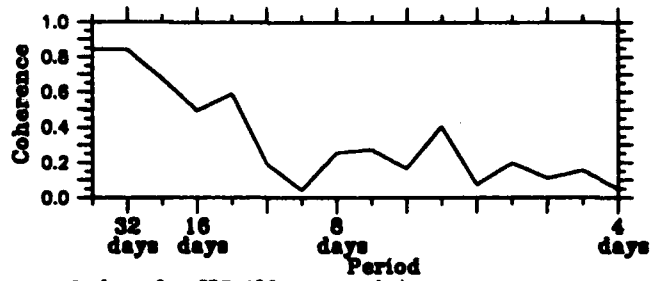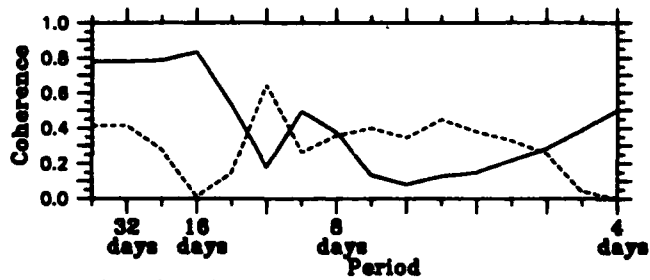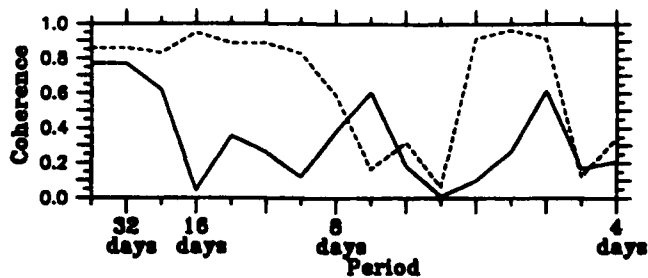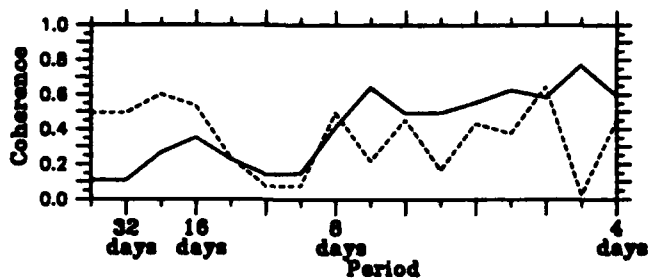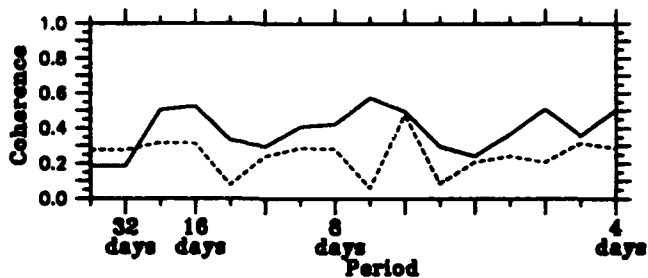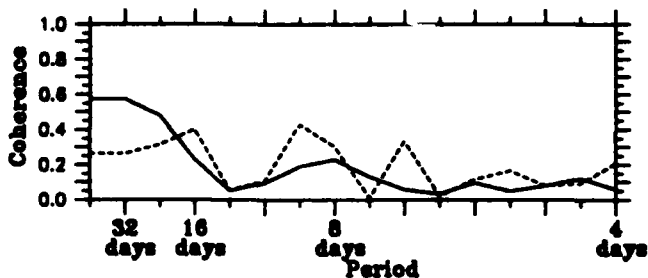


Figure 89: As in Figure 79, but for I4.
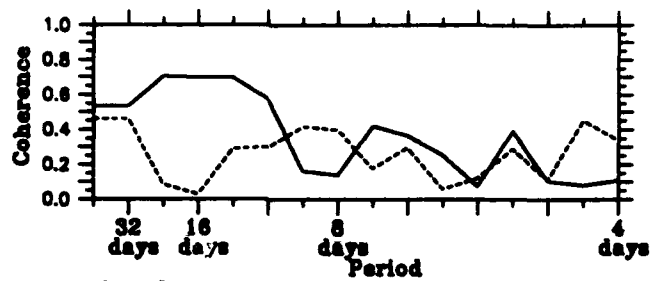
Figure 90: As in Figure 79, but for I5.
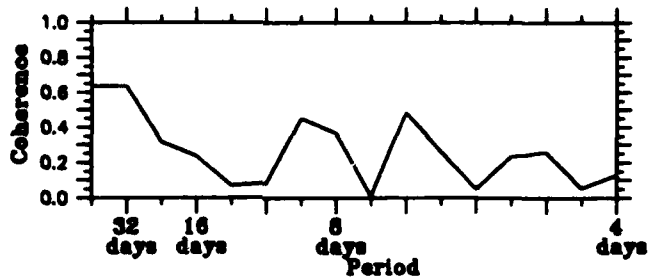


Figure 91: As in Figure 79, but for M13.

# 5 Summary

We have computed and compared vertical motions from three different sources in the Gulf Stream downstream of Cape Hatteras. Magnitudes of vertical motion as measured by RAFOS floats and as estimated from CM data and IES data are 1–2 mm $s^{-1}$, with rare values of up to 3 mm $s^{-1}$. Both the CM and IES vertical motions are smoothly varying fields not dominated by the submesoscale and measurement noise that is present. It is easy to track features from day to day in both datasets; evolution of the fields occurs only slowly as mesoscale jet features evolve.

CM vertical motions agree closely with observations from RAFOS floats. There is also considerable agreement between IES and RAFOS float or CM vertical motions, and very good coherence at long timescales between $w_{IES}$ and $w_{CM}$ timeseries. Indeed, for timescales of greater than $16d$, $w_{CM}$ and $w_{IES}$ show coherence $> 0.5$ at far above the 99% confidence level, but such coherence is absent for timescales of less than $12d$. This lack of coherence may be caused in part by errors related to the presence of strong deep (barotropic) velocities under the meandering Gulf Stream. By combining the IES data with an independent measure of the barotropic velocity, it should be possible to account for the vertical velocity driven by deep currents.

To our knowledge, this is the first study in which vertical motions associated with mesoscale processes in the ocean have been observed and verified by independent measurements and independent dynamical methods. The spatial and temporal structures of the $w$ field can be diagnosed with both CM and IES arrays; the Gulf Stream clearly exhibits secondary circulations on the mesoscale that are consistent with quasi-geostrophic dynamics.

# 6 References

Anderson-Fontana, S. and H. T. Rossby, 1991: *RAFOS floats in the SYNOP experiment 1988–1990*. Technical Report 91-7, University of Rhode Island Graduate School of Oceanography, Narragansett, RI 02882-1197. 155pp.

Árnason, G., 1942: Distribution of mass variations in atmospheric air columns. *Meteorologiske Annaler*, 1, 10, pp. 255-279.

Bane, J. M., L. M. O'Keefe, and D. R. Watts, 1989: Mesoscale eddies and submesoscale coherent vortices: Their existence near and interactions with the Gulf Stream. *Mesoscale/ Synoptic Coherent Structures in Geophysical Turbulence*, J. C. J. Nihoul and B. M. Jamart, eds. Elsevier Science Publishers, Amsterdam. pp. 501-518.

Blanton, S. L., III, 1991: *Computations of vertical velocity in the Gulf Stream northeast of Cape Hatteras, North Carolina*. M.S. Thesis, University of North Carolina Marine Sciences Program, Chapel Hill, NC, 27599-3300. 84pp.

Bryden, H. L., 1976: Horizontal advection of temperature for low-frequency motions. *Deep Sea Res.*, 23, 1165-1174.

Bryden, H. L., 1980: Geostrophic vorticity balance in midocean. *J. Geophys. Res.*, 85C, 2825-2828.

Bower, A. S., 1989: Potential vorticity balances and horizontal divergence along particle trajectories in Gulf Stream meanders east of Cape Hatteras. *J. Phys. Oceanogr.*, 19, 1669-1681.

Bower, A. S., 1991: A simple kinematic mechanism for mixing fluid parcels across a meandering jet. *J. Phys. Oceanogr.*, 21, 173-180.

Bower, A. S. and H. T. Rossby, 1989: Evidence of cross-frontal exchange processes in the Gulf Stream based on isopycnal RAFOS float data. *J. Phys. Oceanogr.*, 19, 1177-1190.

Fields, E. and D. R. Watts, 1990. *THE SYNOP EXPERIMENT: Inverted Echo Sounder data report for May 1988 to Aug 1989*. GSO Technical Report No. 90-2, Graduate School of Oceanography, University of Rhode Island, Narragansett, RI 02882-1197. 231 pp.

Fields, E. and D. R. Watts, 1991. *THE SYNOP EXPERIMENT: Inverted Echo Sounder data report for Jun 1989 to Sep 1990*. GSO Technical Report No. 91-2, Graduate School of Oceanography, University of Rhode Island, Narragansett, RI 02882-1197. 255pp.

Gill, A. E., 1982: *Atmosphere-Ocean Dynamics*. Academic Press. 662pp.

Hall, M. M., 1985: *Horizontal and vertical structure of velocity, potential vorticity and energy in the Gulf Stream*. Ph.D. thesis, MIT/WHOI, WHOI-85-16, Woods Hole, MA, 02543, 165pp.

Hall, M. M., 1986: Horizontal and vertical structure of the Gulf Stream velocity field at 68 W. *J. Phys. Oceanogr.*, 16, 1814-1828.

Hall, M. M., 1989: Energetics of the Kuroshio extension at 35° N, 152° E. *J. Phys. Oceanogr.*, 21, 958-975.

Hogg, N. G., 1991: Mooring motion corrections revisited. *J. Atmos. Ocean. Technol.*, 8, 289-295.

Holton, J. R., 1979: *An Introduction to Dynamic Meteorology*. Academic Press, 391pp.

Kim, H.-S., 1991. *An observational streamfunction in the Gulf Stream*. M.S. thesis, Univ. of Rhode Island Graduate School of Oceanography, Narragansett, RI, 02882-1197, 126pp.

Leach, H., 1987: The diagnosis of synoptic-scale vertical motion in the seasonal thermocline. *Deep-Sea Res.*, 34, 2005-2017.

Lee, T., 1993: *Variability of the Gulf Stream path from Cape Hatteras to 45 west observed from infrared imagery.* Ph.D. thesis, Univ. of Rhode Island Graduate School of Oceanography, Narragansett, RI, 02882-1197, 95pp.

Osgood, K. E., J. M. Bane, Jr., and W. K. Dewar, 1987: Vertical velocities and dynamical balances in Gulf Stream meanders. *J. Geophys. Res.*, **92C**, 13029-13040.

Panofsky, H. A., 1944: The effect of vertical motion on local temperature and pressure tendencies. *Bull. Amer. Meteor. Soc.*, **25**, 271-275.

Pickart, R. S. and D. R. Watts, 1990: Using the inverted echo sounder to measure vertical profiles of Gulf Stream temperature and geostrophic velocity. *J. Atmos. Ocean. Tech.*, **7**, 146-156.

Pollard, R. T. and L. A. Regier, 1992: Vorticity and vertical circulation at an ocean front. *J. Phys. Oceanogr.*, **22**, 609-625.

Rossby, H. T., 1987: On the energetics of the Gulf Stream at 73W. *J. Marine Res.*, **45**, 59-82.

Rossby, H. T., D. Dorson and J. Fontaine, 1986. The RAFOS system. *J. Atmos. Oceanic Technol.*, **3**, 672-679.

Shapiro, R., 1970: Smoothing, filtering and boundary effects. *Rev. Geophys. Space Phys.*, **8**, 359-387.

Shay, T. J., S. Haines, J. M. Bane and D. R. Watts, 1992: SYNOP Central Array current meter data report: Mooring period May 1988-September 1990. University of North Carolina Technical Report.

Tintoré, J., D. Gomis, S. Alonso and G. Parrilla, 1991: Mesoscale dynamics and vertical motion in the Alborán Sea. *J. Phys. Oceanogr*, **21**, 811-823.

Tracey, K. L. and D. R. Watts, 1991: *THE SYNOP EXPERIMENT: Thermocline depth maps for the Central Array October 1987 to August 1990.* GSO Technical Report No. 91-5, Graduate School of Oceanography, University of Rhode Island, Narragansett, Rhode Island, 02882-1197. 193pp.

Watts, D. R. and H. T. Rossby, 1977: Measuring dynamic heights with inverted echo sounders: Results from MODE. *J. Phys. Oceanogr.*, **7**, 346-358.

# REPORT DOCUMENTATION PAGE

| 1a. REPORT SECURITY CLASSIFICATION | 1b. RESTRICTIVE MARKINGS |
|---|---|
| Unclassified | |

| 2a. SECURITY CLASSIFICATION AUTHORITY | 3. DISTRIBUTION/AVAILABILITY OF REPORT |
|---|---|
| | Distribution for Public Release |
| 2b. DECLASSIFICATION/DOWNGRADING SCHEDULE | Distribution is unlimited |

| 4. PERFORMING ORGANIZATION REPORT NUMBER(S) | 5. MONITORING ORGANIZATION REPORT NUMBER(S) |
|---|---|
| Univ. or RI, Graduate School of Oceanography, GSO Technical Report 93-2 | |

| 6a. NAME OF PERFORMING ORGANIZATION | 6b. OFFICE SYMBOL (If applicable) | 7a. NAME OF MONITORING ORGANIZATION |
|---|---|---|
| Univ. of RI Graduate School of Oceanography | 1122 PO | |

| 6c. ADDRESS (City, State, and ZIP Code) | 7b. ADDRESS (City, State, and ZIP Code) |
|---|---|
| South Ferry Road Narragansett, RI 02882-1197 | |

| 8a. NAME OF FUNDING/SPONSORING ORGANIZATION | 8b. OFFICE SYMBOL (If applicable) | 9. PROCUREMENT INSTRUMENT IDENTIFICATION NUMBER |
|---|---|---|
| Office Naval Research National Science Foundation | | |

| 8c. ADDRESS (City, State, and ZIP Code) | 10. SOURCE OF FUNDING NUMBERS | | | |
|---|---|---|---|---|
| 100 N.Quincy St., Arlington, VA 22217 1800 G St., N.W., Washington, DC 20550 | PROGRAM ELEMENT NO. | PROJECT NO. | TASK NO. | WORK UNIT ACCESSION NO. |

**11. TITLE (Include Security Classification)**

Vertical Motion in the SYNOP Central Array

**12. PERSONAL AUTHOR(S)** Scott S. Lindstrom & D. Randolph Watts

| 13a. TYPE OF REPORT | 13b. TIME COVERED | 14. DATE OF REPORT (Year, Month, Day) | 15. PAGE COUNT |
|---|---|---|---|
| Technical | FROM 6/88 TO 8/90 | Oct. 93 | 84 |

**16. SUPPLEMENTARY NOTATION**

| 17. COSATI CODES | | | 18. SUBJECT TERMS (Continue on reverse if necessary and identify by block number) |
|---|---|---|---|
| FIELD | GROUP | SUB-GROUP | Gulf Stream, SYNOP, Vertical Motion |
| | | | |

**19. ABSTRACT (Continue on reverse if necessary and identify by block number)**

As part of the SYNOP (Synoptic Ocean Prediction experiment) field program, twelve tall moorings measured the Gulf Stream's temperature and velocity fields with current meters (CM) at nominal depths of 400 m, 700 m, 1000 m, and 3500 m for two years, from May 1988 through August 1990. Simultaneously, 24 inverted echo sounders (IES) monitored the thermocline topography. A third observational component of the experiment was the release of isopycnal RAFOS floats; 70 such floats traversed the area monitored by the CM and the IES. This report documents the methods used to compute vertical motion for each data source, and the differences and similarities between the three methods. Typical velocities during 'strong' events, as observed by or inferred from all three instruments, was 1-2 mm s$^{-1}$ in regions near the center of the Gulf Stream. The comparison of RAFOS vertical motions and vertical motions diagnosed from CM data showed excellent agreement; furthermore, CM vertical motions and IES vertical motions are statistically coherent for periods longer than 12 days. We conclude that we may map mesoscale fields of w(x,y,t); the fields mapped are consistent with quasi-geostrophic dynamics.

| 20. DISTRIBUTION/AVAILABILITY OF ABSTRACT | 21. ABSTRACT SECURITY CLASSIFICATION |
|---|---|
| ☒ UNCLASSIFIED/UNLIMITED ☐ SAME AS RPT. ☐ DTIC USERS | |

| 22a. NAME OF RESPONSIBLE INDIVIDUAL | 22b. TELEPHONE (Include Area Code) | 22c. OFFICE SYMBOL |
|---|---|---|
| | | |

**DD FORM 1473, 84 MAR**  83 APR edition may be used until exhausted.
All other editions are obsolete.